THÈSE

Présentée à L'Université de Lille 1
École Doctorale Sciences Pour L'Ingénieur

Pour obtenir le grade de

DOCTEUR DE L'UNIVERSITÉ DE LILLE

Spécialité : MICROONDES ET MICROTECHNOLOGIES

Par

Yogadissen ANDEE

Advanced Techniques for Noise Figure and Noise Parameters Measurements of Differential Amplifiers

Soutenue le 10 décembre 2015 devant la Commission d'examen

Membres du Jury:

Pr. Alain Cappy	IEMN	Président
Pr. Laurent Escotte	LAAS	Rapporteur
Pr. Bernard Jarry	XLIM	Rapporteur
Pr. Dominique Schreurs	ESAT-TELEMIC	Membre
Dr. Joel Dunsmore	Keysight	Membre
Pr. François Danneville	IEMN	Directeur de thèse
Dr. Caroline Arnaud	CEA-Leti	Encadrant de thèse
Mr. Steffen Neidhardt	Rohde&Schwarz	Invité
Mr. Philippe Seurre	Rohde&Schwarz	Invité

Thèse préparée en collaboration avec le CEA-Leti, Rohde&Schwarz et l'IEMN

Abstract

Differential circuits have major advantages over single-ended circuits regarding immunity to common-mode noise, double voltage swing and reduction of even-order distortion. Their wide proliferation creates a need for the development of functional techniques for differential noise figure measurement. Chapter 1 shows that the noise figure of a 4-port circuit depends on the correlation of the noise waves at the output ports. However, no standard equipment is capable of measuring directly this correlation. Chapter 2 proposes an original technique for measuring the correlation of output noise waves. It makes use of a hybrid coupler connected to the differential DUT. The correlation is determined by using two configurations of connection between the DUT and the coupler. A rigorous and general technique for the noise figure measurement of differential amplifiers is developed from this approach. Chapter 3 proposes an original approach where no extra coupler is required. A study of the structure of a differential amplifier is performed where an expression of the correlation is calculated in terms of output noise powers and of the 4-port S-parameters. A fast and functional measurement technique using this method is developed on a 4-port network analyzer. This coupler-free approach is extended to the measurement of the noise parameters of differential amplifiers. The noise parameters are determined from differential source-pull measurements using a differential impedance tuner. This is, to the best of our knowledge, the first coupler-free technique developed for measuring differential noise parameters.

Keywords

Noise figure, measurement, differential, network analyzer, correlation, noise waves, low noise amplifier, mixed-mode, tuner, coupler

Résumé

Les circuits différentiels présentent de nombreux avantages par rapport aux circuits 2-ports classiques en termes d'immunité contre les bruits de mode commun, de tensions de sortie doublées et de réduction de distorsion d'ordre pair. Leur usage répandu crée une demande pour le développement de nouvelles techniques de mesures du facteur de bruit différentiel. Le chapitre 1 démontre que le facteur de bruit est fonction de la corrélation des ondes de bruit en sortie du circuit différentiel. Il n'existe toutefois aucun appareil capable de mesurer directement cette corrélation. Le chapitre 2 présente une technique originale pour mesurer cette corrélation. Elle utilise un coupleur hybride connecté aux ports de sortie du circuit différentiel selon 2 configurations de connexion. Cette approche permet de mesurer rigoureusement le facteur de bruit de tous types d'amplificateurs différentiels. Le chapitre 3 propose une technique pour mesurer la corrélation sans utiliser de coupleurs. Une étude de la structure différentielle permet de trouver une expression de la corrélation en fonction des puissances de bruit en sortie et des paramètres S. Une technique rapide et fonctionnelle est ainsi développée sur un analyseur de réseau 4-port pour mesurer le facteur de bruit d'un amplificateur différentiel. Cette approche sans coupleur est étendue à la mesure des paramètres de bruit d'un amplificateur différentiel. L'extraction des 4 paramètres de bruit se fait grâce à la méthode des impédances multiples en utilisant un synthétiseur différentiel d'impédance. Ce travail présente pour la première fois une technique sans coupleur pour la mesure des paramètres de bruit différentiels.

Mots clés

Facteur de bruit, mesure, différentiel, analyseur de réseau, corrélation, ondes de bruit, amplificateur faible bruit, modes mixtes, synthétiseur d'impédance, coupleur

Acknowledgements

I would like to express my special appreciation and thanks to my advisor Pr. François DANNEVILLE for encouraging and supporting my research during the last three years.

I am especially thankful to my advisor Dr. Caroline ARNAUD for her valuable help and support since her arrival at the CEA Leti.

I would like to express appreciation to Mr. Philippe SEURRE and Mr. Steffen NEIDHARDT of Rohde&Schwarz for sharing their knowledge and skills on network analyzer measurements.

I gratefully acknowledge Pr. Bernard JARRY and Pr. Laurent ESCOTTE for their interesting comments and questions after having examined my PhD thesis.

I am also grateful to Pr. Alain CAPPY, Pr. Dominique SCHREURS and Dr. Joel DUNSMORE for participating in the doctoral defense committee. I greatly appreciated the discussions that we had during my thesis defense.

I also thank Mr. Jérôme PROUVÉE and Dr. François GRAUX for creating the research project and for supervising my research works during the first year.

I would especially like to thank the members of the CEA Leti: Dr. Clément JANY, Dr. Alexandre SILIGARIS, Dr. José MORON GUERRA, Dr. Vincent PUYAL and Mr. Frédéric HAMEAU. Your help and friendship have contributed immensely to my personal and professional time in Grenoble.

A special thanks to my colleagues: Mr. Anthony GOAVEC, Dr. Marina DENG, Mrs. Sylvie LÉPILLIET, Mr. Matthieu VERDY, Mr. Simon SOALCA, Mr. Sylvain DUMAS, Dr. Gauthier TANT, Dr. Robert POLSTER, Dr. Alin RATIU and Ms. Jennifer ZAINI. You have been a source of friendships as well as good advice and discussions.

"Distinguishing the signal from the noise requires both scientific knowledge and self-knowledge."

Nate Silver

Contents

List of Figures

Abbreviations

A/D	**A**nalogue to **D**igital
ADS	**A**dvanced **D**esign **S**ystem
BER	**B**it **E**rror **R**atio
CAD	**C**omputer-**A**ided **D**esign
CM	**C**ommon **M**ode
CMRR	**C**ommon **M**ode **R**ejection **R**atio
dA	**d**ifferential **A**mplifier
DC	**D**irect **C**urrent
dLNA	**d**ifferential **L**ow **N**oise **A**mplifer
DM	**D**ifferential **M**ode
dNF	**d**ifferential **N**oise **F**igure
dT	**d**ifferential **T**uner
DUT	**D**evice **U**nder **T**est
ENR	**E**xcess **N**oise **R**atio
FET	**F**ield **E**ffect **T**ransistor
GaAs	**Ga**llium **As**enide
G-R	**G**eneration-**R**ecombination
IEEE	**I**nstitute of **E**lectrical and **E**lectronics **E**ngineers
IF	**I**ntermediate **F**requency
LNA	**L**ow **N**oise **A**mplifier
NF	**N**oise **F**igure
NFA	**N**oise **F**igure **A**nalyzer
PDF	**P**robability **D**ensity **F**unction
RF	**R**adio **F**requency

RMS	**R**oot **M**ean **S**quare
R&S	**R**ohde & **S**chwarz
S-E	**S**ingle-**E**nded
SMA	**S**ub**M**iniature version **A**
SNR	**S**ignal to **N**oise **R**atio
SOLT	**S**hort **O**pen **L**oad **T**hrough
VNA	**V**ector **N**etwork **A**nalyzer

General Introduction

The demand for electronic devices with higher linearity, higher dynamic range and lower noise specifications requires the development of novel architectures of electronic circuits. Components with differential architecture are more and more replacing traditional single-ended circuits in many wireless system applications. The signals in differential circuits are represented by the difference of two voltages rather than a single voltage to ground as in the single-ended circuits. This property offers several important advantages to differential circuits over single-ended ones. They offer a better immunity to common-mode noise and interference. In addition, the phase difference between the outputs of a differential circuit enables the voltage swing to be twice that in single-ended operation. This is particularly interesting for integrated circuits that can only cope with low supply voltages. Moreover, differential circuits have also the ability to reduce even-order distortion.

The wide proliferation of differential circuits in radio-frequency and other high-frequency applications creates an important demand for the development of measurement techniques of these circuits. It is nowadays possible to characterize the small-signal behavior of differential circuits using conventional network analyzers. Performance figures of merits, such as differential gain and common-mode rejection are commonly measured using the mixed-mode scattering parameters.

In contrast, the noise characterization of these circuits remains a challenging subject. Accurate noise measurements are difficult due to the low levels of powers involved. The powers to be measured are often at the femtowatt level or even below. But more particularly, the noise characterization of differential circuits is challenging due to correlated output noises. Indeed, the noises generated at the two output ports of a differential circuit are often correlated and bring some complications when noise performance is measured.

One important figure of merit for noise performance is the noise figure, which describes the amount of excess noise present in a circuit or system. The noise figure of a differential circuit depends on the output noise powers but also on the correlation of the output noises. The issue about differential noise figure concerns mainly the measurement of this correlation. No commercially-available equipment is capable so far to measure directly the correlation of output noises. The correlation is a complex term which depends on the real and imaginary of the output noise waves. Modern equipment are capable of measuring the magnitude of a noise wave but not its real or imaginary part.

In literature, the subject of differential noise figure has been dealt with by bypassing the measurement of the correlation. The classical method for the noise figure measurement of a differential circuit consists of embedding the latter between two hybrid 180° couplers. This technique allows to characterize differentially the circuit without measuring the correlation.

The purpose of this work is to develop advanced methods for the measurement of the noise wave correlation at the output ports of differential circuits. These methods will serve for the development of accurate and functional techniques for the noise figure and noise parameters measurements of differential circuits.

This work is divided into three chapters. In Chapter 1, an expression of differential noise figure is determined in terms of the correlation of the output noise waves. All the basic concepts that are necessary for the determination of the differential noise figure will be discussed. Electronic noise and the conventional techniques for the noise characterization of single-ended circuits are firstly presented. This knowledge is then extended to differential circuits where mixed-mode S-parameters and the four-port noise formalism are described and used to define the noise figure of differential amplifiers.

Chapter 2 presents a technique for determining the correlation of the noise waves at the output ports of a differential amplifier (dA). A non-ideal 180° hybrid coupler is connected to the output ports of the dA according to two different configurations. This two-configuration approach allows a rigorous de-embedding of the correlation by taking into account the amplitude and phase imbalances of the coupler. The calculations for extracting the correlation will be firstly described. This theoretical work is then validated by simulation results of a dA. And, based on the calculations, a general technique will be developed for the noise figure measurement of all sorts of differential amplifiers.

Chapter 3 presents an original technique for measuring the correlation of output noise waves without using any coupler. It is demonstrated that, for a conventional dA, the correlation can be determined in terms of input-referred noise powers and the 4-port S-parameters of the dA. This approach allows fast measurements of the differential noise figure without the need for couplers that require complicated de-embedding procedures. The calculations for determining the correlation will be described and validated by simulations. A fast and functional procedure will then be developed for the noise figure measurement of a differential low noise amplifier (dLNA).

This coupler-free approach will be extended in the second part of Chapter 3 to the measurement of the noise parameters of differential amplifiers. These noise parameters are important figures of merit as they allow the determination of differential noise figure for arbitrary impedances presented to the dA. The approach is based on differential source-pull measurements using a differential impedance tuner. The equations required for extraction of the noise parameters from the source-pull measurements will be described and verified by simulations. An original coupler-free technique is then developed for the noise parameters measurement of a dLNA.

Chapter 1

Differential Noise Figure

1.1 Introduction

This chapter describes the basic concepts necessary for the determination of the noise figure of differential circuits. It serves as a theoretical groundwork for the development of the measurement techniques of Chapters 2 and 3. The first section of Chapter 1 presents the different types of noise in electronic devices. The definition of two-port noise figure is reminded in section 1.3 and the existing techniques (Y-factor and cold source methods) for noise figure measurement of two-port devices are presented in section 1.4. Noise parameters are introduced in section 1.5 and their measurement technique using an impedance tuner is described in section 1.6. The concept of noise waves is then developed in section 1.7 where the noise waves are defined as random variables and represented for two-port circuits. The knowledge of the noise characterization of two-port circuits presented in the first sections is extended in section 1.8 to four-port circuits. The noise figure of differential circuits is then determined using the noise-wave formalism and the mixed-mode scattering parameters.

1.2 Definition of noise in electronics

In common language, noise refers to a loud, unpleasant or disturbing sound. In modern communications, noise is used to designate, not sound itself, but the perturbations that caused undesired sounds to appear at the output of a telephone system, for example. In electronics, noise refers more generally to the spontaneous fluctuations in current, voltage and temperature in a circuit [1]. Before describing the specific types of noise that are present in electronic systems, some common concepts need to be addressed. First, an electronic system has multiple sources of noise, both internal and external. On one side, 'Internal' (or intrinsic) refers to sources that constitute the circuit (resistors, amplifiers, transistors, etc.). On the other side, 'External' refers for example to noise from ignition, sparks or undesired pick-up of spurious signals. It concerns also natural electrical disturbances occurring in the atmosphere or electrical noise emanating from the sun. Such external noise problems are resolved by techniques like relocation, filtering and shielding.

For the purpose of this thesis, only internal noises are considered. There are 4 main types of intrinsic noise sources related to electronic devices: thermal, shot, generation-recombination and flicker noise sources.

1.2.1 Thermal noise

Thermal noise, also referred as Johnson-Nyquist noise, is the most common noise source in electronics and it is present in all conductors. It is generated by the random thermal motion of charge carriers (usually electrons) inside an electrical conductor, as described by J.B. Johnson in 1927 [2]. H. Nyquist established a relation [3] for the mean square voltage $\overline{e_n^2}$ due to the thermal agitation in a conductor of pure resistance R as:

$$\overline{e_n^2} = 4kTR\Delta f \tag{1.1}$$

where k is Boltzmann's constant (1.38 10^{-23} joules/Kelvin). T is absolute temperature in Kelvins. Δf is the bandwidth in Hertz.

In another formulation, the available thermal noise power, P_{av} is given by:

$$P_{av} = kT\Delta f \tag{1.2}$$

Thermal noise is considered as white, meaning that it is spectrally uniform or flat. Said another way, the noise spectral density is constant throughout the frequency spectrum. [1]

1.2.2 Shot noise

Shot noise is caused by the random, quantized nature of current flow [4]. Indeed, current flow is not a continuous flow of electrons, it is rather a discrete flow of electrons with random spacing. This noise current occurs in components such as vacuum Tubes, Schottky-barrier diodes, p-n junctions and bipolar transistors [1]. The mean-square current due to shot noise current, $\overline{i_n^2}$, is given by the Schottky formula [4]:

$$\overline{i_n^2} = 2qI\Delta f \tag{1.3}$$

where q is the charge of an electron and I is the DC current. And like thermal noise, the noise power resulting from shot noise is proportional to the bandwidth.

1.2.3 Generation-recombination noise

Generation-recombination noise, or G-R noise, is caused by the fluctuation of the generation and recombination of carriers in semiconductor [5]. These fluctuations cause the number of free carrier to vary, thereby leading to random variations in conductivity that manifest as noise. The spectral response of G-R noise is almost

[1] At low temperatures or at very high frequencies, for instance in the teraherz bandwidth, the available thermal noise power may not be constant. Quantum correction may cause P_{av} to diminish. Nevertheless, most modern electronic components have a limited frequency bandwidth, for which thermal noise can be considered as 'white'.

uniform up to a frequency determined by the lifetime of the carriers. In most RF circuits, G-R is negligible compared to the other sources of noise.

1.2.4 Flicker noise

Flicker noise is observed in any circuit with DC signals. It appears due to fluctuating configurations of defects in metals, fluctuating occupancies of traps in semiconductors, fluctuating domain structures in magnetic materials, etc [6]. Its spectrum density is inversely proportional to the frequency and it is often called $1/f$ noise. It is commonly neglected at microwave frequencies in linear circuits such as low noise amplifiers.

The typical power spectral density of electronic components has the shape illustrated in Fig. 1.1:

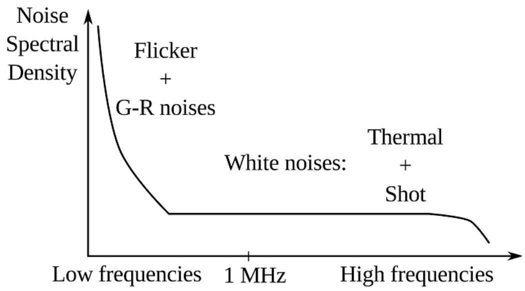

FIGURE 1.1: Schematic of a noise spectral density showing flicker, G-R, shot and thermal noise sources at increasing frequencies

In the next chapters high frequency and linear systems will be dealt with. Consequently, only the white noises will be considered as the contributions of flicker and G-R noises are negligible.

1.3 Noise figure

Electronic systems often have to deal with low-level signals which are difficult to extract in the presence of noise. Parameters such as sensitivity, bit error ratio (BER) and noise figure are used to measure the ability to process low-level signals.

Noise figure (NF) is particularly interesting as it is suitable not only for the characterization of the whole system, but also for the characterization of components that form the system. These components can be pre-amplifiers, mixers, IF amplifiers, etc. By controlling their noise figures, the noise figure of the whole system is controlled. NF is therefore a key parameter that differentiates a component from another and a system from another. The noise figure of an electronic circuit was first defined by H.T.Friis [7] as the degradation of the signal-to noise ratio (SNR):

$$F = \frac{S_i/N_i}{S_o/N_o} = \frac{S_i/N_i}{(GS_i)/(N_A + GN_i)} = \frac{N_A + GN_i}{GN_i} \tag{1.4}$$

where S_i and N_i represent respectively the signal and noise powers available at the input of the circuit, as shown in Fig. 1.2. S_o and N_o represent respectively the signal and noise powers available at the output. The aspects of available signal and noise powers are described in Appendix A. G is the available gain of the circuit. N_A is the circuit intrinsic noise power available at its output.

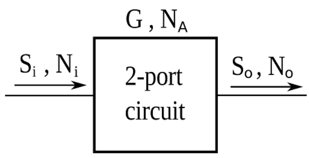

FIGURE 1.2: Represention of a noisy 2-port circuit with input and output signal and noise powers

The degradation of the SNR depends on the temperature of the source impedance. The noise figure is defined for a standard source temperature of 290K.

An equivalent IEEE definition [8] states that the noise figure is the ratio of the total available output noise power per unit bandwidth to the portion of the output noise power that is due to the input noise, evaluated for the case where the input noise power is kT_0 with $T_0 = 290K$. Then, equation (1.4) becomes:

$$F = \frac{N_A + GkT_0\Delta f}{GkT_0\Delta f} = 1 + \frac{N_A}{GkT_0\Delta f} \tag{1.5}$$

which is the definition adopted in the following sections. [2] Equation (1.5) demonstrates that the noise figure depends on two parameters: the available gain G and the intrinsic noise N_A of the circuit. The measurement of the NF requires therefore the measurement of these 2 parameters.

1.4 Noise figure measurement techniques

There are two main techniques for making noise figure measurements of two-port devices. The traditional technique is called the Y-factor or hot/cold method. It is commonly used with a noise figure analyzer or with a signal analyzer. The second technique is called the cold source or direct-noise method and it is performed using network analyzers.

1.4.1 Y-factor method

This technique consists of using a noise source that provides two levels of noise power when it is turned on or off. The noise outputs for these two noise levels provide the required two points that will be used to solve for G and N_A. The noise source consists of an avalanche diode that generates considerable noise when reversed biased [9]. A photograph of a broadband calibrated noise source from Noisecom is shown in Fig. (1.3).

FIGURE 1.3: Noisecom's broadband calibrated noise source

When the source is on (with the biased diode), it has an available noise power of $kT_h\Delta f$. T_h is the hot noise temperature, it can be as high as 10,000 K. When the source is off (without bias), it has an available noise power of $kT_c\Delta f$. T_c is

[2] It is common in literature to call the quantity F 'noise factor' and NF 'noise figure' which represents the noise factor in dB. In this work, the term noise figure is used for both the 'linear terms' and the terms in dB.

the cold noise temperature, it is equal to the ambient temperature, i.e. close to $T_0 = 290K$. The noise source has calibrated output noise levels represented the excess noise ratio (ENR). This ratio is expressed in terms of the hot and cold noise temperatures as:

$$ENR = \frac{T_h - T_c}{T_0} = \frac{T_h}{T_0} - 1 \tag{1.6}$$

The noise source is connected to the device under test (DUT) and the output noise powers are measured with a noise figure analyzer (NFA) or a signal analyzer, as shown in Fig. (1.4).

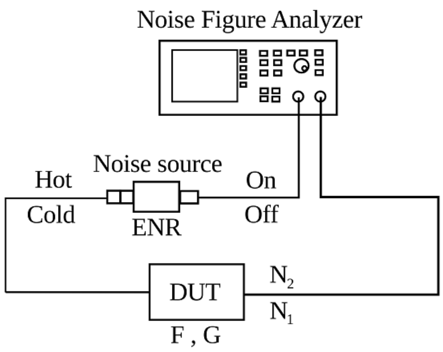

FIGURE 1.4: Setup for the noise figure measurement using the Y-factor method

The measured noise powers correspond to the noise powers delivered to the 50Ω port of the NFA. However, in the definition of the noise figure, available noise powers are required. An available power can be calculated from a delivered power using the output reflection coefficient of the DUT and the input reflection coefficient of the NFA, as explained it will be explained in section 1.4.2. For a DUT and an NFA with matched ports, the available power is equal to the delivered power. Otherwise, the reflection coefficients are measured using a network analyzer as described in 1.4.2 and the available power is determined afterwards.

The noise power available at the output of the DUT when the source is turned off is (assuming $T_c = T_0$):

$$N_1 = GkT_0\Delta f + N_A \tag{1.7}$$

The noise power available at the output of the DUT when the source is turned on is:

$$N_2 = GkT_h\Delta f + N_A \tag{1.8}$$

As output noise power is linearly proportional to source temperature, N_1 and N_2 can be depicted on Fig. (1.5).

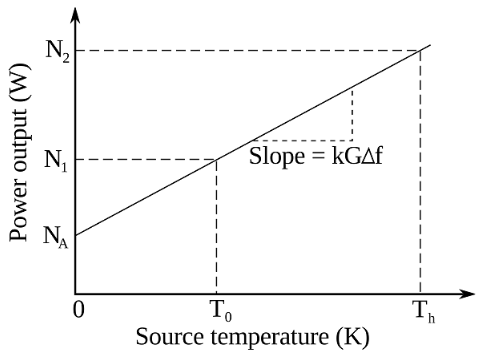

FIGURE 1.5: Output noise powers versus source temperature for a constant bandwidth

And using (1.6) and (1.8), the hot output noise power is given by:

$$N_2 = GkT_0(ENR + 1)\Delta f + N_A \tag{1.9}$$

The ratio of N_2 and N_1 is defined by Y-factor ($Y = N_2/N_1$).

Using (1.7) and (1.8),

$$\begin{aligned} Y &= \frac{GkT_0(ENR\ + 1)\Delta f + N_A}{GkT_0\Delta f + N_A} \\ &= 1 + \frac{GkT_0\ ENR\ \Delta f}{GkT_0\Delta f + N_A} \\ &= 1 + \frac{ENR}{F} \end{aligned} \tag{1.10}$$

The noise figure is then determined from ENR and Y as:

$$F = \frac{ENR}{Y - 1} \tag{1.11}$$

This hot/cold method has the advantage of not requiring absolute power calibrations as the approach is based on the measurement of hot power to cold power ratios. However, the use of a noise source brings some complications. The noise source calibration (for T_h) is challenging and is performed by only a few metrology laboratories. Also, the ENR of noise sources tends to deviate, so calibrations need to be performed quite regularly. Moreover, the reflection coefficient of the noise source changes when it is turned on and off. This could lead to measurement errors, particularly for DUTs with low input return losses [10]. In practice, these mismatch errors are minimized by connecting an attenuator to the output of the noise source.

1.4.2 Cold source method

This direct noise measurement method allows the determination of the noise figure without the use of a calibrated noise source. A simpler and better controlled noise source, generally a 50Ω termination at room temperature (cold source) is used. A source at only one temperature is sufficient for this method as the available gain of the DUT is measured using a Vector Network Analyzer (VNA). The unknown term is the noise generated by the DUT. It can also be measured by the VNA. Fig. 1.6 shows a block diagram of a basic noise measurement setup using a VNA.

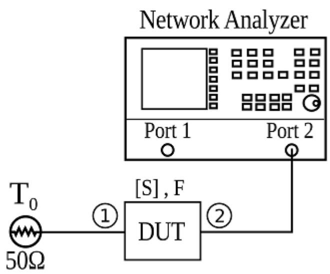

FIGURE 1.6: Setup for the noise figure measurement using the cold source method

The input port of the DUT is connected to a 50Ω termination and the output port is connected to a 50Ω VNA receiver. The measured output noise power consists of the noise contributions of the 50Ω termination, of the DUT and of the VNA receiver. The available noise power N_{sys} at the output of the whole system (cascade of the cold source, DUT and the VNA receiver) is given by:

$$N_{sys} = (N_A + GkT_0\Delta f)G_{rec} + N_{rec} \tag{1.12}$$

where:

- N_A is the available noise power at the output of the DUT due to its intrinsic noise sources. N_A is the unknown term that needs to be extracted from (1.12) for the calculation of the noise figure.

- N_{sys} is the available noise power at the output of the system, as shown in Fig. 1.7. In practice, the noise power measured at the output of the system is the power delivered N_{del} to a 50Ω load. N_{sys} can be expressed in terms of N_{del}, of Γ_{rec} the input reflection coefficient of the receiver and of Γ_{dut} the output reflection coefficient of the DUT as:

$$\begin{aligned} N_{sys} &= \frac{N_{del}|1-\Gamma_{rec}\Gamma_{dut}|^2}{(1-|\Gamma_{dut}|^2)(1-|\Gamma_{rec}|^2)} \\ &= \frac{N_{del}}{1-|\Gamma_{dut}|^2} \text{ as } \Gamma_{rec}=0 \text{ (matched to } 50\Omega) \end{aligned} \tag{1.13}$$

For the practical case where the DUT and the receiver are matched to 50Ω ($\Gamma_{dut} = 0$ and $\Gamma_{rec} = 0$), the available power is equal to the delivered power ($N_{sys} = N_{del}$). For a DUT with low output return loss, an isolator or attenuator can be used to improve output matching.

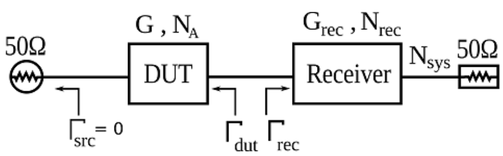

FIGURE 1.7: Block diagram of noise measurement setup

- G is the available gain of the DUT. It is calculated from the S-parameters as:

$$G = \frac{|S_{21}|^2(1-|\Gamma_{src}|^2)}{|1-S_{11}\Gamma_{src}|^2(1-|\Gamma_{dut}|^2)} \tag{1.14}$$

where Γ_{src} is the source reflection coefficient presented to the DUT. In the cold method, a 50Ω termination ($\Gamma_{src} = 0$) is used as source. G simplifies to:

$$G = \frac{|S_{21}|^2}{(1-|\Gamma_{dut}|^2)} \tag{1.15}$$

And for a DUT with its output port matched to 50Ω ($\Gamma_{dut} = 0$), the available gain is equal to the insertion gain, i.e. $G = |S_{21}|^2$.

- G_{rec} is the available gain of the receiver; it is set generally to 1 by making a conventional receiver power calibration. Contrary to the hot/cold method where ratios of noise powers are determined, the cold method requires an absolute noise power measurement. This absolute power measurement is carried out after performing power calibration in the receiver plane using a thermal sensor. A consequence of receiver power calibration is that the receiver is considered to have unity gain. Receiver power calibrations will be discussed in Chapter 2. Another consequence is that the intrinsic noise of the receiver N_{rec} can be determined directly by connecting a 50Ω match to the receiver port and measuring the absolute output power.

In a 50Ω environment, (1.12) simplifies to:

$$N_{del} = (N_A + |S_{21}|^2 kT_0 \Delta f) + N_{rec} \tag{1.16}$$

From (1.16) and (1.4), the noise figure is calculated as:

$$\begin{aligned} F &= 1 + \frac{N_{del} - |S_{21}|^2 kT_0 \Delta f - N_{rec}}{|S_{21}|^2 kT_0 \Delta f} \\ &= \frac{N_{del} - N_{rec}}{|S_{21}|^2 kT_0 \Delta f} \end{aligned} \tag{1.17}$$

The noise figure is thereby obtained from the noise power measured at the output of the DUT and from the latter's gain.

The cold source method has the advantage of not having to deal with the mismatches that a calibrated noise source might bring. It offers also the possibility of performing both S-parameters and noise figure measurements on a DUT with a single set of connections, as described in [11]. The differential noise figure techniques developped in the next chapters will make use of the cold source approach.

1.5 Noise parameters

The previous methods characterize the noise figure at one source impedance, 50Ω in a 50Ω environment. However, the noise figure varies with the source impedance presented to the device. This variation can be expressed in terms of noise parameters which allow noise characterization for arbitrary source impedances/admittances. The relation between noise figure and noise parameters [12] is given by:

$$F = F_{min} + \frac{R_n}{G_s}|Y_s - Y_{opt}|^2 \tag{1.18}$$

where F_{min} is the minimum noise figure obtained when the source admittance Y_s ($Y_s = G_s + jB_s$) is equal to the optimum source admittance Y_{opt} ($Y_{opt} = G_{opt} + jB_{opt}$). And R_n is the equivalent noise resistance which represents how fast the noise figure increases as Y_s deviates from Y_{opt}. There are therefore 4 noise parameters F_{min}, R_n, G_{opt} and B_{opt} that allow a complete noise characterization.

The noise figure may also be calculated using reflection coefficients instead of admittance:

$$F = F_{min} + \frac{4R_n}{Z_0}\frac{|\Gamma_s - \Gamma_{opt}|^2}{|1 + \Gamma_{opt}|^2(1 - |\Gamma_s|^2)} \tag{1.19}$$

where Γ_s is the source reflection coefficient seen by the device. Γ_{opt} is the optimum source reflection coefficient and Z_0 is the characteristic impedance.

The relation between noise figure and the real and imaginary parts of the source reflection coefficient is shown graphically in Fig. (1.8).

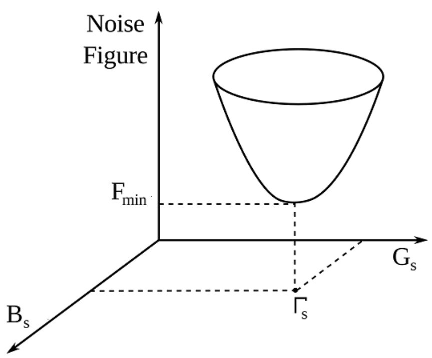

FIGURE 1.8: 3D representation of noise figure vs. source reflection coefficient

1.6 Noise parameters measurement technique

The commonly used technique for measuring noise parameters is based on a multi-impedance approach. In theory, the four parameters are solved by measuring the noise figure of the device for four different sources impedances. In practice, the noise figure measurements are sensitive to experimental errors. More than four source impedances are therefore presented to the device. A least-square algorithm is then used to reduce the over-determined data and to solve for the noise parameters [13]. This classical multi-impedance technique, called source-pull, consists of connecting an impedance tuner to the input port of the DUT as shown in Fig. (1.9).

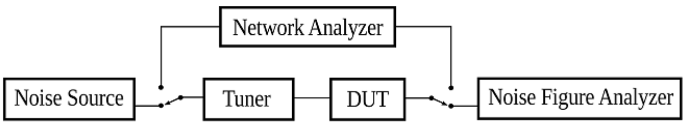

FIGURE 1.9: Block diagram of the setup for the determination of the differential noise parameters from source-pull measurements

For each source impedance presented by the tuner, the noise figure F_{casc} of the cascaded system is measured using the classical hot/cold method. The cascaded system consists of tuner, the DUT and the receiver of the NFA. The noise figure F_{dut} of the DUT is extracted using Friis equation [7]:

$$\begin{aligned} F_{casc} &= F_{tun} + \frac{F_{dut}-1}{G_{tun}^{av}} + \frac{F_{rec}-1}{G_{tun}^{av}G_{dut}^{av}} \\ F_{dut} &= 1 + (F_{casc} - F_{tun})G_{tun}^{av} - \frac{F_{rec}-1}{G_{dut}^{av}} \end{aligned} \tag{1.20}$$

where F_{tun} is the noise figure of the tuner. The tuner used for source-pull measurement consists generally of only passive components (see Chapter 3 for an explanation of the architecture of the passive tuner). Its noise figure is therefore equal to the inverse of the available gain: $F_{tun} = 1/G_{tun}^{av}$ with G_{tun}^{av} being calculated from the scattering parameters of the tuner as:

$$G_{tun}^{av} = \frac{|S_{21}^{tun}|^2(1-|\Gamma_{src}|^2)}{|1-S_{11}^{tun}\Gamma_{src}|^2(1-|\Gamma_{tun}|^2)} \tag{1.21}$$

where Γ_{src} and Γ_{tun} are the output reflection coefficients of the source and of the tuner respectively. These reflection coefficients, as well as the S-parameters, are measured using a conventional network analyzer.

F_{rec} is the noise figure of the receiver of the NFA. It depends on the impedance presented to the NFA. In fact, the NFA sees Γ_{dut} which is the reflection coefficient at the output of the system 'Tuner + DUT'. So, prior to the noise measurements of the DUT, the noise parameters of the receiver must be determined. This is done by connecting the tuner directly to the receiver and performing source-pull measurements.

This receiver characterization can be simplified by placing an isolator between the DUT and the receiver. The isolator is used to improve the matching and therefore to present the same impedance, typically 50Ω to the receiver. This simplicity however comes at a price. An isolator is effective over a limited bandwidth, thus restricting the bandwidth of measurement. For wideband measurements, it is therefore necessary to have a set of isolators with covers the measurement bandwidth.

In Chapter 3, this tuner-based technique will be extended to the measurement of the noise parameters of differential amplifiers.

1.7 Noise waves

In this work, differential noise figure will be defined in terms of noise waves. A noise wave formalism will be preferred to the voltage and current representation. A wave interpretation of noise has advantages for high frequency circuit applications. The strength of the noise wave representation is that simple relations can often be found between a circuit's scattering and noise wave parameters [14]. There exist nowadays accurate methods for the measurement of scattering parameters which contribute to accurate noise analysis. Moreover noise waves are numerically stable. Reflections and resonances are common in high frequency circuits. This may cause huge variations in voltage and current quantities. On the contrary, noise waves quantities have limited range which is useful for example in CAD applications [15]. The noise wave interpretation has served for several applications since its introduction by Penfield [16]. In [17], Bosma used noise waves to solve the Haus and Adler [18] optimum noise performance problem. Hecken [19] has calculated the noise performance of linear networks through signal-flow theory using noise waves. In [15], Kanaglekar et al. used the noise wave representation for the development of CAD programs that compute the noise analysis of multiport networks.

1.7.1 Random variables

Noise waves are continuous-time random variables. A continuous random variable X is characterized by the values that it can take in the interval [a,b], with each interval associated with a probability $P(a \leq X \leq b)$. This probability is related to a function f(x) called the probability density function (PDF) as:

$$P(a \leq X \leq b) = \int_a^b f(x)\, dx \qquad (1.22)$$

This relation suggests that the probability $P(a \leq X \leq b)$ is the area under the density curve between a and b as depicted by Fig. (1.10).

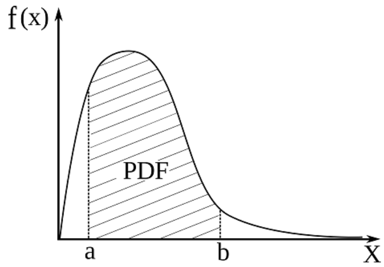

FIGURE 1.10: Representation of an arbitrary probability density function

Probability density functions are characterized by parameters called moments which have interesting practical interpretations. The nth moment of a continuous random variable is given by:

$$\overline{X^n} = \int_{\infty}^{\infty} x^n f(x)\, dx \qquad (1.23)$$

The first-order moment is the mean and is defined as:

$$\overline{X} = \int_{\infty}^{\infty} x f(x)\, dx \tag{1.24}$$

The second-order moment is the 'mean-square' calculated as:

$$\overline{X^2} = \int_{\infty}^{\infty} x^2 f(x)\, dx \tag{1.25}$$

This second-order moment is a measure of the strength of the variable and represents the expected power.

If we consider two random variables X and Y, the 'cross' moment, called correlation is given by:

$$\overline{XY} = \int \int_{\infty}^{\infty} xy f(x,y)\, dx\, dy \tag{1.26}$$

When the two random variables X and Y are uncorrelated or independent, $\overline{XY} = 0$. In this case:

$$\overline{(X+Y)^2} = \overline{X^2 + Y^2 + 2XY} = \overline{X^2} + \overline{Y^2} \tag{1.27}$$

Consequently, for two uncorrelated variables, the quadratic mean of the sum is equal to the sum of the mean-squares. This definition will be particularly useful when dealing with uncorrelated noise waves.

Noise waves are defined as stationary and ergodic random variables [14]. A random variable is stationary if its statistical properties (first and second moment) do not change over time. And a stationary variable is generally ergodic, i.e. the first and second order moments are equal to the first and second order time averages:

$$\overline{X} = \int_{\infty}^{\infty} x f(x)\, dx = \frac{1}{T}\int_{0}^{T} x(t)\, dt =< X > \tag{1.28}$$

$$\overline{X^2} = \int_{\infty}^{\infty} x^2 f(x)\, dx = \frac{1}{T}\int_{0}^{T} x^2(t)\, dt =< X^2 > \tag{1.29}$$

Therefore, for ergodic variables, the second-order moment refers to time-average power. This definition is particularly interesting as the time-average power of noise waves will be used in section 1.8.2 for the determination of the differential noise figure.

1.7.2 Noise wave representation

In the noise wave representation, a circuit's noise is described using waves that emanate from its ports. A linear two-port represented by noise waves and scattering parameters is shown in Fig. (1.11) [14].

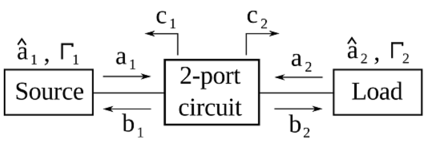

FIGURE 1.11: Noise wave representation of a two-port circuit

The relation between the noise waves and the 2x2 scattering matrix is given by :

$$\begin{pmatrix} b_1 \\ b_2 \end{pmatrix} = \begin{pmatrix} S_{11} & S_{12} \\ S_{21} & S_{22} \end{pmatrix} \begin{pmatrix} a_1 \\ a_2 \end{pmatrix} + \begin{pmatrix} c_1 \\ c_2 \end{pmatrix} \tag{1.30}$$

where a_1 and a_2 are the incident noise waves, b_1 and b_2 are the outgoing noise waves and c_1 and c_2 are the emerging noise waves due to the internal noises of the two-port.

The incident noise waves can be expressed in terms of the generator waves $\hat{a}_1$ and $\hat{a}_2$ and of the terminations' reflection coefficients Γ_1 and Γ_2:

$$\begin{pmatrix} a_1 \\ a_2 \end{pmatrix} = \begin{pmatrix} \hat{a}_1 \\ \hat{a}_2 \end{pmatrix} + \begin{pmatrix} \Gamma_1 & 0 \\ 0 & \Gamma_2 \end{pmatrix} \begin{pmatrix} b_1 \\ b_2 \end{pmatrix} \tag{1.31}$$

The noise waves are time-varying complex random variables characterized by correlation matrices. In particular, the correlation matrix of the outgoing noise waves is given by:

$$\mathbf{B} = \begin{pmatrix} \overline{|b_1|^2} & \overline{b_1 \cdot b_2^*} \\ \overline{b_2 \cdot b_1^*} & \overline{|b_2|^2} \end{pmatrix} \tag{1.32}$$

where the overbar indicates time averaging with assumption of stationary and ergodicity for the noise waves. The diagonal terms of **B**, give the noise powers going out of the two ports. The off-diagonal terms are correlation products of the emerging noise waves.

This noise wave formalism will be extended in 1.8.2 to four-port circuits in order to build an expression for noise figure of differential circuits.

1.8 Differential circuits

There is an increase in the use of differential circuits for high-frequency and microwave applications. Some structures such as many mixers and A/D converters are naturally balanced thus making circuit design somewhat simpler if all devices in the chain are balanced [20]. While this trend has begun in the IF sections, it is propagating up the RF chain and the proper characterization of differential devices is increasingly important. An example of a basic receiver system with differential components is shown in Fig. (1.12).

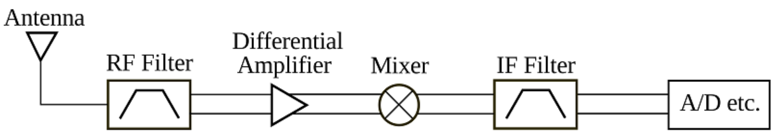

FIGURE 1.12: Receiver architecture with balanced topologies

The advantages of using differential circuits instead of single-ended devices are:

1. They offer a better immunity to common-mode noise and interference. Noise from power supplies and signals that appear as common-mode are rejected by differential circuits.

2. The phase difference between the outputs of a differential circuit enables the voltage swing to be twice that in single-ended (S-E) operation. This is particularly interesting for integrated circuits that can only cope with low supply voltages. Indeed, the same signal swing can be obtained using a lower voltage power supply, with lower dissipation.

3. The even-order harmonic distortion are reduced.

This work will focus on the noise characterization of differential amplifiers. Fig. (1.13) shows the photograph of a differential low noise amplifier that will be used in this work to demonstrate the validity of the proposed measurement techniques. It is an RF amplifier with a differential gain of more than 10 dB and a differential noise figure of around 4 dB in the frequency bandwdith of 100MHz to 500 MHz.

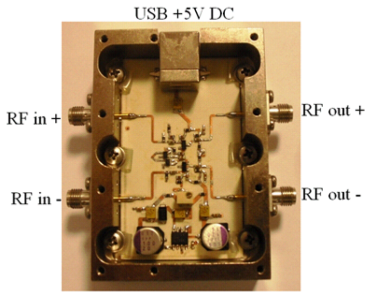

FIGURE 1.13: Photograph of an RF differential amplifier from Rohde&Schwarz

1.8.1 Mixed-mode scattering parameters

Mixed-mode scattering parameters are used to characterize the small-signal behavior of differential circuits. A method for full mixed-mode DUT characterization (including differential and common mode as well as conversion from one mode into the other) has been shown in [21] for the first time. The principle of the mixed-mode approach consists of considering the 2 input ports of the differential circuit as 1 balanced port, similarly for the 2 output ports. At each balanced port, there are both common-mode and differential-mode excitations, as shown in Fig. (1.14).

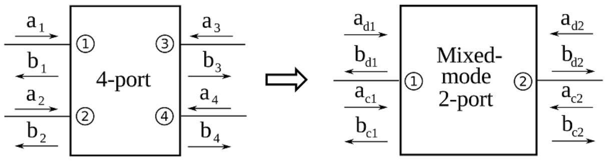

FIGURE 1.14: Mixed-mode representation: $a_{d1(2)}$ and $b_{d1(2)}$ are the differential-mode waves and $a_{c1(2)}$ and $b_{c1(2)}$ are the common-mode noise waves.

The common-mode and differential-mode waves are defined from the standard input and output waves as follows [21]:

$$\text{Differential mode} \begin{cases} a_{d1(2)} = \dfrac{a_{1(3)} - a_{2(4)}}{\sqrt{2}} \\ b_{d1(2)} = \dfrac{b_{1(3)} - b_{2(4)}}{\sqrt{2}} \end{cases} \tag{1.33}$$

$$\text{Common mode} \begin{cases} a_{c1(2)} = \dfrac{a_{1(3)} + a_{2(4)}}{\sqrt{2}} \\ b_{c1(2)} = \dfrac{b_{1(3)} + b_{2(4)}}{\sqrt{2}} \end{cases} \tag{1.34}$$

These equations allow the conversion of the classical S-parameters to the mixed-mode S-parameters as follows:

$$\mathbf{S_{mm}} = \mathbf{M} \cdot \ \mathbf{S_{std}} \cdot \ \mathbf{M}^{-1} \tag{1.35}$$

where $\mathbf{M} = \frac{1}{\sqrt{2}} \begin{bmatrix} 1 & -1 & 0 & 0 \\ 0 & 0 & 1 & -1 \\ 1 & 1 & 0 & 0 \\ 0 & 0 & 1 & 1 \end{bmatrix}$ and $\mathbf{S_{std}}$ is: $\begin{bmatrix} S_{11} & S_{12} & S_{13} & S_{14} \\ S_{21} & S_{22} & S_{23} & S_{24} \\ S_{31} & S_{32} & S_{33} & S_{34} \\ S_{41} & S_{42} & S_{43} & S_{44} \end{bmatrix}$

The 4x4 matrix of mixed-mode S-parameters $\mathbf{S_{mm}}$ consists of four blocks which are actually submatrices, as shown below. $\mathbf{S_{dd}}$ corresponds to the four purely differential S-parameters while $\mathbf{S_{cc}}$ corresponds to the four purely common-mode parameters. The other two quadrants $\mathbf{S_{dc}}$ and $\mathbf{S_{cd}}$ represent the mode-conversion terms.

$$\begin{array}{rl} \text{DM} \ \Big\{ & \\ \text{DM to CM} \ \Big\{ & \end{array} \left[\begin{array}{cc|cc} S_{dd11} & S_{dd12} & S_{dc11} & S_{dc12} \\ S_{dd21} & S_{dd22} & S_{dc21} & S_{dc22} \\ \hline S_{cd11} & S_{cd12} & S_{cc11} & S_{cc12} \\ S_{cd21} & S_{cd22} & S_{cc21} & S_{cc22} \end{array} \right] \begin{array}{ll} \Big\} & \text{CM to DM} \\ \Big\} & \text{CM} \end{array}$$

The differential parameter S_{dd21} and the mode-conversion parameter S_{dc21} will be used in section 1.8.2 for the calculation of the differential noise figure. They are calculated in terms of the classical S-parameters using 1.35 as:

$$\begin{aligned} S_{dd21} &= \frac{1}{2}(S_{31} + S_{42} - S_{32} - S_{41}) \\ S_{dc21} &= \frac{1}{2}(S_{31} - S_{42} + S_{32} - S_{41}) \end{aligned} \tag{1.36}$$

1.8.2 Noise wave formalism for 4-port circuits

The expression of the differential noise figure is determined by using the noise-wave formalism introduced in 1.7.2 and the mixed-mode S-parameters presented in 1.8.1. The two-port noise-wave formalism of 1.7.2 is extended to four-port circuits. Fig. (1.15) shows the noise-wave representation of a 4-port circuit connected to two sources and two loads.

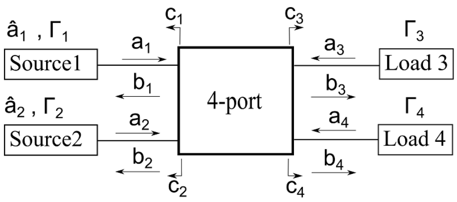

FIGURE 1.15: Noise wave formalism for a 4-port circuit, where a_i is incident noise wave at port i, b_i is the outgoing noise wave and c_i is the internal noise wave. The input ports are connected to 2 sources with generator wave $\hat{a}_i$ and reflection coefficient of Γ_i.

The incident noise wave a_i is defined as the sum of the generator wave from the source $\hat{a}_i$ and the reflected wave coming from the 4-port:

$$a_i = \hat{a}_i + \Gamma_i b_i \tag{1.37}$$

The emerging noise wave b_i is defined as:

$$b_i = \mathbf{S} a_i + c_i \tag{1.38}$$

where S is the 4x4 matrix of standard S-parameters. c_i is the noise wave emerging at the output port i produced by the intrinsic noise sources of the 4-port circuit. Combining (1.37) and (1.38), yields the expression for b_i in terms of the generator waves:

$$\begin{aligned} b_i &= \mathbf{S}[\hat{a}_i + \Gamma_i b_i] + c_i \\ b_i[1 - \mathbf{S}\Gamma_i] &= [\mathbf{S}\hat{a}_i + c_i] \\ b_i &= [1 - \mathbf{S}\Gamma_i]^{-1}[\mathbf{S}\hat{a}_i + c_i] \end{aligned} \tag{1.39}$$

In the following paragraphs, the terminations will be considered to be reflectionless, i.e. $\Gamma_i = 0$. This simplification is of some practical use for clarifying the 4-port noise-figure definition. As it will be explained in the next chapters, measurements are performed using sources and loads that are well matched. These terminations have return losses of at least 20dB in the measurement bandwidths. Consequently the $\Gamma_i = 0$ simplification is accepted.

The noise waves at the output ports of the 4-port connected to reflectionless terminations therefore simplify to:

$$\begin{aligned} b_3 &= S_{31}\,\hat{a}_1 + S_{32}\,\hat{a}_2 + c_3 \\ b_4 &= S_{41}\,\hat{a}_1 + S_{42}\,\hat{a}_2 + c_4 \end{aligned} \tag{1.40}$$

The output return parameters S_{33} and S_{44} and the output cross parameters S_{34} and S_{43} have been neglected. This works deals with the noise definition of differential amplifiers. It is admitted that for these particular types of 4-port circuits, these parameters are negligible compared to the transmission parameters S_{31}, S_{32}, S_{41} and S_{42}.

The output differential-mode noise wave is defined as $b_{d2} = \dfrac{b_3 - b_4}{\sqrt{2}}$ and the input differential and common-mode noise waves are $\hat{a}_{d1} = \dfrac{\hat{a}_1 - \hat{a}_2}{\sqrt{2}}$ and $\hat{a}_{c1} = \dfrac{\hat{a}_1 + \hat{a}_2}{\sqrt{2}}$ respectively. An expression of b_{d2} is calculated in terms of $\hat{a}_{d1}$ and $\hat{a}_{c1}$ using the mixed-mode formalism introduced in section 1.8.1 [22]:

$$b_{d2} = S_{dd21}\,\hat{a}_{d1} + S_{dc21}\,\hat{a}_{c1} + c_{d2} \tag{1.41}$$

where c_{d2} is the output differential-mode noise wave generated by the internal noise sources of the circuit.

The input ports of the circuit are connected to two independent sources having available noise powers of $N^{av}_{1(2)} = \dfrac{\overline{|\hat{a}_{1(2)}|^2}}{1 - |\Gamma_{1(2)}|^2} = kT_0\Delta f$. As the sources are considered as reflectionless ($|\Gamma_{1(2)}|^2 = 0$), the noise powers at the input ports of the circuit are $|\hat{a}_{1(2)}|^2 = kT_0\Delta f$. The differential-mode noise power at the input of the amplifier is therefore given by:

$$\begin{aligned}\overline{|\hat{a}_{d1}|^2} = \overline{\hat{a}_{d1} \cdot \hat{a}_{d1}^*} &= \overline{\left(\frac{\hat{a}_1 - \hat{a}_2}{\sqrt{2}}\right) \cdot \left(\frac{\hat{a}_1^* - \hat{a}_2^*}{\sqrt{2}}\right)} \\ &= \frac{\overline{|\hat{a}_1|^2} + \overline{|\hat{a}_2|^2} - 2\Re e(\overline{\hat{a}_1 \cdot \hat{a}_2^*})}{2}\end{aligned} \tag{1.42}$$

And as the 2 input sources are uncorrelated, $\overline{\hat{a}_1 \cdot \hat{a}_2^*} = 0$. So, (1.42) becomes

$$\overline{|\hat{a}_{d1}|^2} = \frac{\overline{|\hat{a}_1|^2} + \overline{|\hat{a}_2|^2}}{2} = kT_0\Delta f \tag{1.43}$$

Likewise, the common-mode noise power $\overline{|\hat{a}_{c1}|^2}$ at the input of the circuit is equal to $kT_0\Delta f$.

The correlation between $\hat{a}_{d1}$ and $\hat{a}_{c1}$ is null as:

$$\begin{aligned}\overline{\hat{a}_{d1} \cdot \hat{a}_{c1}^*} &= \overline{\left(\frac{\hat{a}_1 - \hat{a}_2}{\sqrt{2}}\right) \cdot \left(\frac{\hat{a}_1^* + \hat{a}_2^*}{\sqrt{2}}\right)} \\ &= \frac{\overline{|\hat{a}_1|^2} - \overline{|\hat{a}_2|^2}}{2} = 0\end{aligned} \tag{1.44}$$

Consequently, as $\hat{a}_{d1}$, $\hat{a}_{c1}$ and c_{d2} are all uncorrelated, the differential-mode noise power at the output of the amplifier can be calculated from (1.41):

$$\overline{|b_{d2}|^2} = (|S_{dd21}|^2 + |S_{dc21}|^2)kT_0\Delta f + \overline{|c_{d2}|^2} \tag{1.45}$$

$\overline{|b_{d2}|^2}$ consists of two elements. The first one is $(|S_{dd21}|^2 + |S_{dc21}|^2)kT_0\Delta f$ which corresponds to the differential output noise power due to the two uncorrelated sources. The second one is $\overline{|c_{d2}|^2}$ which corresponds to the differential output noise power due to the intrinsic noise sources of the circuit.

1.9 Differential noise figure definition

The differential noise figure (dNF) is defined as the ratio of the total differential-mode noise at the output to the portion of the differential-mode noise power that is due to two sources [22] [3]:

$$F_{diff} = \frac{\overline{|b_{d2}|^2}}{kT_0\Delta f \left(|S_{dd21}|^2 + |S_{dc21}|^2\right)} \tag{1.46}$$

This definition of the differential noise figure is an extension of the two-port noise figure definition given in section 1.3. The expression is valid for a differential circuit connected to two independent and reflectionless sources.

The issue of differential noise figure is the difficulty of measuring $\overline{|b_{d2}|^2}$. It can be expressed in terms of the output noise powers $\overline{|b_3|^2}$ and $\overline{|b_4|^2}$ [23]:

$$\overline{|b_{d2}|^2} = \frac{\overline{|b_3|^2} + \overline{|b_4|^2} - 2\Re e(\overline{b_3 \cdot b_4^*})}{2} \tag{1.47}$$

(1.47) is injected in (1.46) to obtain:

$$F_{diff} = \frac{\overline{|b_3|^2} + \overline{|b_4|^2} - 2\Re e(\overline{b_3 \cdot b_4^*})}{2kT_0\Delta f \left(|S_{dd21}|^2 + |S_{dc21}|^2\right)} \tag{1.48}$$

This analytical expression of dNF shows that the measurement of the latter requires the determination of the output noise powers $\overline{|b_3|^2}$ and $\overline{|b_4|^2}$ and the mixed-mode gains S_{dd21} and S_{dc21}. These parameters can be measured using standard equipment such as network analyzers. (1.48) depends also on the term $\overline{b_3 \cdot b_4^*}$ which represents the correlation between the noise waves at the outputs of the differential amplifier. No standard equipment offers direct solutions for the measurement of this noise correlation term.

[3] A similar procedure described in [22] for the determination of the differential noise figure yielded a same expression.

1.9.1 Noise wave correlation

The concept of correlation between the output noise waves is crucial in understanding the difficulties of differential noise figure measurement.

If the two noises waves b_3 and b_4 are fully correlated, they will differ by only a scaling factor ($b_3 = \alpha\ b_4$). Full correlation happens when the noise waves are generated by the same physical sources. However, if b_3 and b_4 are completely uncorrelated (or independent), each wave will be random and unrelated to the other one. For differential amplifiers, the amount of correlation is between these two extremes. The intrinsic noise sources of the DA contribute to both noise waves b_3 and b_4 emerging at the two output ports and as a consequence, are correlated. But these internal sources send noise waves with different magnitude and phase at the two output ports (which tends away from correlation). b_3 and b_4 are therefore partially correlated and related as:

$$b_3 = \alpha\ b_4 + \gamma \tag{1.49}$$

where $\alpha\, b_4$ represents the fully correlated component and γ is the independent one.

Direct measurement of the noise wave correlation is not possible with signal or network analyzers as the magnitude and phase (also real and imaginary part) of noise waves are not measurable. This is the main reason why no electronics company has proposed so far equipment capable of measuring directly the noise figure of differential circuits.

Traditional equipment cannot characterize noise waves but they can easily measure noise powers. Chapters 2 and 3 will deal with two different techniques that allow the determination of the noise wave correlation from measured noise powers at the output ports of differential amplifiers.

1.10 Conclusion

The basic concepts required for the calculation of the differential noise figure have been developed. Electronic noise was firstly presented and the prevalence of white noises at radio-frequencies was discussed. The classical two-port noise figure and noise parameters measurement techniques have been presented. This will serve as groundwork for the development of measurement techniques of differential noise figure and parameters. An expression of the differential noise figure has been derived using the noise-wave formalism and the mixed-mode scattering parameters. It has been demonstrated that the differential noise figure depends on the correlation of the noise waves at the output ports of the differential circuit. Chapters 2 and 3 will provide some solutions to evaluate this correlation in order to measure the noise figure of RF differential amplifiers.

Chapter 2

De-embedding differential noise figure using the correlation of output noise waves

2.1 Introduction

This chapter proposes a technique for noise figure measurement of differential amplifiers (dAs). As explained in Chapter 1, the measurement of the differential noise figure (dNF) is challenging subject due to the difficulty of measuring the correlation of output noise powers. In literature, the subject has been dealt for the first time by connecting the dA to 180° hybrid couplers [24]. This allows single-ended (S-E) measurements with standard 2-port equipment. This technique has some accuracy limitations as major assumptions are made on the properties of couplers, as it will be demonstrated in section 2.1.1. Other techniques based on this 2-coupler method have been developed [25], [26],[27]. In [25], a procedure to de-embed the noise figure of dAs using non-ideal couplers is proposed. This technique is more accurate than the previously cited one as practically no assumptions are made on the couplers. It has however the disadvantage of working only for specific dAs, as it will be explained in section 2.1.2.

In this chapter, a more general technique than [25] is proposed. It is based on the measurement of the correlation of the noise waves at the output ports of the dA [28]. It makes use of a 180° hybrid coupler and takes into account the non-ideal properties of the latter. The calculations and procedure for the extraction of the correlation are explained in section 2.2.1. This theoretical work is validated by simulation results presented in section 2.2.2. The test setup and measurement results are dealt with in section 2.2.3. And concluding remarks are given in section 2.3.

2.1.1 Classical two-coupler technique

The classical technique using 180° hybrid couplers or baluns was first presented by A.Abidi and J.C.Leete [24]. The approach consists of connecting two hybrid couplers at the input and output ports of the differential amplifier. This allows hot/cold measurements [29] in a single-ended (S-E) configuration using a calibrated noise source and a noise figure analyzer, as shown in Fig. 2.1.

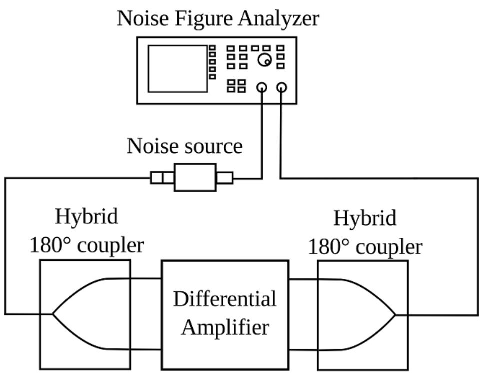

FIGURE 2.1: Measurement setup for hot/cold measurements of cascaded system

The authors use the following definition for the noise figure of the cascaded system [8]:

$$F_{\text{casc}} = \frac{\text{Total noise power at the output}}{\text{Noise power at the output due to the source at } T_0 = 290K} \tag{2.1}$$

where the total noise power at the output port is due to the contributions from the source, from the two couplers, and from the amplifier. Using (2.1) and the expressions of these contributions calculated in [24], the cascade noise figure is given by:

$$F_{casc} = \frac{1}{2}F_1 + \frac{F-1}{2G_1} + \frac{F_2-2}{4AG_1} \tag{2.2}$$

where F is the noise figure of the differential amplifier, A is its differential gain. G_1 is the S-E gain of the input coupler. F_1 and F_2 are the S-E noise figures of the input coupler and output coupler respectively [1]. These S-E characteristics are measured using the Y-factor method [29] with a noise figure analyzer and a noise source as shown in Fig. 2.2.

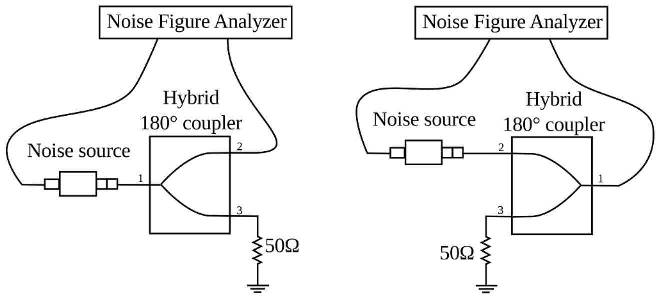

FIGURE 2.2: Single-ended measurements of hybrid couplers

In this approach, the noise figure of the cascaded system is calculated from (2.2) by making the following assumptions:

1. The noise source, couplers and NFA are considered as reflectionless (matched to 50Ω). The noise figures of the couplers and of the amplifier are measured at a 50Ω impedance. The available gains of 2.2 are therefore equal to to the insertion gains.

2. Both paths in each coupler have symmetrical losses.

3. The phase difference between the output ports of each coupler is exactly 180°.

The noise figure of the differential amplifier is de-embedded from the cascaded noise figure using (2.2). This de-embedding method assumes a simplified model of

[1]As the couplers are passive components, the noise figures should be equal to the losses. But due to measurement inaccuracies, the measured noise figures differ slightly from the losses. This explains why the authors considered both the noise figures and the losses of the couplers separately.

the coupler, with symmetrical losses and ideal 180° phase difference between the output ports. With this simplified coupler model, only differential-mode signals are propagated so the effect of common-mode signals is not taken into account. In practice, the hybrid couplers have non-ideal characteristics. The couplers have non-symmetrical losses and the phase difference between their output ports differs from 180°. The simplifications made in this technique yield significant measurement errors as demonstrated in [25].

2.1.2 De-embedding technique using non-ideal couplers

In [25], a general model of the hybrid couplers is considered. Arbitrary losses and phase/amplitude imbalances are defined for the 2 branches of the couplers. The main improvement with this analysis is that it considers the presence of both differential and common-mode signals due to the imbalances in the couplers, and therefore, provides a more accurate measurement. The approach is valid for two types of differential amplifiers: balanced and fully differential. The two different topologies are illustrated in Fig. 2.3.

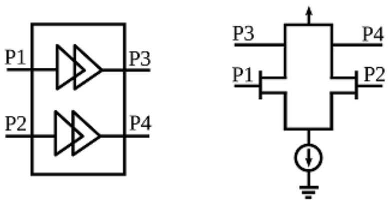

FIGURE 2.3: Simplified schematic diagrams of a balanced amplifier (left) and fully-differential amplifier (right)

As schematized in Fig. 2.3, a balanced amplifier consists of two independent single-ended amplifiers. It equally amplifies both differential- and common-mode signals, which means $CMRR = 1$ (common-mode rejection ratio).

A fully differential amplifier consists of two amplifying devices with a common bias current source. It only amplifies differential signals since common-mode excitations are rejected by the structure (i.e., $CMRR = \infty$).

For both topologies, the measurement setup consists of emdedding the dA between two hybrid couplers. The noise figure of the dA is de-embedded using two different equations for the two topologies. These detailed explanations of the equations are presented in [25].

For the balanced amplifiers, the cascaded noise figure is given by:

$$F_{casc} = \frac{F(|S_{31}^{A}S_{12}^{B2}|^2 + |S_{42}^{A}S_{13}^{B2}|^2) + 1 - (|S_{12}^{B2}|^2 + |S_{13}^{B2}|^2)}{|S_{21}^{B1}S_{31}^{A}S_{12}^{B2} + S_{31}^{B1}S_{42}^{A}S_{13}^{B2}|^2} \tag{2.3}$$

For fully differential amplifiers,

$$F_{casc} = \frac{F(|S_{31}^{A}S_{12}^{B2} + S_{41}^{A}S_{13}^{B2}|^2 + |S_{32}^{A}S_{12}^{B2} + S_{42}^{A}S_{13}^{B2}|^2) + 1 - 0.5|S_{12}^{B2} - S_{13}^{B2}|^2}{|(S_{21}^{B1}S_{31}^{A} + S_{31}^{B1}S_{32}^{A})S_{12}^{B2}|^2 + (S_{21}^{B1}S_{41}^{A} + S_{31}^{B1}S_{42}^{A})S_{13}^{B2}|^2} \tag{2.4}$$

where S_{31}^{A}, S_{32}^{A}, S_{41}^{A} and S_{42}^{A} are the S-parameters of the amplifier, S_{21}^{B1} and S_{31}^{B1} are the S-parameters of the input coupler and S_{12}^{B2} and S_{13}^{B2} are the S-parameters of the output coupler.

These 2 equations demonstrate that the de-embedding of the noise figure of the amplifier depends on the S-parameters of the couplers. And characterizing the couplers by their S-parameters takes into account their phase/amplitude imbalances.

The characterization of the couplers are performed using a conventional 2-port network analyzer. Fig. 2.4 shows the connection diagram for the measurement of the single-ended gains S_{21}^{B1} and S_{12}^{B2}. Measurements are performed similarly for S_{31}^{B1} and S_{13}^{B2}.

This de-embedding technique is more time-consuming than method [24] but it presents more precise results as no assumptions are made on the properties of the couplers. However, it is valid for only two types of differential amplifiers, balanced and fully-differential. It is no more appropriate for general models of differential amplifiers having for e.g. arbitrary CMRR.

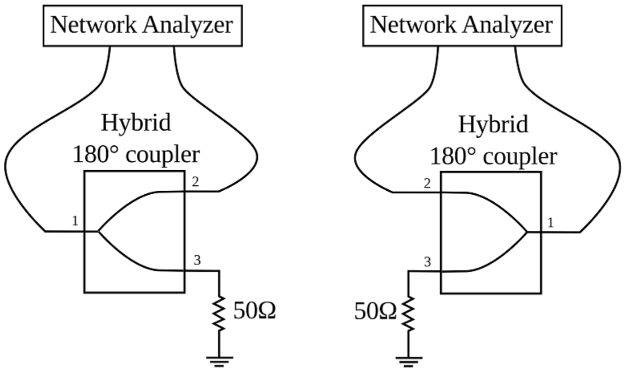

FIGURE 2.4: S-parameters measurements of hybrid couplers using a network analyzer

2.2 General technique

A more general approach [28] than the previous techniques is proposed in this chapter. It is based on the measurement of the correlation of the noise waves at the output ports of a differential amplifier (dA). It makes use of a 180° hybrid coupler connected to the dA according to two different configurations. The non-ideal properties of the coupler, such as amplitude and phase imbalances are considered in a rigorous manner. The calculations and procedure for the extraction of the correlation using the two configurations are explained in section 2.2.1. This theoretical work is validated by simulation results of a dA, presented in section 2.2.2. A differential noise figure measurement technique using a 4-port network analyzer is then developed. The test setup and measurement results are dealt with in section 2.2.3.

2.2.1 Theory

This section presents the calculations that are necessary for understanding the new method for differential noise figure measurement. This new approach consists of connecting the dA to a non-ideal coupler according to two configurations. These two configurations are described in sections 2.2.1.1 and 2.2.1.4. The main objective of the calculations is to extract the correlation of the noise waves at the output ports of the dA. This extraction is performed using the noise-wave formalism described in Chapter 1 and it is developed in the following sections.

2.2.1.1 Configuration 1

The technique consists of firstly connecting a 180° hybrid coupler to the output ports of the differential amplifier, as shown in Fig. 2.5. The noise wave at the output port of a non-ideal 180° hybrid coupler connected to a differential amplifier is given by:

$$b_{out} = S^c_{31}\, b_3 + S^c_{32}\, b_4 + c^c_3 \tag{2.5}$$

where S^c_{31} and S^c_{41} represent the singled-ended scattering parameters of the coupler. b_3 and b_4 are the noise waves at the outputs of the differential amplifier. c^c_3 is the noise wave generated by the hybrid coupler at its output port. It must be noted that this equation is valid for a system of reflectionless components. In our study, the components are assumed to have high input and output return losses and are therefore considered to be reflectionless. The more general case for components having low return losses is left for future work.

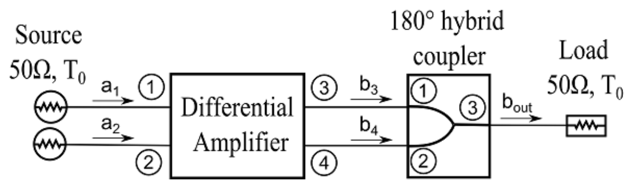

FIGURE 2.5: Configuration 1: The output ports 3 and 4 of the amplifier are connected respectively to the input ports 1 and 2 of the coupler

The output noise power of the cascaded system is calculated from (2.5) by:

$$\begin{aligned}\overline{|b_{out}|^2} &= \overline{b_{out} \cdot b^*_{out}} \\ &= \overline{(S^c_{31}\, b_3 + S^c_{32}\, b_4 + c^c_3) \cdot (S^{c*}_{31}\, b^*_3 + S^{c*}_{32}\, b^*_4 + c^{c*}_3)}\end{aligned} \tag{2.6}$$

As the noises emerging at the output ports of the dA are independent of the intrinsic noises of the coupler, $\overline{b_3 \cdot c^{c*}_3} = 0$ and $\overline{b_4 \cdot c^{c*}_3} = 0$. So, (2.5) becomes:

$$\begin{aligned}
\overline{|b_{out}|^2} &= |S^c_{31}|^2\overline{|b_3|^2} + |S^c_{32}|^2\overline{|b_4|^2} + \overline{|c^c_3|^2} + S^c_{31}\cdot S^{c*}_{32}\,\overline{b_3\cdot b^*_4} + S^{c*}_{31}\cdot S^c_{32}\,\overline{b^*_3\cdot b_4} \\
&= |S^c_{31}|^2\overline{|b_3|^2} + |S^c_{32}|^2\overline{|b_4|^2} + \overline{|c^c_3|^2} + 2\Re e\left(S^c_{31}\cdot S^{c*}_{32}\,\overline{b_3\cdot b^*_4}\right) \qquad (2.7)
\end{aligned}$$

where $\overline{|c^c_3|^2}$ is the noise power generated by the coupler at its output port 3. This intrinsic noise of the coupler can be calculated from its S-parameters as stated by Bosma's theorem [17].

2.2.1.2 Intrinsic noise of the hybrid coupler

Bosma's theorem states that the noise wave correlation matrix of a passive multiport can be derived directly from the scattering matrix as follows [2] :

$$C_s = kT(I - SS^\dagger) \qquad (2.8)$$

where k is Boltzmann's constant and T is the physical temperature in kelvin. Here, I is the unit matrix, S is the scattering matrix of the n-port, and $S^\dagger$ is the transposed complex conjugate of S. This relation is obtained using the second law of thermodynamics by assuming that lossy passive multiports introduce only thermal noise. The demonstration is made by Bosma in [17].

This theorem makes the computation of the noise correlation matrix for a passive multiport easier than for an active multiport. The diagonal elements of the C_s matrix give the noise power generated by the multiport at its different ports.

[2] The noise wave correlation matrix is valid if the passive multiport is matched to reflectionless loads. In our study, the components have high input and output losses, they are assumed to be reflectionless.

In the case of the hybrid coupler which is a passive 3-port [3], the noise generated at its output port 3 is given by:

$$\overline{|c_3^c|^2} = kT_0\Delta f(1 - (|S_{31}^c|^2 + |S_{32}^c|^2 + |S_{33}^c|^2)) \tag{2.9}$$

As the coupler is considered to have a high output return loss, $|S_{33}^c|^2$ is negligible compared to the transmission parameters. $\overline{|c_3^c|^2}$ is therefore given by:

$$\overline{|c_3^c|^2} = kT_0\Delta f(1 - |S_{31}^c|^2 - |S_{32}^c|^2) \tag{2.10}$$

2.2.1.3 Extraction of the correlation term

The correlation of the output noise waves is determined using the noise powers determined in the sections 2.2.1.1 and 2.2.1.3. The correlation is extracted as follows:

Let $\alpha = 2\Re e\left(S_{31}^c \cdot S_{32}^{c*}\,\overline{b_3 \cdot b_4^*}\right)$, α is calculated from (2.6) and (2.10) as:

$$\alpha = \overline{|b_{out}|^2} - |S_{31}^c|^2\overline{|b_3|^2} - |S_{32}^c|^2\overline{|b_4|^2} - \left(1 - |S_{31}^c|^2 - |S_{32}^c|^2\right) kT_0\Delta f \tag{2.11}$$

It depends on the scattering parameters of the hybrid coupler and on the output noise powers $\overline{|b_3|^2}$, $\overline{|b_4|^2}$ and $\overline{|b_{out}|^2}$ which can all be measured with a network analyzer. α can be expressed in terms of the correlation term as follows [4]:

$$2\Re e\left(S_{31}^c \cdot S_{32}^{c*}\,\overline{b_3 \cdot b_4^*}\right) = 2\Re e(S_{31}^c \cdot S_{32}^{c*})\Re e(\overline{b_3 \cdot b_4^*}) - 2\Im m(S_{31}^c \cdot S_{32}^{c*})\Im m(\overline{b_3 \cdot b_4^*}) \tag{2.12}$$

(2.12) shows that α depends on both the real part $\Re e(\overline{b_3 \cdot b_4^*})$ and the imaginary part $\Im m(\overline{b_3 \cdot b_4^*})$ of the correlation term. As the real and imaginary parts are 2 unknown terms, another equation is necessary to solve for the real part of the

[3]A hybrid coupler is usually a 4-port circuit (0, 180, Δ and $\sum$ ports). In this work, the $\sum$ port is not used, it is terminated with a 50Ω match. The coupler is therefore considered as a 3-port circuit. Moreover, the Δ and $\sum$ ports are well isolated, so the noise contributions of the $\sum$ port can be neglected.

[4]This calculation is detailed in Appendix B

correlation (only $\Re e(\overline{b_3 \cdot b_4^*})$ is required to determine the dNF). This equation is found using configuration 2.

2.2.1.4 Configuration 2

In configuration 2, the output ports 3 and 4 of the amplifier are connected respectively to the input ports 2 and 1 of the coupler, as shown in Fig. 2.6.

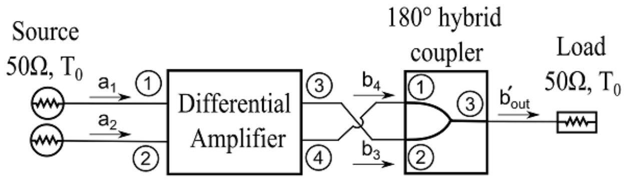

FIGURE 2.6: Configuration 2: The output ports 3 and 4 of the amplifier are connected respectively to the input ports 1 and 2 of the coupler

The noise wave at the output of the cascaded system is given by:

$$b'_{out} = S^c_{31}\, b_4 + S^c_{32}\, b_3 + c^c_3 \tag{2.13}$$

The output noise power is given by:

$$\overline{|b'_{out}|^2} = |S^c_{31}|^2\overline{|b_4|^2} + |S^c_{32}|^2\overline{|b_3|^2} + 2\Re e\left(S^c_{32} \cdot S^{c*}_{31}\,\overline{b_3 \cdot b_4^*}\right) + \overline{|c^c_3|^2} \tag{2.14}$$

Let $\alpha' = 2\Re e\left(S^c_{32} \cdot S^{c*}_{31}\,\overline{b_3 \cdot b_4^*}\right)$, α' is calculated from (2.14) and (2.10):

$$\alpha' = \overline{|b'_{out}|^2} - |S^c_{31}|^2\overline{|b_4|^2} - |S^c_{32}|^2\overline{|b_3|^2} - \left(1 - |S^c_{31}|^2 - |S^c_{32}|^2\right) kT_0\Delta f \tag{2.15}$$

α' depends on the the noise powers and scattering parameters which can be easily measured using commercially-available network analyzers. α' can be expressed in terms of the correlation term as [5]:

$$2\Re e\left(S^c_{32} \cdot S^{c*}_{31}\,\overline{b_3 \cdot b_4^*}\right) = 2\Re e(S^c_{32} \cdot S^{c*}_{31})\Re e(\overline{b_3 \cdot b_4^*}) - 2\Im m(S^c_{32} \cdot S^{c*}_{31})\Im m(\overline{b_3 \cdot b_4^*})$$
$$= 2\Re e(S^c_{31} \cdot S^{c*}_{32})\Re e(\overline{b_3 \cdot b_4^*}) + 2\Im m(S^c_{31} \cdot S^{c*}_{32})\Im m(\overline{b_3 \cdot b_4^*}) \quad (2.16)$$

2.2.1.5 Determination of the real part of the correlation

The real part of the correlation is determined from (2.12) and (2.16) as follows:

$$\begin{aligned}
\alpha &= 2\Re e(S^c_{31} \cdot S^{c*}_{32})\Re e(\overline{b_3 \cdot b_4^*}) - 2\Im m(S^c_{31} \cdot S^{c*}_{32})\Im m(\overline{b_3 \cdot b_4^*})\\
\alpha' &= 2\Re e(S^c_{31} \cdot S^{c*}_{32})\Re e(\overline{b_3 \cdot b_4^*}) + 2\Im m(S^c_{31} \cdot S^{c*}_{32})\Im m(\overline{b_3 \cdot b_4^*})\\
\alpha + \alpha' &= 4\Re e(S^c_{31} \cdot S^{c*}_{32})\Re e(\overline{b_3 \cdot b_4^*})\\
\implies \Re e(\overline{b_3 \cdot b_4^*}) &= \frac{\alpha + \alpha'}{4\Re e(S^c_{31} \cdot S^{c*}_{32})}
\end{aligned} \quad (2.17)$$

An expression of the correlation of the noise waves at the output ports of a dA is obtained. It depends on the following elements:

- The S-parameters of the hybrid coupler
- The noise powers at the output ports of the dA
- The output noise powers for configurations 1 and 2

As explained in Chapter 1, the correlation is then injected in (1.48) for the determination of the differential noise figure.

The equations and this novel procedure for the measurement of dNF have been successfully verified by circuit simulations in Keysight's Advanced Design System (ADS).

[5]See Appendix B for the detailed calculations

2.2.2 Validation by simulation

A C-band differential amplifier, shown in Fig. 2.7 is designed and simulated in ADS.

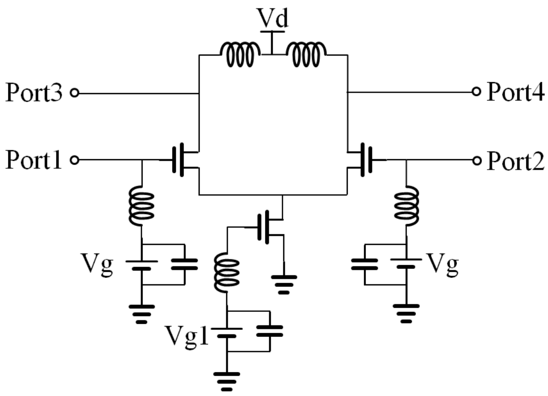

FIGURE 2.7: Simplified schematic diagram of differential amplifier made of GaAs field-effect transistors (FETs)

The dA has a differential gain of least 10 dB and a common-mode gain of -10 to -3 dB on its specified frequency bandwidth (6 to 8 GHz), as shown in Fig. 2.8. A low common-mode rejection is chosen to demonstrate that the procedure is valid for arbitrary CMRR.

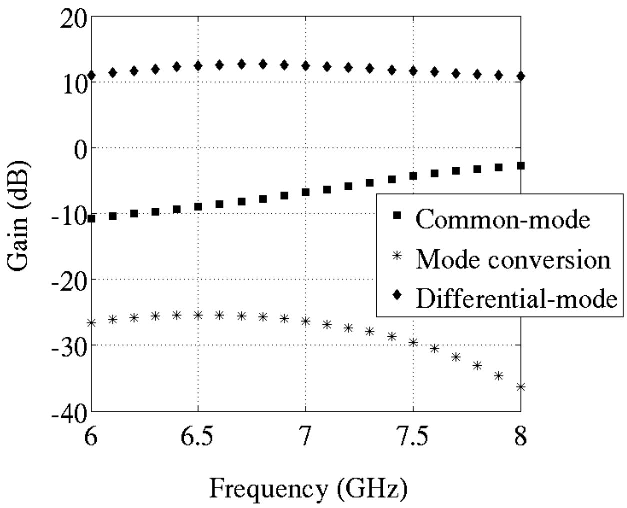

FIGURE 2.8: Mixed-mode gains required for the calculation of the differential noise figure

The input and output ports of the dA are connected to 50Ω terminations. The output noise powers are measured within 1 MHz bandwidth and are shown in Fig. 2.9.

The dA is then connected to a non-ideal hybrid coupler as in Configuration 1. A hybrid coupler with a constant gain imbalance of 1 dB and a constant phase imbalance of 10° is chosen. The noise power measured at the output port of the cascaded system is shown in Fig. 2.9. The last step consists of connecting the dA and the coupler according to Configuration 2. The output noise power of Config.2 cascaded system is also shown in Fig. 2.9.

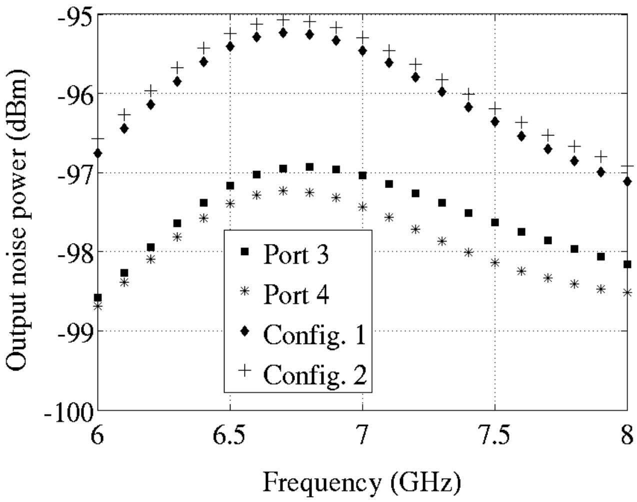

FIGURE 2.9: Noise powers at the output ports of the dA and at the output of the cascaded system of configurations 1 & 2.

The real part of the correlation of output noise waves is calculated using simulation data and equations given in the previous sections. It is illustrated in Fig. 2.10.

This real part of the correlation is then injected in (1.48) for the calculation of the differential noise figure (dNF). For verification issues, the dNF is compared to the one obtained when the dA is placed between two ideal couplers. In this case, the couplers have neither amplitude nor phase imbalance. In such configuration, the dNF of the dA is obtained directly by measuring the single-ended NF of the cascaded system. The dNF measured with both methods are shown in Fig. 2.11.

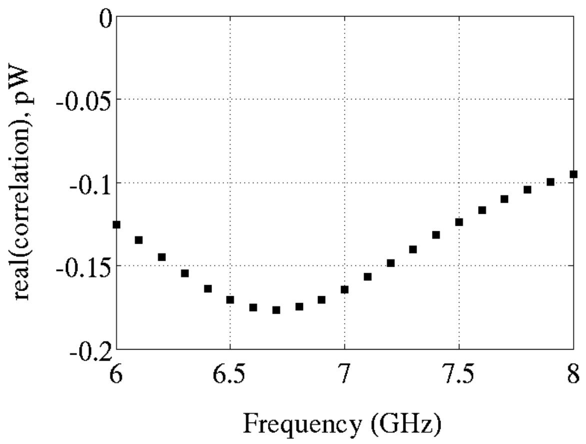

FIGURE 2.10: Real part of the correlation of output noise waves

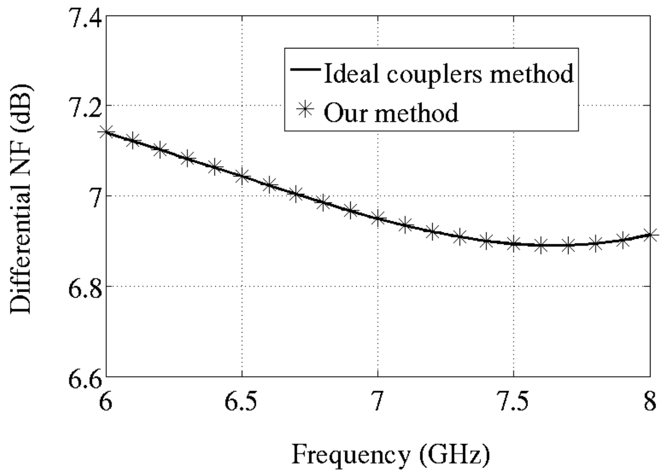

FIGURE 2.11: Comparison between the dNF obtained with our procedure and with the ideal couplers method

Fig. 2.11 shows that there is a complete agreement between the two dNF. This means that the equations given in the previous sections are correct. It also validates our dNF de-embedding procedure where the phase and amplitude imbalances of the hybrid coupler are taken into account.

2.2.3 Measurement setup and experimental results

The measurement procedure is developed for the noise figure measurement of a differential amplifier. The dNF is obtained after the measurement of the following elements:

- The mixed-mode gains of the dA

- The 3-port S-parameters of the hybrid coupler
- The noise powers at the 2 output ports of the differential amplifier
- The output noise power of the cascaded system for configuration 1
- The output noise power of the cascaded system for configuration 2

All these elements are measured using a R&S ZVA24 4-port Network analyzer [30], Fig. 2.12. The following sections describe the procedure for the measurement of these parameters.

FIGURE 2.12: R&S ZVA24 four-port vector network analyzer

2.2.3.1 Scattering parameters measurement

The first step of the measurement procedure consists of measuring the S-parameters of the differential amplifier and of the hybrid coupler. An UOSM (Unknown through - Open - Short - Match) calibration is performed on all four analyzer ports. The calibration is carried out using a R&S ZV-Z52 calibration unit [31], Fig. 2.13. An automatic calibration is preferred to a manual calibration as it is faster and more secured:

- There is no need to connect several standards manually. In our case, a 4-port manual calibration can be very long.
- Invalid calibration due to operator errors (e.g wrong standards or improper connections) are almost excluded.

FIGURE 2.13: R&S ZV-Z52 calibration unit

Differential amplifier

This automatic calibration is applied firstly to the S-parameters measurement of a radio-frequency R&S differential low noise amplifier (dLNA). The input and output ports of the amplifier are interfaced with 50Ω SMA connectors, as shown in Fig. 2.14, which allow measurements with standard 50Ω equipment. The circuit is made of discrete elements, namely NPN transistors from NXP semiconductors.

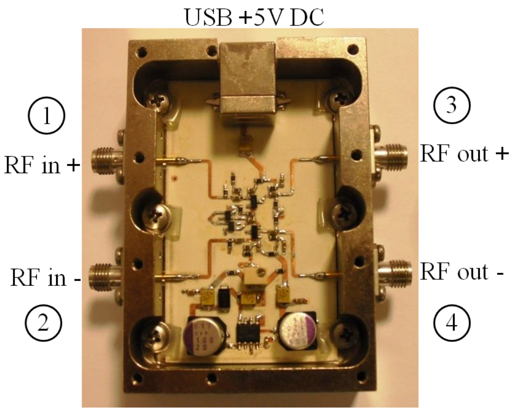

FIGURE 2.14: Rohde&Schwarz RF differential amplifier with SMA connectors

Measurements of the amplifier are performed in the 100MHz to 500MHz frequency range.

Using the mixed-mode S-parameters, the following characteristics are measured:

- The dLNA has a differential gain of at least 10 dB.
- The conversion gain between common-mode and differential mode is around -10 dB.

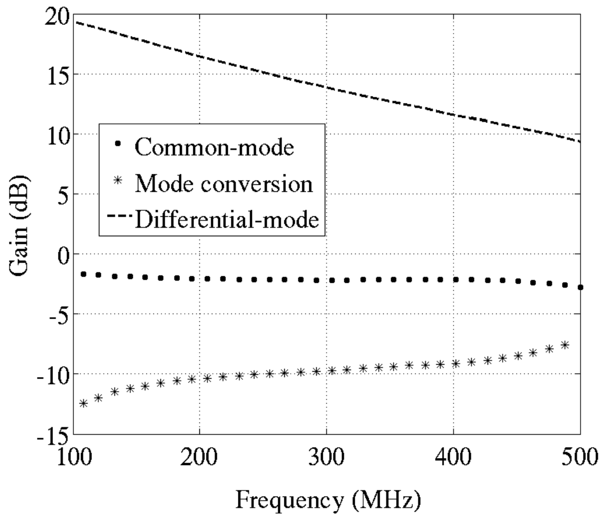

FIGURE 2.15: Mixed-mode gains of R&S RF differential amplifier

- The dLNA has a common-mode rejection of at most 3 dB. The circuit has a variable common-mode rejection. A poor common-rejection is chosen in order to demonstrate that the technique works for arbitrary CMRR.

The amplifier has differential 100Ω input and output impedances. The input and output return losses are of at least 15 dB, as shown in Fig. 2.16. This allows us to assume that the dA has reflectionless input and output ports.

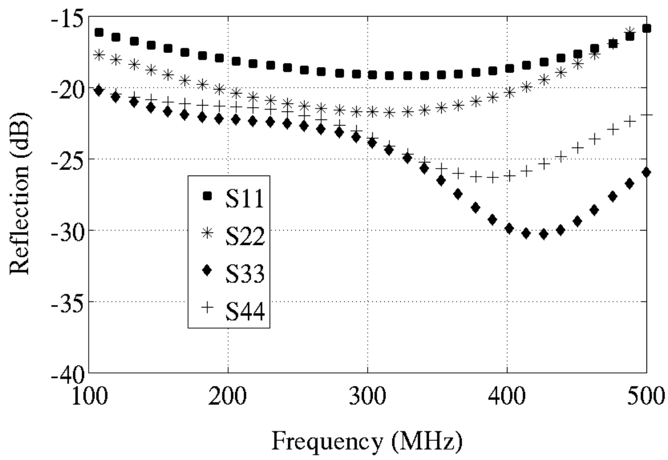

FIGURE 2.16: Reflection coefficients of the input and output ports of the dA

Hybrid coupler

The next step consists of measuring the S-parameters of the hybrid coupler that is used in configuration 1 and 2. An UMCC 180°/3 dB hybrid coupler is used. A diagram of the coupler is shown in Fig. 2.17 [6]. Its insertion losses, gain and

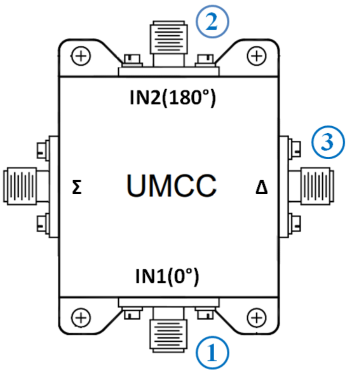

FIGURE 2.17: UMCC 0°/180° hybrid coupler

phase imbalances are characterized in the frequency range of 100MHz to 500MHz using the ZVA24 Network analyzer. These characteristics are shown in Fig. 2.18. An amplitude imbalance of around 0.4 dB and a phase imbalance of maximum 5°

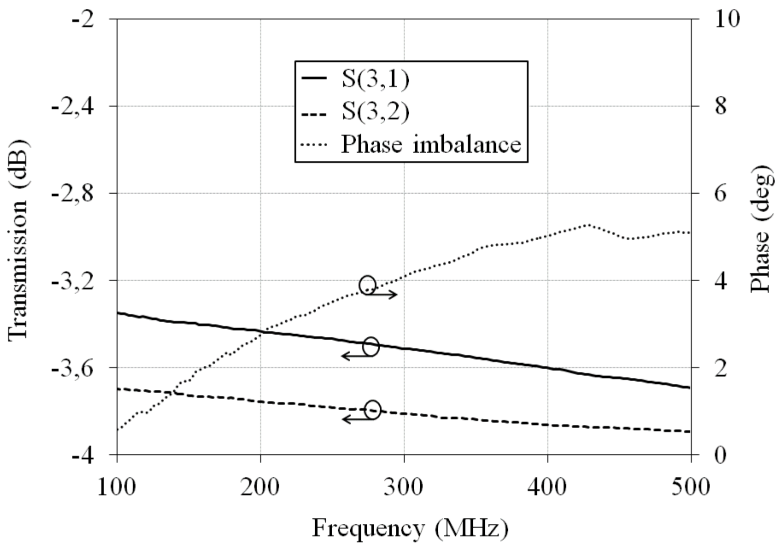

FIGURE 2.18: Transmission parameters and phase imbalance of the coupler

are observed. It should be noticed that the phase imbalance is computed as the difference with respect to the ideal 180° phase difference. These imbalances show

[6]The sum port of the coupler is not used. It is terminated with a 50Ω termination

that the coupler cannot be considered as symmetrical as assumed in [24]. The input and output return losses and the isolation are of at least 15 dB, as shown in Fig. 2.19. The return losses are sufficiently high to assume that the ports of the coupler are reflectionless.

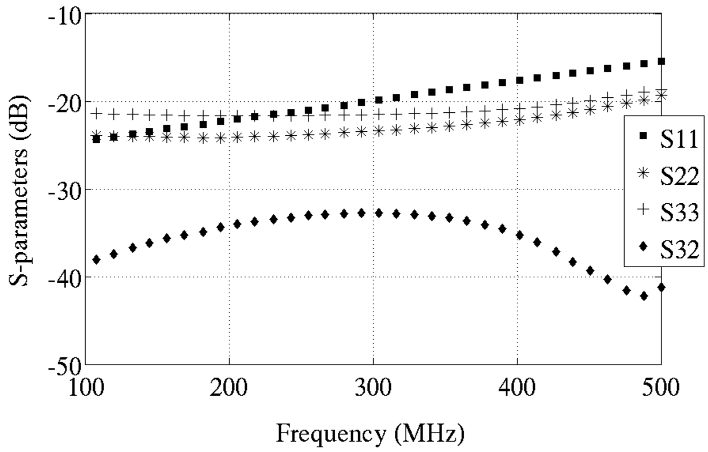

FIGURE 2.19: Return losses and isolation of the hybrid coupler

2.2.3.2 Noise power measurement

The next step of the procedure deals with the measurement of the noise powers at the output ports of the dLNA. The noise measurements are also done using the R&S ZVA24 network analyzer. The principle consists of connecting two 50Ω sources at the two input ports of the differential amplifier and measuring the output noise powers using 2 VNA receivers. Prior to the noise measurements, the receivers need to be characterized.

Receiver

In the simplest case the output ports of the differential amplifier are connected to two ports of the analyzer without any further components. Although this is the easiest setup, it does not guarantee accurate noise power measurements. Indeed the receivers of the analyzer have a noise figure of around 42 dB in the frequency range of 100MHz to 500MHz [11]. During measurements, these noisy receivers would tend to mask the noise generated by the dLNA. A high noise figure receiver is often the main contributor to uncertainties in noise power measurements [32]. It is therefore necessary to reduce the noise figure of the receivers in order to provide accurate noise power measurements [7]. This can be done by using the direct receiver connections of the ZVA24 analyzer.

Direct receiver access

The measurement ports of the ZVA24 analyzer is equipped with direct receiver access connections as shown in Fig. 2.20.

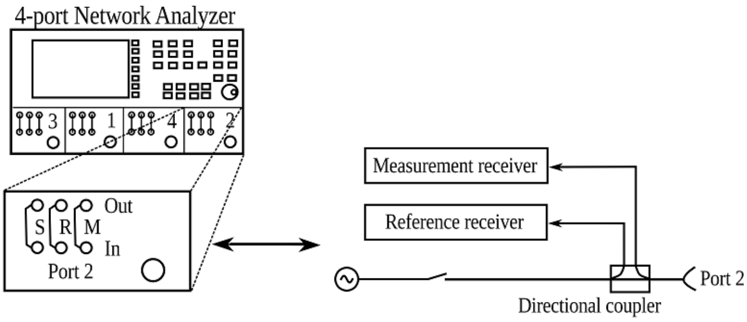

FIGURE 2.20: Basic scheme of ZVA24 analyzer test port. The direct receiver connectors are abbreviated as : S: Source path, R: Reference path and M: Meas path.

The sensitivity of the receiving ports can be increased by connecting directly the output ports of the dLNA to the 'Meas in' direct receiver access connectors. Indeed, this direct access allows to by-pass the directional coupler found in the test ports of the analyzer. The noise figure of each receiver are reduced by about 12 dB which corresponds to the coupling loss of the directional coupler.

Consequently, the receivers have a lower noise figure of about 30 dB. This is however not sufficient to guarantee accurate noise measurement. The receiver noise figure can be further reduced by connecting a pre-amplifier to the direct receiver access.

[7]The noise power related to the DUT should be higher than the Minimum Detectable Signal

Pre-amplifiers

Two low noise amplifiers (LNAs) from KUHNE electronic [33], Fig. 2.21, are used as pre-amplifiers. They have around 25 dB gain and 4 dB noise figure between 100MHz and 500MHz. One pre-amplifier is connected to each receiver access, as shown in Fig. 2.22.

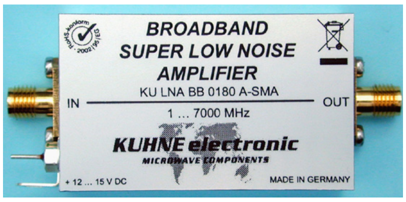

FIGURE 2.21: Low noise pre-amplifier from Kuhne Electronic

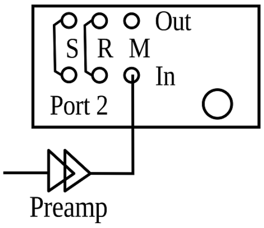

FIGURE 2.22: Connection diagram for the pre-amplifier and the direct access

The noise figure F_{rec}^{vna} of the receiver is thereby reduced by about the gain G_{preamp} of the pre-amplifier according to Friis equation:

$$F_{rec}^{sys} = F_{preamp} + \frac{F_{rec}^{vna} - 1}{G_{preamp}} \tag{2.18}$$

As F_{rec}^{vna} is much bigger than 1 and F_{preamp} is small,

$$\begin{aligned} F_{rec}^{sys} &\approx \frac{F_{rec}^{vna}}{G_{preamp}} \\ F_{rec}^{sys}(dB) &\approx F_{rec}^{vna}(dB) - G_{preamp}(dB) \end{aligned} \tag{2.19}$$

Consequently, the receivers have a noise figure of about 5 dB which allows noise measurements with sufficiently low uncertainties.

Receiver calibration

Before noise power measurements can be done, it is necessary to calibrate the receiver setups. Receiver power calibrations are important to ensure accurate noise power measurements. These calibrations mathematically remove the frequency response errors in the receivers and adjust readings to the same source power calibration level. The concept of receiver calibration is to take a known source power at some source reference plane and transfer that knowledge to the receiver at a desired receiver reference plane. The calibration is performed as follows:

1. A power source calibration is done at the Port 1 reference plane using a R&S NRP-Z55 thermal power sensor. A picture of the sensor is shown in Fig. 2.23. The thermal power sensor is used as an absolute power reference in order to calibrate the source. The connection diagram for the source calibration is represented in Fig. 2.24.

FIGURE 2.23: R&S NRP-Z55 thermal power sensor

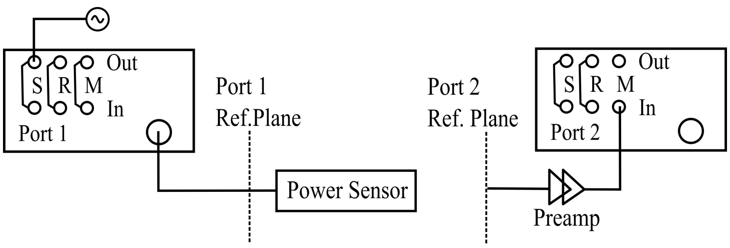

FIGURE 2.24: Connection diagram for source calibration

2. The receiver calibration is performed by connecting Port 1 reference plane to each receiver reference plane, as shown in Fig. 2.25.

The last step in the receiver characterization consists of measuring the inherent noise of the receivers. As a receiver power calibration has been performed, the

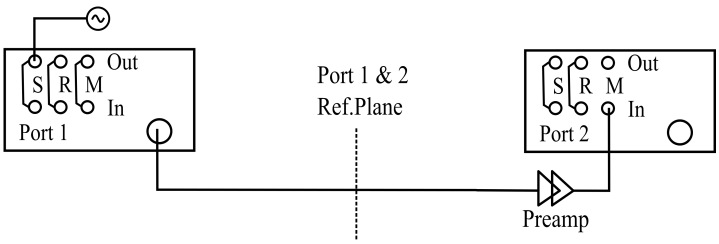

FIGURE 2.25: Connection diagram for receiver calibration

intrinsic noise of the receivers is measured directly by connecting a 50Ω match to each receiver [8]. The measured RMS powers correspond to the noise generated by the receivers at their outputs. The connection diagram is shown in Fig. 2.26.

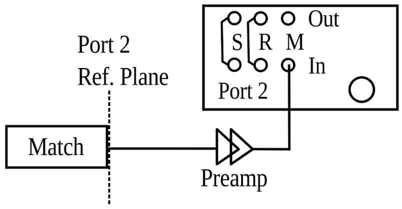

FIGURE 2.26: Connection diagram for receiver noise calibration

Output noise powers

As the receivers have been properly characterized, the next step consists of measuring the noise powers at the output ports of the dLNA. Two 50Ω SMA terminations are connected to the input ports of the amplifier. The output noise powers are measured using the receivers described previously. The measurement setup is represented in Fig. 2.27.

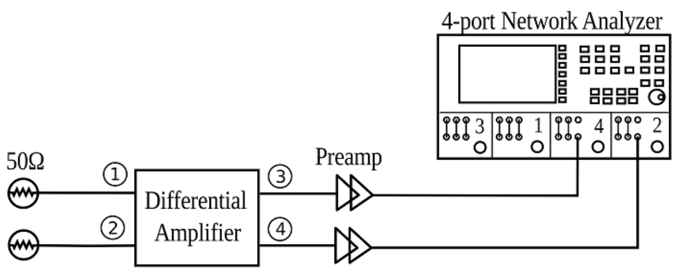

FIGURE 2.27: Measurement setup for output noise powers

[8]If the receiver power calibration is not performed, the inherent noise of the receivers can be determined using the Y-factor method with a calibrated noise source.

The noise power measurements are performed within a 5MHz bandwidth with a measurement time of at least 50 ms. [9]. The measured noise powers comprise the contributions of the 50Ω terminations, of the dA and of the receivers. The output noise powers are obtained by subtracting the noise contributions of the receivers measured in 2.2.3.2. The output noise powers are shown in Fig. 2.28.

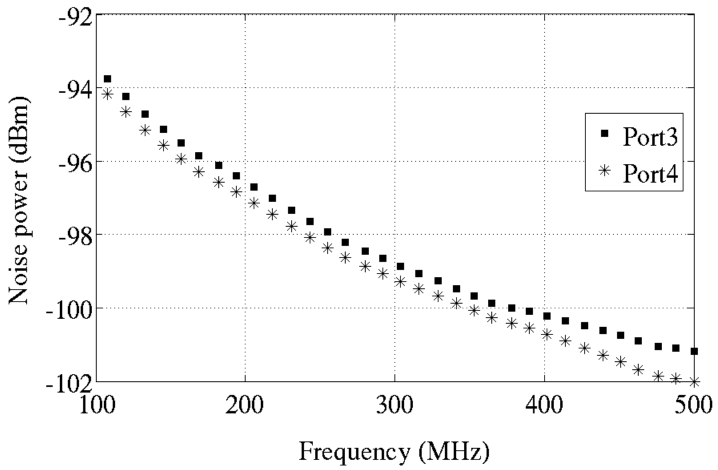

FIGURE 2.28: Output noise powers measured using a R&S ZVA24 Network Analyzer

Noise power measurement for configuration 1

The next step of the procedure consists of measuring the noise power at the output of the cascaded system. The UMCC 180° hybrid coupler is connected to the dLNA according to the configuration 1, where the output ports 3&4 of the amplifier are connected respectively to the input ports 1&2 of the coupler. The cascaded system is connected to the VNA receiver and the output noise power is measured. The block diagram of the setup is shown in Fig. 2.29. A photograph of the measurement setup is also presented in Fig. 2.30. And the measured output noise power is shown in Fig. 2.32.

[9]Longer measurement time leads to less rapid measurements. But this decreases the measurement inaccuracies. Indeed, by increasing the measurement time the variance of the power measurement decreases, yielding into a more stable power value.

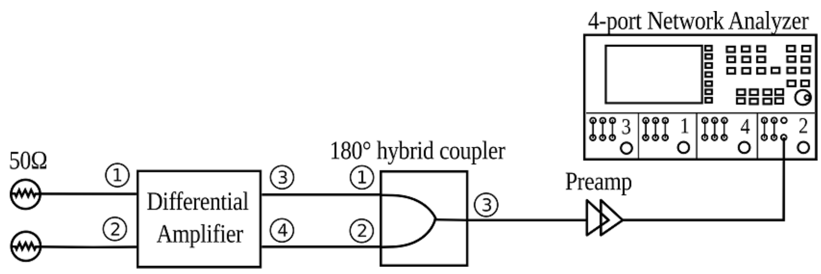

FIGURE 2.29: Measurement setup for configuration1

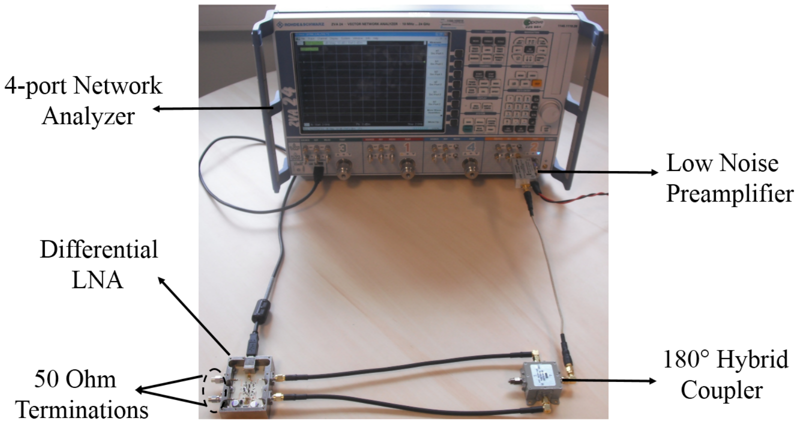

FIGURE 2.30: Photograph of the measurement setup

Noise power measurement for configuration 2

The last step of the measurement procedure consists of connecting the hybrid coupler according to configuration 2. The output ports 3 and 4 of the amplifier are connected respectively to the input ports 2 and 1 of the coupler, as shown in Fig. 2.31. The noise power at the output port of the cascaded system is shown in Fig. 2.32.

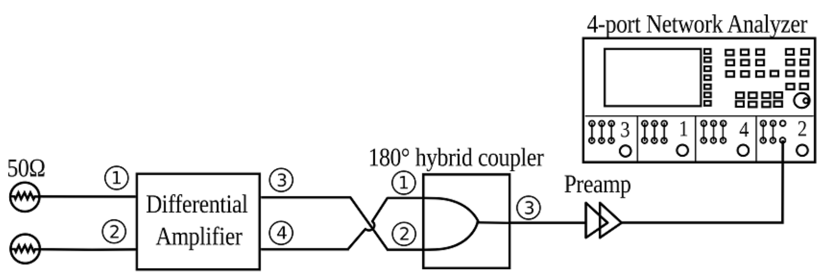

FIGURE 2.31: Measurement setup for configuration2

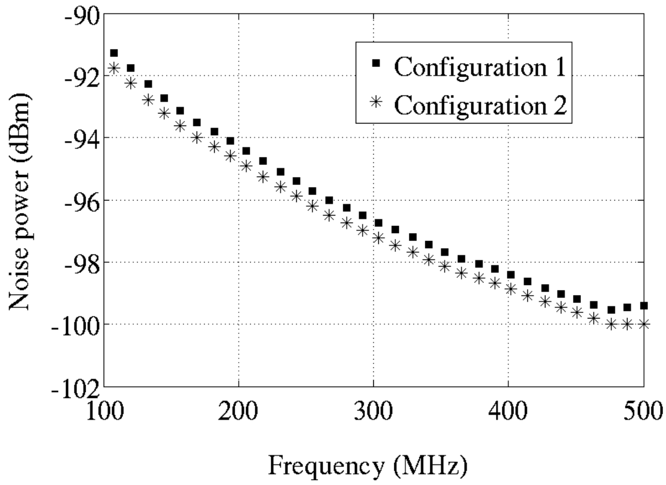

FIGURE 2.32: Output noise powers measured for the two configurations

2.2.3.3 Real part of correlation

The previous sections have dealt with the measurement of several parameters that serve for the extraction of the real part of the correlation of output noise waves. This real part is calculated from the measurement data and equations developed in section 2.2.1. It has the same dimension as a power and is shown in Fig. 2.33.

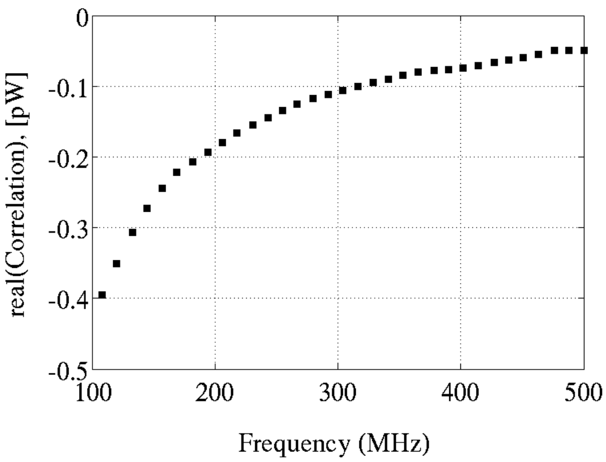

FIGURE 2.33: Real part of the correlation

Fig. 2.33 shows that the real part of the correlation is given to the tenths of a picowatt. It is of the same order of magnitude as the output noise powers. As explained in Chapter 1, the differential mode (DM) noise power at the output of the dLNA can be expressed in terms of the output noise powers and the correlation as:

$\overline{|b_{d2}|^2} = (\overline{|b_3|^2} + \overline{|b_4|^2} - 2\Re e(\overline{b_3 \cdot b_4^*}))/2$. This shows that a correct evaluation of the correlation is the sine qua non for having accurate DM noise power measurements. Moreover, the real part of the correlation corresponds here to a negative power. The correlation can be a negative power as it is in fact a mathematical concept; it does not correspond to a physical quantity.

2.2.3.4 Differential noise figure

The differential noise figure (dNF) is calculated by injecting the real part of the correlation in (1.48). A dNF of 3.9 to 4.5 dB is obtained in the operating frequency range of 100MHz to 500MHz, as shown in Fig. 2.34.

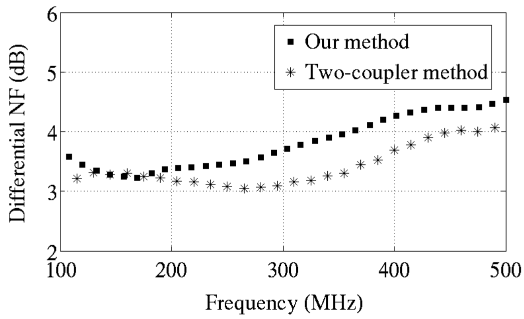

Figure 2.34: Measurement results obtained with the 2 different methods

Evaluation of the measurement results

For comparison and verification issues, the noise figure of the R&S dLNA is measured using the classical two-coupler technique [24] described in section 2.1.1. The dLNA is embedded between 2 UMCC hybrid couplers. The S-E noise figures and gains of the cascaded system and of the couplers are measured using the Y-factor method. Measurements are performed with an R&S FSV13 Signal Analyzer and a Noisecom's NC346D Noise Source. The noise figure of the dLNA is de-embedded using (2.2). As shown in Fig. 2.34, a differential noise figure of 3.3 to 4 dB is obtained.

As expected, the noise figures given by both techniques are of the same order of magnitude. There are somehow some differences which are partly caused by the measurement uncertainties which depend on multiple factors such as the noise figure of the receivers, the small-signal characteristics of the amplifier, the ENR of the noise source, etc [32].

However, the main reason for such deviations comes from the simplifications made in the two-coupler technique. As explained in section 2.1.1, the 2-coupler approach assumes that the couplers have symmetrical paths as their phase and amplitude imbalances are neglected. This assumption is not true in practice and causes some measurement errors [25]. On the contrary, our de-embedding methodology developed in this chapter does not yield these errors as the imbalances are rigorously taken into account.

2.3 Conclusion

This chapter has dealt with the development of an accurate technique for the differential noise figure measurement of differential amplifiers. The method consists of connecting a hybrid coupler at the output ports of a differential amplifier according to two configurations. It allows an exact extraction of the correlation of the noise waves at the output ports of the dA, which is essential for the determination of the dNF.

This measurement technique is more time-consuming than the existing coupler-based methods. It requires also an expensive 4-port network analyzer. But it proposes a rigorous noise figure de-embedding for dAs with arbitrary CMRRs. Moreover, our method does not require any calibrated noise source as only cold measurements are performed. The approach can be further developed for the measurement of dAs having low input and output return losses. This is left for future work.

This chapter has shown that the proper de-embedding of the dNF with non-ideal hybrid couplers requires a long measurement procedure. In Chapter 3, a more straightforward approach for measuring differential noise figure without using couplers is presented.

Chapter 3

Differential noise figure and noise parameters measurement without any coupler

3.1 Differential noise figure measurement: Coupler-free technique

3.1.1 Introduction

A technique for measuring differential noise figure using a hybrid coupler has been proposed in Chapter 2. It has been demonstrated that the proper de-embedding of a non-ideal hybrid coupler can prove to be a difficult task. Moreover, couplers often have limited bandwidths. Therefore a set of several hybrid couplers is required for wideband measurements. The purpose of this chapter is to present a different approach than the classical coupler techniques for the noise figure measurement of differential amplifiers. A coupler-free technique based on the calculation of the correlation of output noises will be developed. The calculations are explained in section 3.1.2. The method will then be verified by simulations and measurements of differential amplifiers in sections 3.1.3 and 3.1.4.

3.1.2 Theory

As explained in section 1.9, the measurement of correlated output noise signals remains one of the main issues for the noise characterization of differential circuits. This section will present a new coupler-free approach for measuring the correlation of noise waves at the output ports of a differential amplifier. The determination of the correlation is addressed by examining the architecture of a differential amplifier. A dA can be seen as two single-ended amplifiers connected to a common network as shown in Fig. 3.1 [23]. The intrinsic noises generated by

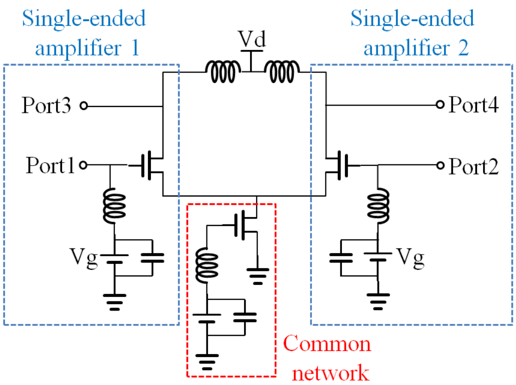

FIGURE 3.1: Simplified architecture of a differential amplifier with two single-ended amplifiers connected to a common network

the single-ended amplifiers are not correlated and are represented in Fig. 3.2 by two independent input-referred noise sources N_{s1} and N_{s2}. These 2 input-referred noise sources contribute to the noises at the two output ports of the dA and produce the correlation between the output noises. The common network may cause some additional slight correlation. Its noises appear however in the common mode and are therefore rejected by the fully-differential amplifier [23]. In Fig. 3.2, each

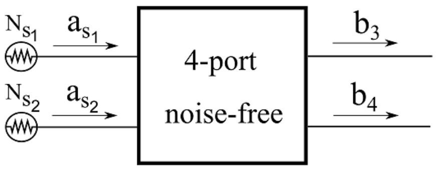

FIGURE 3.2: Noisy differential circuit represented by a noise-free 4-port circuit connected to 2 input-referred noise sources N_{s1} and N_{s2} delivering the noise waves a_{s1} and a_{s2}; a_{si} is the sum of the noise wave from the source and the input-referred noise wave at Port i.

input-referred noise source consists of the noise contributions of the S-E amplifier and of the 50Ω termination connected at each input port. The noise waves from the two input-referred noise sources are denoted by a_{s1} and a_{s2}. The noise waves b_3 and b_4 at the output ports of the dA can be expressed in terms of a_{s1} and a_{s2} and of the S-parameters of the dA by:

$$\begin{aligned} b_3 &= S_{31}\, a_{s1} + S_{32}\, a_{s2} \\ b_4 &= S_{41}\, a_{s1} + S_{42}\, a_{s2} \end{aligned} \tag{3.1}$$

The correlation between the output noise waves is calculated as:

$$\begin{aligned} \overline{b_3 \cdot b_4^*} &= \overline{(S_{31}\, a_{s1} + S_{32}\, a_{s2}) \cdot (S_{41}^*\, a_{s1}^* + S_{42}^*\, a_{s2}^*)} \\ &= S_{31}S_{41}^*\overline{|a_{s1}|^2} + S_{32}S_{42}^*\overline{|a_{s2}|^2} + S_{31}S_{42}^*\overline{a_{s1} \cdot a_{s2}^*} + S_{32}S_{41}^*\overline{a_{s2} \cdot a_{s1}^*} \end{aligned} \tag{3.2}$$

As the input-referred noise sources are uncorrelated, $\overline{a_{s1} \cdot a_{s2}^*} = 0$ and $\overline{a_{s2} \cdot a_{s1}^*} = 0$.

The correlation is therefore given by:

$$\overline{b_3 \cdot b_4^*} = S_{31}S_{41}^*\overline{|a_{s1}|^2} + S_{32}S_{42}^*\overline{|a_{s2}|^2} \tag{3.3}$$

where the input-referred noise powers can be calculated in terms of the output noise powers and the S-parameters by using (3.1):

$$\begin{aligned} \overline{|a_{s1}|^2} &= \frac{|S_{42}|^2\overline{|b_3|^2} - |S_{32}|^2\overline{|b_4|^2}}{|S_{31}|^2||S_{42}|^2| - |S_{41}|^2||S_{32}|^2|} \\ \overline{|a_{s2}|^2} &= \frac{|S_{31}|^2\overline{|b_4|^2} - |S_{41}|^2\overline{|b_3|^2}}{|S_{31}|^2||S_{42}|^2| - |S_{41}|^2||S_{32}|^2|} \end{aligned} \tag{3.4}$$

An analytical expression of the correlation of the noise waves at the output ports of a differential amplifier has been found. The correlation is measured by using the output noise powers and the S-parameters of the dA. The correlation is then injected in (3.5) for the measurement of the differential noise figure:

$$F_{diff} = \frac{\overline{|b_3|^2} + \overline{|b_4|^2} - 2\Re e(\overline{b_3 \cdot b_4^*})}{2kT_0\Delta f \left(|S_{dd21}|^2 + |S_{dc21}|^2\right)} \tag{3.5}$$

This section has dealt with the calculations of the differential noise figure without the use of couplers. The extraction of the correlation of the output noise waves is simpler than with the coupler-method. Only the S-parameters and the output noise powers of the differential circuit are required for the calculations. This coupler-free approach will be verified by ADS simulations of a differential amplifier in the following section.

3.1.3 Validation by simulation

The expressions of section 3.1.2 are validated by simulating a differential amplifier on ADS. The simulation results will be compared to those obtained by using the technique described in section 2.2. An X-band differential amplifier is designed and simulated on ADS. The simplified schematic diagram of the circuit ressembles that of Fig. 2.7. An S-parameter simulation is firstly performed and the mixed-mode S-parameters of the dA are calculated using (1.35). The differential gain, common-mode gain and the conversion gain between common-mode and differential-mode are displayed in Fig. 3.3. The amplifier has a differential gain of about 10 dB in

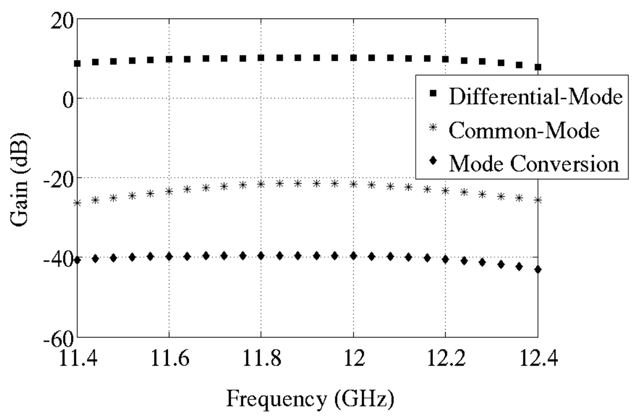

FIGURE 3.3: The differential gain, common-mode gain and the conversion gain between common-mode and differential-mode of the differential amplifier simulated in the 11.4-12.4 GHz bandwidth

the 11.4-12.4 GHz bandwidth. The common-mode rejection is of a least 20 dB. A good common-mode rejection is chosen in order to ensure that common-mode noise correlation does not affect the extraction of the differential noise figure. And the conversion between common-mode and differential-mode is around -40 dB.

A noise simulation is then performed on the dA. The input and output ports are connected to 50Ω terminations and the output noise powers are measured with a bandwidth Δf of 1 MHz. The noise powers $\overline{|b_3|^2}$ and $\overline{|b_4|^2}$ measured at the output ports 3 and 4 of the dA are shown in Fig. 3.4.

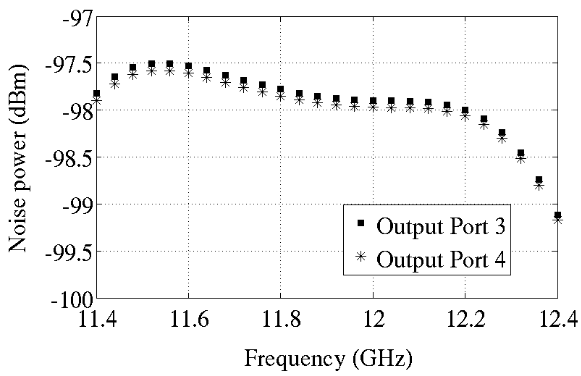

FIGURE 3.4: The noise powers measured in a bandwidth Δf of 1 MHz at the output ports 3 and 4 of the fully-differential amplifier

The correlation of the output noise waves $\overline{b_3 \cdot b_4^*}$ is then calculated from the S-parameters and the output noise powers by using (3.3) and (3.4). The real part of the correlation is shown in Fig. 3.5. It is compared in Fig. 3.5 to $\Re e(\overline{b_3 \cdot b_4^*})$ measured using the coupler-technique described in section 2.2. Indeed, the differential amplifier has also been simulated by connecting its output ports to a hybrid coupler. The real part of the correlation of the output noise waves has been extracted by using the procedure described in section 2.2.1.

There is a good agreement between the correlations obtained with the two techniques. There is somehow a slight difference which is explained by some common-mode correlation that has not been completely eliminated by the dA.

$\Re e(\overline{b_3 \cdot b_4^*})$ is finally injected in (3.5) to determine the differential noise figure. Fig. 3.6 shows the differential noise figures obtained with the two techniques. The

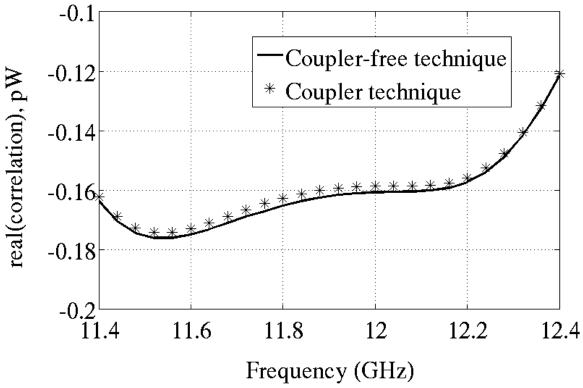

FIGURE 3.5: The real part of the correlation of output noise waves calculated using the coupler-free technique and the coupler-technique of (3.4)

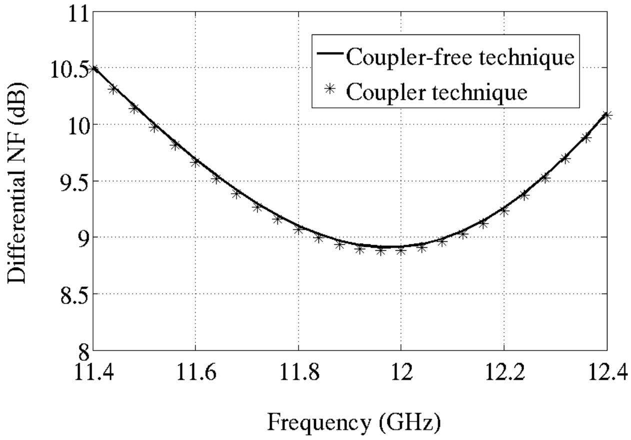

FIGURE 3.6: Comparison between the differential noise figures obtained with the coupler-free technique and the coupler technique of section 2.2

two noise figures agree well in the bandwidth of the dA. These simulation results therefore confirm the relevance of the theoretical work described in section 3.1.2. The next step is to test the technique in real measurement conditions.

3.1.4 Measurement procedure

A measurement procedure is developed for the noise figure measurement of the dLNA used in section 2.2.3. The dLNA has a variable common-mode rejection. In this section, a good common-mode rejection of at least 20 dB is set in order to guarantee that common-mode noise correlation does not affect the measurements. The input and output ports are well-matched to 50Ω, with input and output return losses of at least -15 dB.

3.1.4.1 S-parameters measurement

Both S-parameters and noise measurements are performed with the R&S ZVA24 4-port Network Analyzer. The first step consists of measuring the 4-port S-parameters of the dLNA after performing an UOSM calibration on the four analyzer ports. Fig. 3.7 shows the mixed-mode S-parameters of the dLNA determined from its 4-port S-parameters using (1.35).

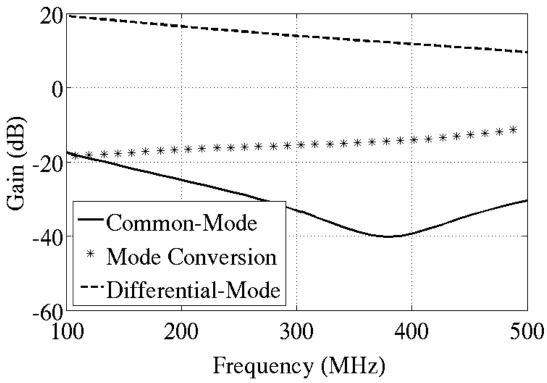

FIGURE 3.7: The differential gain, common-mode gain and the conversion gain between common-mode and differential-mode of the differential amplifier measured in the 100-500 MHz bandwidth

3.1.4.2 Noise powers measurement

The second step consists of measuring the noise powers at the output ports of the dLNA. The setup for the noise power measurements is similar to the one described in section 2.2.3.2. Cold-source measurements are performed with the two input ports of the dLNA connected to two 50Ω terminations. The output ports of the dLNA are connected to two VNA receivers via two low-noise preamplifiers. A photograph of the setup is shown in Fig. 3.8.

The output noise powers are measured in a 5 MHz bandwidth (Δf=5 MHz) after performing power calibrations in the two receiver reference planes. The calibration procedures have been explained in section 2.2.3.2. Fig. 3.9 shows the noise powers measured in the frequency range of 100-500 MHz at the output ports 3 and 4 of the dLNA. Output noise powers of around -94 to -104 dBm are measured for a bandwidth Δf of 1 MHz, which correspond to 4x10^{-19} to 6x10^{-20} W/Hz.

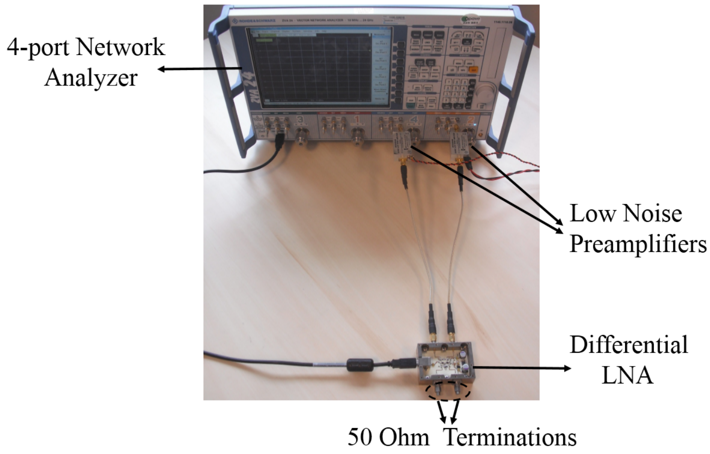

FIGURE 3.8: Photograph of the setup for the noise power measurements at the output ports of the differential amplifier

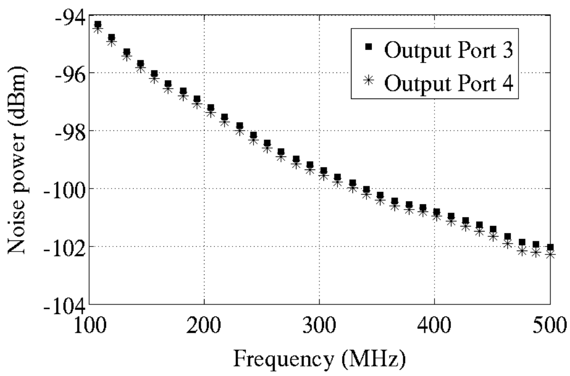

FIGURE 3.9: The noise powers at the output ports 3 and 4 of the dLNA measured with a R&S ZVA24 4-port Network Analyzer

3.1.4.3 Correlation of output noise waves

The output noise powers and the S-parameters of the dLNA are injected in (3.3) and (3.4) to calculate the correlation of the output noise waves. The real part of the correlation measured for a bandwidth Δf of 5 MHz and is shown in Fig. 3.10. $\Re e(\overline{b_3 \cdot b_4^*})$ varies from around -0.4 pW to -0.06 pW. This corresponds to $-4\text{x}10^{-19}$ to $-6\text{x}10^{-20}$ W/Hz, which is of the same order of magnitude as the output noise powers.

This correlation is compared to the one obtained with the coupler technique. Measurements are carried out by using the UMCC hybrid coupler (see section 2.2.3.1) at the output ports of the dLNA as described in section 2.2.3. The real part of the correlation obtained with the coupler-technique is also shown in Fig. 3.10. There is a good agreement between the correlations measured with the two techniques.

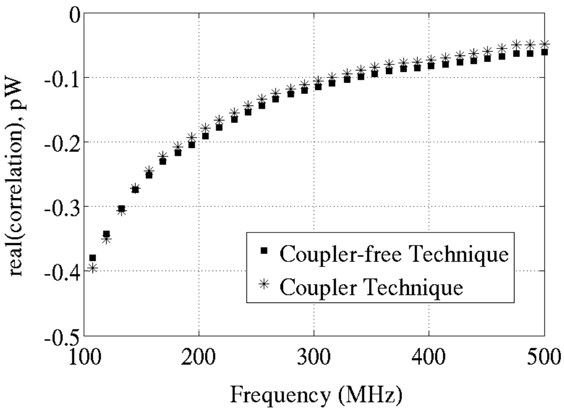

FIGURE 3.10: The real part of the correlation of the output noise waves measured with the coupler-free technique and the coupler-technique of section 2.2.3

3.1.4.4 Differential noise figure

$\Re e(\overline{b_3 \cdot b_4^*})$ is then injected in (3.5) to determine the differential noise figure. Fig. 3.11 shows the differential noise figures obtained with the two techniques. The

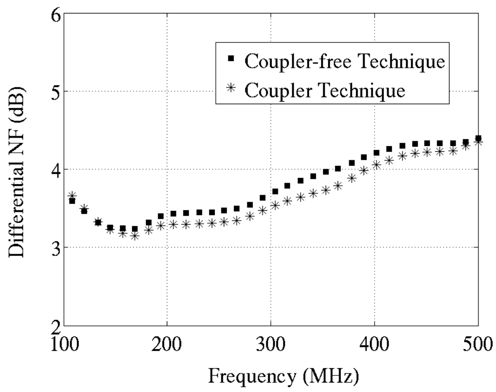

FIGURE 3.11: Comparison between the differential noise figures obtained with the coupler-free technique and the coupler technique of section 2.2.3

two noise figures agree well in the bandwidth of the dLNA, a dNF of around 3.6 to 4.4 dB is obtained in the operating frequency range of 100 MHz to 500 MHz. The slight difference between the traces is explained firstly by the measurement uncertainties that can cause some deviations between the results of both methods. And secondly, there is some common-mode noise correlation that has not been totally eliminated by the dLNA and therefore affects slightly the results of the coupler-free technique. These measurement results therefore confirm the relevance of our new coupler-free technique for differential noise figure measurements.

3.1.5 Conclusion

A new coupler-free technique for the noise figure measurement of differential amplifiers has been proposed. It is based on the determination of the correlation of output noises. The calculations of the correlation of output noise waves have been described in section 3.1.2. The correlation is obtained from the 4-port S-parameters and the output noise powers of the differential amplifier, without requiring any coupler. The calculations have been successfully verified in section 3.1.3 by ADS simulations of a differential amplifier. And in section 3.1.4, the technique has been tested in real measurement conditions where the noise figure of a differential low noise amplifier has been measured by using a 4-port Network Analyzer. The measurement procedure is simple and functional as no de-embedding of couplers is required and all the measurements are performed on the analyzer.

This technique can be extended to the noise figure measurements of on-wafer differential amplifiers. An on-wafer measurement technique has been presented at the ARFTG 2014 conference and published in [34].

In this section, the technique has been limited to differential amplifiers where the input and output ports are considered to be reflectionless. In the following sections, the approach will be extended to differential amplifiers with arbitrary input and output impedances. A technique for the measurement of differential noise parameters will be proposed where the differential noise figure is measured for various source impedances.

3.2 Differential noise parameters measurement: Coupler-free technique

3.2.1 Introduction

This section proposes a coupler-free technique for the noise parameters measurement of differential amplifiers. It is based on the coupler-free differential noise figure measurement technique presented in section 3.1.2. In section 3.1.2, the noise figure of differential amplifiers with well-matched input and output ports was determined in a 50Ω (100Ω for differential-mode) environment. In this section, the noise parameters of amplifiers with arbitrary input and output impedances will be measured. The differential noise parameters are F_{min}^{diff}, the minimum differential noise figure, R_n^{diff}, the differential equivalent noise resistance, G_{opt}^{diff} and B_{opt}^{diff}, the real and imaginary parts of the optimum source admittance Y_{opt}^{diff}. These noise parameters allow the determination of the differential noise figure for arbitrary differential sources impedances.

The existing methods for measuring differential noise parameters use hybrid couplers or baluns for converting the 4-port circuit into a 2-port system [27], [26], [35]. This allows traditional 2-port source-pull measurements by using a single-ended impedance tuner. The extraction of the noise parameters using the coupler technique will be presented in section 3.2.1.1. As explained previously, the couplers have limited bandwidth and their proper de-embedding can be somehow complicated. A coupler-free approach is therefore proposed in this work. The calculations and procedure for the determination of the differential noise parameters are explained in section 3.2.2. This theoretical work is validated by simulation results presented in section 3.2.3. The test setup and measurement results are dealt with in section 3.2.4.

3.2.1.1 Traditional coupler-technique

This section describes the traditional approach for the determination of the differential noise parameters. The method consists of embedding the differential DUT between two hybrid couplers. Conventional single-ended source-pull measurements are performed by using a two-port impedance tuner, as shown in Fig. (3.12). The basic principle consists of using the impedance tuner to present different impedances to the two-port 'couplers+differential amplifier' cascaded system.

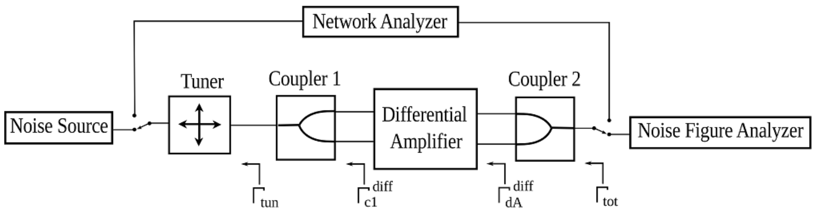

FIGURE 3.12: Block diagram of conventional measurement setup for differential noise parameters

For each source impedance, the noise figure F_{casc}^{diff} of the cascaded system is measured by using either the Y-factor method (see section 1.4.1) or the cold source method (see section 1.4.2). The noise figure F_{dA}^{diff} of the differential amplifier is then de-embedded from F_{casc}^{diff} by using Friis equation applied to differential excitations:

$$F_{casc}^{diff} = F_{c1}^{diff} + \frac{F_{dA}^{diff} - 1}{G_{c1}^{av^{diff}}} + \frac{F_{c2}^{diff} - 1}{G_{c1}^{av^{diff}} G_{dA}^{av^{diff}}} \tag{3.6}$$

where F_{c1}^{diff} and F_{c2}^{diff} are the differential noise figure of the couplers 1 and 2 respectively. As the couplers consists of only passive elements, their differential noise figures are calculated from their available differential gains $G_{c1}^{av^{diff}}$ and $G_{c2}^{av^{diff}}$ as:

$$F_{c1}^{diff} = \frac{1}{G_{c1}^{av^{diff}}} \quad \text{and} \quad F_{c2}^{diff} = \frac{1}{G_{c2}^{av^{diff}}} \tag{3.7}$$

Using (3.6) and (3.7), F_{casc}^{diff} simplifies to:

$$F_{casc}^{diff} = \frac{F_{dA}^{diff}}{G_{c1}^{av^{diff}}} + \frac{1 - G_{c2}^{av^{diff}}}{G_{casc}^{av^{diff}}} \tag{3.8}$$

where $G_{casc}^{av^{diff}}$ is the available gain of the cascaded system. It is given by $G_{casc}^{av^{diff}} = G_{c1}^{av^{diff}} G_{dA}^{av^{diff}} G_{c2}^{av^{diff}}$.

The issue of using couplers is to properly eliminate the influence introduced by them in the gain and noise measurements. In the state of the art techniques [27], [26] and [35], the couplers are characterized by using the mixed-mode formalism. This allows a proper characterization where non-idealities such as losses, amplitude and phase imbalances are taken into account.

Using the mixed-mode formalism [21], the 3-port couplers are represented as equivalent two-ports: 1 single port and 1 balanced port. The representation of the input coupler as a 2-port mixed-mode circuit is illustrated in Fig. (3.13).

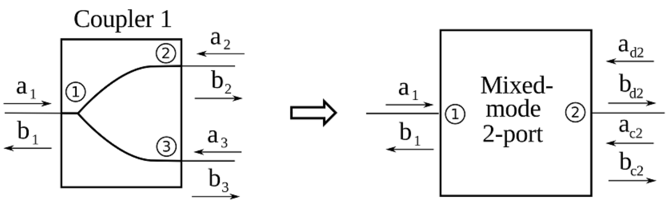

FIGURE 3.13: Mixed-mode representation of the input coupler

The matrix of mixed-mode S-parameters $\mathbf{S_{c1}^{mm}}$ of the input coupler is calculated from the matrix of standard S-parameters $\mathbf{S_{c1}^{std}}$ as:

$$\mathbf{S_{c1}^{mm}} = \mathbf{M_{c1}} \quad \mathbf{S_{c1}^{std}} \quad \mathbf{M_{c1}^{-1}} \tag{3.9}$$

where $\mathbf{S_{c1}^{mm}} = \frac{1}{\sqrt{2}} \begin{bmatrix} S_{ss11} & S_{sd12} & S_{sc12} \\ S_{ds21} & S_{dd22} & S_{dc22} \\ S_{cs21} & S_{cd22} & S_{cc22} \end{bmatrix}$ and $\mathbf{M_{c1}}$ is: $\begin{bmatrix} \sqrt{2} & -0 & 0 \\ 0 & 1 & -1 \\ 0 & 1 & 1 \end{bmatrix}$

For each source impedance, the available gain $G_{c1}^{av^{diff}}$ of the input coupler is calculated from the mixed-mode S-parameters as:

$$G_{c1}^{av^{diff}} = \frac{|S_{ds21}^{c1}|^2(1 - |\Gamma_{tun}|^2)}{|1 - S_{ss11}^{c1}\Gamma_{tun}|^2(1 - |\Gamma_{c1}^{diff}|^2)} \tag{3.10}$$

where Γ_{tun} is the output reflection coefficient of the tuner and Γ_{c1}^{diff} is the differential reflection coefficient seen at the output of Coupler 1, as shown in Fig. (3.12).

It is calculated from the mixed-mode S-parameters of the coupler as:

$$\Gamma_{c1}^{diff} = S_{dd22}^{c1} + \frac{S_{ds21}^{c1} S_{sd12}^{c1} \Gamma_{tun}}{1 - S_{ss11}^{c1} \Gamma_{tun}} \tag{3.11}$$

The mixed-mode representation of the output coupler is shown in Fig.(3.14). The

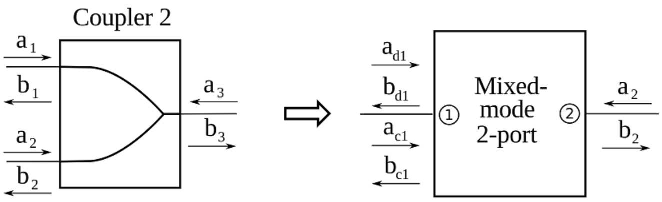

FIGURE 3.14: Mixed-mode representation of the output coupler

matrix of mixed-mode S-parameters $\mathbf{S_{c2}^{mm}}$ of the output coupler is calculated from the matrix of standard S-parameters $\mathbf{S_{c2}^{std}}$ as:

$$\mathbf{S_{c2}^{mm}} = \mathbf{M_{c2}} \quad \mathbf{S_{c2}^{std}} \quad \mathbf{M_{c2}^{-1}} \tag{3.12}$$

where: $\mathbf{S_{c2}^{mm}} = \frac{1}{\sqrt{2}} \begin{bmatrix} S_{dd11} & S_{dc11} & S_{ds12} \\ S_{cd11} & S_{cc11} & S_{cs12} \\ S_{sd21} & S_{sc21} & S_{ss22} \end{bmatrix}$ and $\mathbf{M_{c2}}$ is: $\begin{bmatrix} 1 & -1 & 0 \\ 1 & 1 & 0 \\ 0 & 0 & \sqrt{2} \end{bmatrix}$

For each tuner position, the available gain of Coupler2 is calculated as:

$$G_{c2}^{av^{diff}} = \frac{|S_{sd21}^{c2}|^2 (1 - |\Gamma_{dA}^{diff}|^2)}{|1 - S_{dd11}^{c2} \Gamma_{dA}^{diff}|^2 (1 - |\Gamma_{tot}|^2)} \tag{3.13}$$

where Γ_{tot} is the reflection coefficient at the output of the whole system and Γ_{dA}^{diff} is the differential reflection coefficient seen at the output of differential amplifier, as shown in Fig. (3.12). It is calculated from the mixed-mode S-parameters of the coupler as:

$$\Gamma_{dA}^{diff} = S_{dd22}^{dA} + \frac{S_{dd21}^{dA} S_{dd12}^{dA} \Gamma_{c1}^{diff}}{1 - S_{dd11}^{dA} \Gamma_{c1}^{diff}} \tag{3.14}$$

The available gains $G_{c1}^{av^{diff}}$ and $G_{c2}^{av^{diff}}$ of the couplers are then injected in (3.8) for de-embedding the noise figure F_{dA}^{diff} of the differential amplifier. F_{dA}^{diff} is therefore obtained for several impedances synthesized by the tuner. The four noise parameters are then calculated from F_{dA}^{diff} and from the impedances presented to the dA (related to Γ_{c1}^{diff}). [1]

Simulation and measurement results of this coupler technique applied to differential noise figure measurement will serve as verification tools for the coupler-free technique described in section 3.2.2. A least square fit is performed on the overdetermined data as described in Lane's procedure [13]. Lane's procedure applied to differential noise parameters will be briefly presented in section 3.2.2.4.

3.2.2 Coupler-free technique: Theory

An original technique without couplers is developed for the measurement of the noise parameters of differential amplifiers. The principle relies on differential source-pull measurements by using a differential impedance tuner. The noise figure of the differential amplifier is measured for the different source impedances synthesized by the tuner. The noise figure measurements are carried out by using an extension of the coupler-free approach of section 3.1 to non 50Ω environments. Lane's procedure is then applied to the measured noise figures for the determination of the four differential noise parameters. The calculations for the extraction of the parameters are firstly explained in this section.

A differential source-pull technique is developed to determine the noise parameters of differential amplifiers. The block diagram of the setup for differential source-pull measurements is shown in Fig. (3.15).

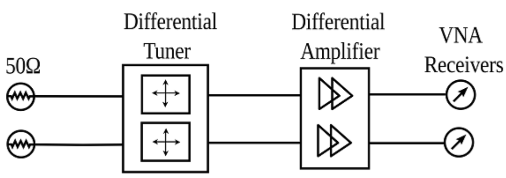

FIGURE 3.15: Block diagram of the differential noise parameters measurement setup

[1] The impedance seen from the input ports of the DUT is not actually the impedance synthesized by the tuner, but it is the impedance seen through the input coupler.

The technique relies on the cold source approach where two 50Ω terminations are connected to the input ports of the differential tuner (dT). The dT presents several impedances to the differential amplifier (dA) and the output noises are measured with two receivers. In our case, the receivers are those of a 4-port Network Analyzer. For each impedance synthesized by the tuner, the noise figure of the dA needs to be calculated. It will be calculated in the following paragraphs from elements that are measurable with conventional equipment. The different elements required for the extraction of the differential noise parameters from the differential source-pull measurements are represented in Fig. (3.16).

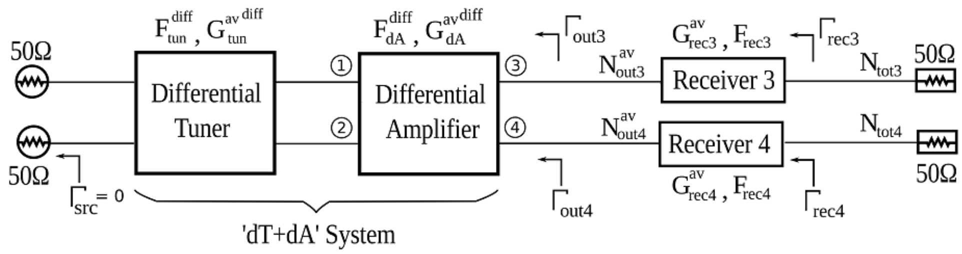

FIGURE 3.16: Representation of the noise and gain elements necessary for the extraction of the differential noise parameters

The noise powers measured at the output ports of the whole system are denoted by N_{tot3} and N_{tot4}, as shown in Fig. (3.16). These noise powers consist of the noise contributions of the dT, the dA and the receivers. The first step of the calculations consists of subtracting the contributions of the receivers from N_{tot3} and N_{tot4} so as determine the noise powers available at the outputs of the 'dT+dA' cascaded system.

3.2.2.1 Output noise powers of the 'dT+dA' system

This section deals with the calculations to determine the noise powers available at the output ports of the 'dT+dA' cascaded system, shown in Fig. (3.16). Only the calculations for the noise power available at the output port 3 of the 'dT+dA' system will be detailed. Similar calculations shall be applied to the output port 4, but they will not be developed.

First of all, the available noise power N^{av}_{tot3} at the output port 3 of the whole system is given by :

$$N^{av}_{tot3} = \frac{N_{tot3}}{1 - |\Gamma_{rec3}|^2} \tag{3.15}$$

where Γ_{rec3} is the reflection coefficient at the output of the whole system. N^{av}_{tot3} can also be expressed as:

$$N^{av}_{tot3} = G^{av}_{rec3} N^{av}_{out3} + N^{av}_{rec3} \tag{3.16}$$

where G^{av}_{rec3} is the available gain of receiver 3, N^{av}_{out3} is the noise power available at the output port 3 of the 'dT+dA' cascaded system and N^{av}_{rec3} is the intrinsic noise power of receiver 3 available at its output. G^{av}_{rec3} is calculated from the S-parameters of the receivers and from Γ_{out3}, the reflection coefficient at the output port 3 of the 'dT+dA' system:

$$G^{av}_{rec3} = \frac{|S^{rec3}_{21}|^2 (1 - |\Gamma_{out3}|^2)}{|1 - S^{rec3}_{11} \Gamma_{out3}|^2 (1 - |\Gamma_{rec3}|^2)} \tag{3.17}$$

As specified in 2.2.3.2, a power calibration is performed in the receivers' reference planes. The receiver can therefore be considered as having unity gain, i.e. $|S^{rec3}_{21}|^2 = 1$.

N^{av}_{rec3} is calculated from F_{rec3}, the noise figure of receiver 3 as:

$$N^{av}_{rec3} = (F_{rec3} - 1) G^{av}_{rec3} k T_0 \Delta f \tag{3.18}$$

The noise figure F_{rec3} depends on the impedance presented to the receiver. For each tuner position, this impedance changes and therefore F_{rec3} also varies. It is possible to keep the impedance constant to a certain extent by placing an isolator between the amplifier and the receiver. This solution has however the disadvantage of being bandwidth limited as isolators often work in a short frequency range. In our approach, no isolator is used. Instead, the noise parameters of the receivers are measured. This allows the determination of the noise figure of the receivers for the different impedances presented to them. The noise parameters of each receiver are obtained from conventional two-port source-pull measurements by using the two independent paths of the differential tuner. The calculations for evaluating the receivers' noise parameters are described in Appendix C.

The available noise power N_{out3}^{av} at the output of the 'dT+dA' cascaded system is calculated from (3.16) and (3.18) as:

$$\begin{aligned} N_{out3}^{av} &= \frac{N_{tot3}^{av} - N_{rec3}^{av}}{G_{rec3}^{av}} \\ &= \frac{N_{tot3}^{av}}{G_{rec3}^{av}} - (F_{rec3} - 1)kT_0\Delta f \end{aligned} \tag{3.19}$$

And using (3.15) and (3.17):

$$\begin{aligned} N_{out3}^{av} &= \frac{N_{tot3}}{1 - |\Gamma_{rec3}|^2} \frac{|1 - S_{11}^{rec3}\Gamma_{out3}|^2(1 - |\Gamma_{rec3}|^2)}{|S_{21}^{rec3}|^2(1 - |\Gamma_{out3}|^2)} - (F_{rec3} - 1)kT_0\Delta f \\ &= N_{tot3}\frac{|1 - S_{11}^{rec3}\Gamma_{out3}|^2}{1 - |\Gamma_{out3}|^2} - (F_{rec3} - 1)kT_0\Delta f \end{aligned} \tag{3.20}$$

This expression allows the subtraction of the noise contributions of receiver 3 from the noise power at the output of the whole system. Similar calculations are performed for the determination of N_{out4}^{av}, the noise power available at the output port 4 of the 'dT+dA' cascaded system:

$$N_{out4}^{av} = N_{tot4}\frac{|1 - S_{11}^{rec4}\Gamma_{out4}|^2}{1 - |\Gamma_{out4}|^2} - (F_{rec4} - 1)kT_0\Delta f \tag{3.21}$$

3.2.2.2 Noise figure of the 'dT+dA' cascaded system

The next step consists of calculating the differential noise figure of the 'dT+dA' cascaded system shown in Fig. (3.17). The noise figure of 'dT+dA' system is

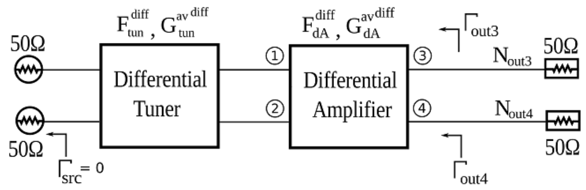

FIGURE 3.17: Block diagram of the cascaded system of the differential tuner and the differential amplifier

calculated by using the approach described in section 3.1 . As explained in section

3.1, the differential noise figure is determined from the 4-port S-parameters and the output noise powers. These output noise powers are in fact the output noise powers delivered to 50Ω terminations. The noise powers at the output ports of 'dT+dA' system delivered to 50Ω terminations will be denoted by N_{out3} and N_{out4}. They are calculated from the available noise powers N^{av}_{out3} and N^{av}_{out4} as:

$$\begin{aligned} N_{out3} &= N^{av}_{out3}(1 - |\Gamma_{out3}|^2)) \\ N_{out4} &= N^{av}_{out4}(1 - |\Gamma_{out4}|^2)) \end{aligned} \tag{3.22}$$

From (3.20), (3.21) and (3.22),

$$\begin{aligned} N_{out3} &= N_{tot3}|1 - S^{rec3}_{11}\Gamma_{out3}|^2 - (F_{rec3} - 1)(1 - |\Gamma_{out3}|^2)kT_0\Delta f \\ N_{out4} &= N_{tot4}|1 - S^{rec4}_{11}\Gamma_{out4}|^2 - (F_{rec4} - 1)(1 - |\Gamma_{out4}|^2)kT_0\Delta f \end{aligned} \tag{3.23}$$

N_{out3} and N_{out4} correspond respectively to the terms $\overline{|b_{out3}|^2}$ and $\overline{|b_{out4}|^2}$ if we use the noise wave formalism described in section 1.8.2. The expression of the differential noise figure F^{diff}_{sys} of 'dT+dA' system is given in terms of output noise waves b_{out3} and b_{out4} and the mixed-mode gains of the system:

$$F^{diff}_{sys} = \frac{\overline{|b_{out3}|^2} + \overline{|b_{out4}|^2} - 2\Re e(\overline{b_{out3} \cdot b^*_{out4}})}{2kT_0\Delta f\,(|S^{sys}_{dd21}|^2 + |S^{sys}_{dc21}|^2)} \tag{3.24}$$

The correlation of output noise waves is given by:

$$\overline{b_{out3} \cdot b^*_{out4}} = S^{sys}_{31}S^{sys*}_{41}\overline{|a_{s1}|^2} + S^{sys}_{32}S^{sys*}_{42}\overline{|a_{s2}|^2} \tag{3.25}$$

where the input-referred noise powers $\overline{|a_{s1}|^2}$ and $\overline{|a_{s2}|^2}$ can be expressed in terms of the output noise powers as:

$$\overline{|a_{s1}|^2} = \frac{|S^{sys}_{42}|^2\overline{|b_{out3}|^2} - |S^{sys}_{32}|^2\overline{|b_{out4}|^2}}{|S^{sys}_{31}|^2||S^{sys}_{42}|^2| - |S^{sys}_{41}|^2||S^{sys}_{32}|^2|} \tag{3.26}$$

$$\overline{|a_{s2}|^2} = \frac{|S^{sys}_{31}|^2\overline{|b_{out4}|^2} - |S^{sys}_{41}|^2\overline{|b_{out3}|^2}}{|S^{sys}_{31}|^2||S^{sys}_{42}|^2| - |S^{sys}_{41}|^2||S^{sys}_{32}|^2|} \tag{3.27}$$

The noise figure of the 'dT+dA' system is therefore obtained using the output noise powers and the S-parameters of the system.

3.2.2.3 Noise figure of the differential amplifier

The third step consists of de-embedding the noise figure F_{dA}^{diff} of the dA from F_{sys}^{diff}. This is done by using Friis equation applied to differential-mode excitations:

$$F_{sys}^{diff} = F_{tun}^{diff} + \frac{F_{dA}^{diff} - 1}{G_{tun}^{av^{diff}}} \tag{3.28}$$

where F_{tun}^{diff} is the differential noise figure of the tuner. As the tuner consists of only passive components, its noise figure is equal to the inverse of its available gain, i.e $F_{tun}^{diff} = 1/G_{tun}^{av^{diff}}$. Therefore (3.28) simplifies to :

$$F_{dA}^{diff} = F_{sys}^{diff} G_{tun}^{av^{diff}} \tag{3.29}$$

where the differential available gain of the tuner is calculated from the latter's differential S-parameters as:

$$G_{tun}^{av^{diff}} = \frac{|S_{dd21}^{tun}|^2}{1 - |S_{dd22}^{tun}|^2} \tag{3.30}$$

The equations and procedure explained in this section allow us to de-embed the dNF of the differential amplifier from the whole system 'dT+dA+receivers'. The noise figure of the dA is therefore obtained for each impedance synthesized by the dT.

3.2.2.4 Differential noise parameters

The last step consists of extracting the differential noise parameters from the noise figures and the source admittances presented to the dA. An expression analogue to the 2-port noise figure [12] is applied to the differential noise figure definition. The dNF is expressed in terms of the differential source admittance Y_s^{diff} ($Y_s^{diff} =$

$G_s^{diff} + jB_s^{diff}$) as:

$$F_{dA}^{diff} = F_{min}^{diff} + \frac{R_n^{diff}}{G_s^{diff}} |Y_s^{diff} - Y_{opt}^{diff}|^2 \tag{3.31}$$

where F_{min}^{diff} is the minimum differential noise figure obtained when the differential admittance Y_s^{diff} presented to the dA is equal to the optimum differential source admittance Y_{opt}^{diff}. Y_{opt}^{diff} consists of a real and an imaginary part, i.e. $Y_{opt}^{diff} = G_{opt}^{diff} + jB_{opt}^{diff}$. And R_n^{diff} is the equivalent differential noise resistance which represents how fast the differential noise figure increases as Y_s^{diff} deviates from Y_{opt}^{diff}. There are therefore four differential noise parameters F_{min}^{diff}, R_n^{diff}, G_{opt}^{diff} and B_{opt}^{diff} that have to be determined. In theory, four measurements of dNF from four source admittances give four simultaneous equations, which should be sufficient to solve for the four noise parameters. However, measurements of the differential noise figure and of the admittances are sensitive to experimental errors, so in practice it is common to measure the noise figure at more than four values of source admittance, and then use a least-mean-squares algorithm to reduce the overdetermined data [13]. This least-square fit is done by firstly writting (3.31)in a form that is linear with respect to four new parameters A, B, C and D [36]:

$$F_{dA}^{diff} = A + BG_s^{diff} + \frac{C + BB_s^{diff^2} + DB_s^{diff}}{G_s^{diff}} \tag{3.32}$$

The four differential noise parameters can be expressed in terms of A, B, C and D as:

$$F_{min}^{diff} = A + \sqrt{4BC - D^2} \tag{3.33}$$

$$R_n^{diff} = B \tag{3.34}$$

$$G_{opt}^{diff} = \frac{\sqrt{4BC - D^2}}{2B} \tag{3.35}$$

$$B_{opt}^{diff} = \frac{\sqrt{-D}}{2B} \tag{3.36}$$

The least square fit is applied to the linear equation (3.32) where the following error criterion ε is minimized in order to determine A, B, C and D:

$$\varepsilon = \frac{1}{2}\sum_{i=1}^{n}\left[A + B\left(G_{s_i}^{diff} + \frac{B_{s_i}^{diff^2}}{G_{s_i}^{diff}}\right) + \frac{C}{G_{s_i}^{diff}} + \frac{DB_{s_i}^{diff}}{G_{s_i}^{diff}} - F_{dA_i}^{diff}\right]^2 \tag{3.37}$$

A weighting factor is generally used in the error criterion if certain data are known to be less reliable than the average [13], [37]. For simplicity considerations, no weighting factor has been used. In future research works, a weighting factor shall be introduced to improve the accuracy of the noise parameters.

The error criterion ε is minimized when its partial derivatives with respect to A, B, C and B are equal to zero, i.e:

$$\frac{\partial\varepsilon}{\partial A} = \sum_{i=1}^{n} P = 0 \tag{3.38}$$

$$\frac{\partial\varepsilon}{\partial B} = \sum_{i=1}^{n}\left(G_{s_i}^{diff} + \frac{B_{s_i}^{diff^2}}{G_{s_i}^{diff}}\right) P = 0 \tag{3.39}$$

$$\frac{\partial\varepsilon}{\partial C} = \sum_{i=1}^{n}\frac{1}{G_{s_i}^{diff}} P = 0 \tag{3.40}$$

$$\frac{\partial\varepsilon}{\partial D} = \sum_{i=1}^{n}\frac{B_{s_i}^{diff}}{G_{s_i}^{diff}} P = 0 \tag{3.41}$$

where $P = A + B\left(G_{s_i}^{diff} + \frac{B_{s_i}^{diff^2}}{G_{s_i}^{diff}}\right) + \frac{C}{G_{s_i}^{diff}} + \frac{DB_{s_i}^{diff}}{G_{s_i}^{diff}} - F_{dA_i}^{diff}$

The four equations (3.38) to (3.41) are solved for the unknown terms A, B,C and D. And the four noise parameters F_{min}^{diff}, R_n^{diff}, G_{opt}^{diff} and B_{opt}^{diff} are finally calculated by using (3.33) to (3.36) [2].

This section has presented the theoretical work that is required for the determination of the differential noise parameters from differential source-pull measurements. The equations and procedure have to be validated by ADS simulations and by measurements of a real differential amplifier, as described in the next sections.

[2]The equations are solved using a script written in Matlab

3.2.3 Validation by simulation

The equations and procedure developed in section 3.2.2 are verified by ADS simulations of a differential amplifier. The schematic diagram of the setup is shown in Fig. (3.18). It consists of a differential tuner, an X-band differential amplifier and two receivers. The differential tuner consists of two independent paths. Each path

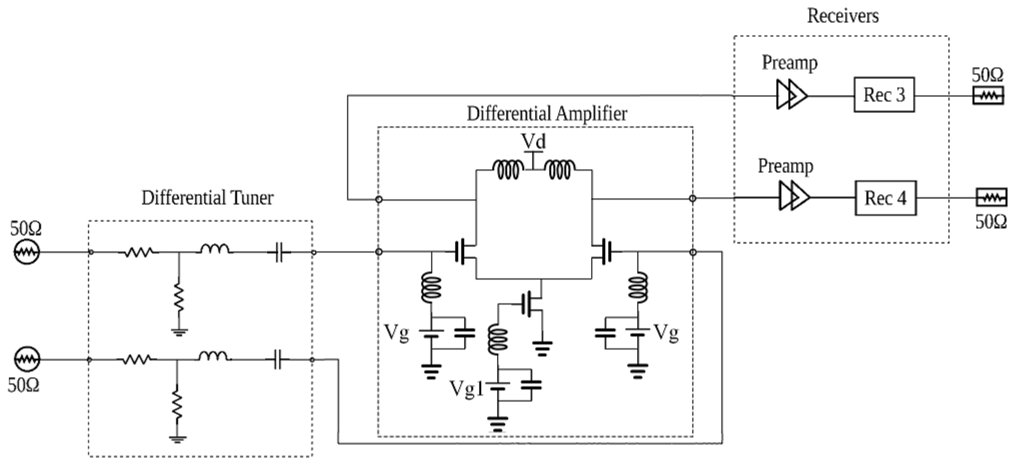

FIGURE 3.18: Simplified schematic diagram for the differential source-pull simulations on ADS

consists of some passive elements that are tuned to present different impedances to the dA. A simplified schematic diagram of the dT is shown in Fig. (3.19). In

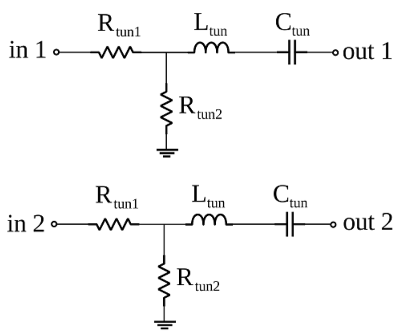

FIGURE 3.19: Simplified schematic diagram of the differential tuner

the simulation environment, only 4 source impedances are required as there is no measurement errors that affect the extraction of the noise parameters. But for the purpose of simulating the procedure as in measurement conditions, more than 4 impedances will be used. Fig. (3.20) shows the constellation of 7 reflection coefficients presented at 12 GHz by each of the two paths of the tuner.

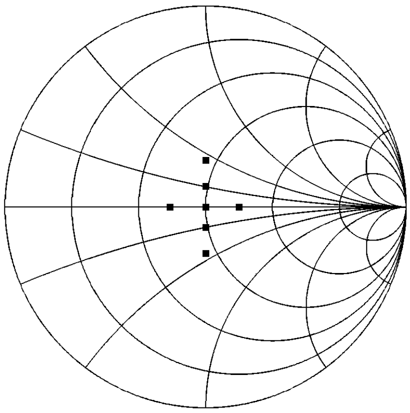

FIGURE 3.20: Smith chart plot of the seven impedances presented by the differential impedance tuner

Two independent receivers are connected at the output ports of the dA. Each receiver consists of a low-noise pre-amplifier which is useful during noise measurements as explained in section 2.2.3.2. Prior to the noise characterization of the dA, the 2-port noise parameters of each receiver need to be determined.

3.2.3.1 Noise parameters of the receivers

The four noise parameters of the two receivers are determined from source-pull measurements by connecting the differential tuner directly to the receivers. The receivers are characterized from conventional 2-port source-pull measurements by using the two independent paths of the tuner. The calculations for the extraction of the noise parameters of the receivers are explained in Appendix C. Fig. (3.21) shows the noise parameters of the two receivers simulated on ADS.

These noise parameters are used to calculate the noise figures F_{rec3} and F_{rec4} of the receivers for the different impedances presented to them during the differential source-pull measurements:

$$F_{rec3} = F_{min}^{rec3} + \frac{4R_n^{rec3}}{Z_0}\frac{|\Gamma_{out3} - \Gamma_{opt}^{rec3}|^2}{|1+\Gamma_{opt}^{rec3}|^2(1-|\Gamma_{out3}|^2)} \tag{3.42}$$

$$F_{rec4} = F_{min}^{rec4} + \frac{4R_n^{rec4}}{Z_0}\frac{|\Gamma_{out4} - \Gamma_{opt}^{rec4}|^2}{|1+\Gamma_{opt}^{rec4}|^2(1-|\Gamma_{out4}|^2)} \tag{3.43}$$

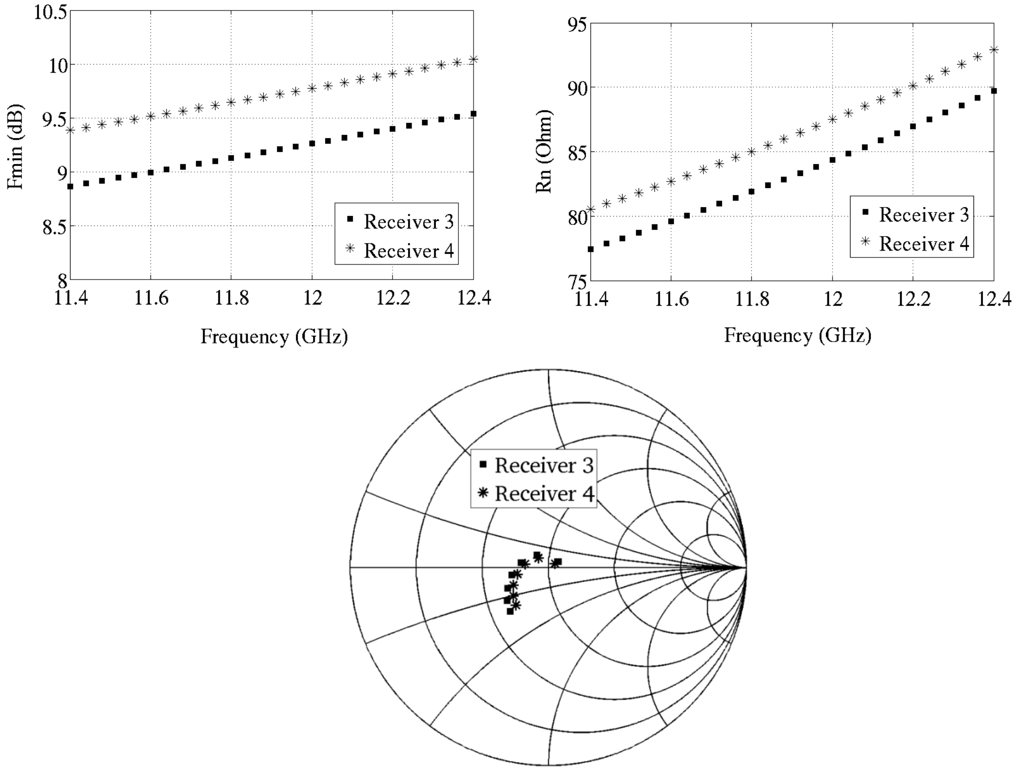

FIGURE 3.21: Single-ended noise parameters of the two receivers: minimum noise figures (left), equivalent noise resistances (right) and optimum source reflection coefficients (bottom)

3.2.3.2 Noise parameters of the differential amplifier

The next step consists of performing the differential source-pull measurements on the dA. Seven different impedances are presented by the tuner and for each impedance, the noise powers N_{tot3} and N_{tot4} at the output ports of the whole 'dT+dA+recs' system are measured.

The noise powers N_{out3} and N_{out4} at the output ports of the 'dT+dA' system are then extracted from N_{tot3} and N_{tot4} and from the noise figures F_{rec3} and F_{rec4} of the receivers simulated previously.

The following step consists of measuring the differential noise figure of 'dT+dA' system for each impedance. This is done by firstly determining the correlation between the output noise waves b_{out3} and b_{out4}. The correlation is calculated from the 4-port S-parameters of the 'dT+dA' system and from the output noise powers N_{out3} and N_{out4} by solving (3.25), (3.26) and (3.27).

The real part of the correlation, the output noise powers and the mixed-mode S-parameters of the 'dT+dA' system are then injected in (3.24) to calculate F_{sys}^{diff}, the dNF of the 'dT+dA' system.

And the differential noise figure F_{dA}^{diff} of the dA is finally calculated from F_{sys}^{diff} and from the available differential gain of the tuner using (3.29).

Seven differential noise figures are therefore obtained for seven source impedances. The four noise parameters of the dA are extracted by using Lane's procedure [13] as described in section 3.2.2. They are shown in Fig. (3.22).

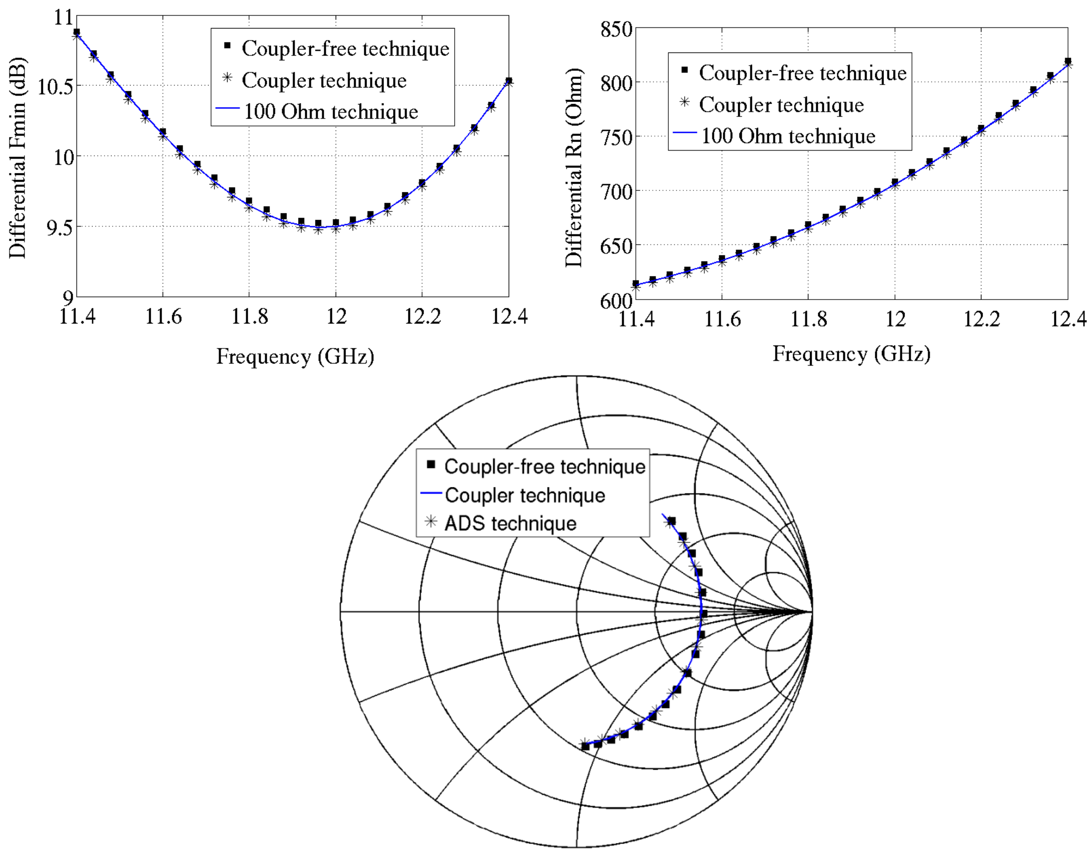

FIGURE 3.22: Differential noise parameters of the amplifier simulated with the coupler-free technique, the coupler-technique and the 100Ω-method: minimum differential noise figures (left), equivalent differential noise resistances (right) and optimum differential source reflection coefficients (bottom)

The differential noise parameters are compared firstly to those obtained with the coupler method developed in section 3.2.1.1. As explained in section 3.2.1.1, the dA is embedded between two hybrid couplers and single-ended source-pull measurements are done using a two-port tuner. Seven impedances are synthesized by the tuner, and for each of them, the differential noise figure of the amplifier is de-embedded by solving the equations described in section 3.2.1.1.

The differential noise parameters are then determined from the seven noise figures and source admittances by using Lane's procedure. The noise parameters obtained with this coupler technique are also shown in Fig. (3.22).

The noise parameters are also compared to those given directly by ADS. Indeed, the differential noise parameters are obtained by doing a noise simulation with the input and output ports connected to 100Ω terminations, as shown in Fig (3.23). ADS is capable of computing the noise parameters from all the noise contributors of the simulated circuit. The noise parameters obtained from the noise simulation with 100Ω terminations are also shown in Fig. (3.22).

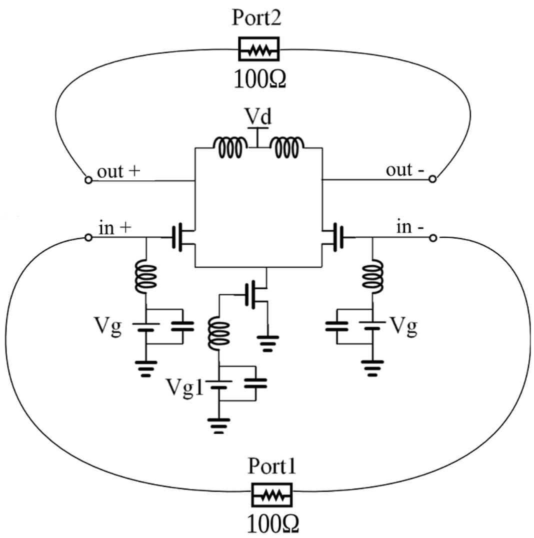

FIGURE 3.23: Schematic diagram of dA with 100Ω terminations for differential noise parameters simulation on ADS

There is a complete agreement between the simulation results obtained with the three methods. This allows us to validate the equations of section 3.2.2 and the coupler-free approach for differential noise parameters measurement. The next step is to test the technique in real measurement conditions.

3.2.4 Measurement procedure and results

This section describes the measurement setup and procedure for the extraction of the differential noise parameters of a low noise amplifier. The setup consists mainly of a Focus Microwaves iDMT-1820 differential impedance tuner, an S-band dLNA and a R&S ZVA24 4-port Network analyzer. The differential impedance tuner consists of two passive single-ended tuners. The tuners utilize broadband slab line transmission structures and passive probes to create impedances. A photograph of the differential tuner is shown in Fig. (3.24).

FIGURE 3.24: Photograph of the Focus Microwaves iDMT-1820 differential impedance tuner

The differential source-pull measurements will be performed in the 2 to 3 GHz frequency range with a frequency step of 200MHz. The measurements are done for a single frequency at a time. This means that the procedure has to be repeated for each frequency point; in our case the procedure will be performed for six frequency points. This single-frequency approach is time-consuming but it is justified for source impedances considerations. Indeed the differential tuner is calibrated at one frequency at a time and generates the appropriate impedance constellation for only that frequency. For the other frequencies, the constellation generated by the differential tuner is completely scattered. This might cause some serious measurement errors as the choice of the constellation is an important factor in the proper extraction of the noise parameters[38],[39].

3.2.4.1 Source impedance constellation

A tuner calibration is therefore performed at each of the frequency points so as to have the proper impedance constellation for each of them. A constellation of 15 impedances is chosen. A compromise between accuracy and time is made. Indeed, a large number of measurements decreases the effect of measurement errors and ensures a more robust method. But doing a lot of measurements is obviously time and effort consuming. In practice, it seems to us that 15 impedances provide sufficient redundancy without being too much time-consuming. Fig. (3.25) shows the constellation of 15 reflection coefficients presented by the tuner at 2 GHz.

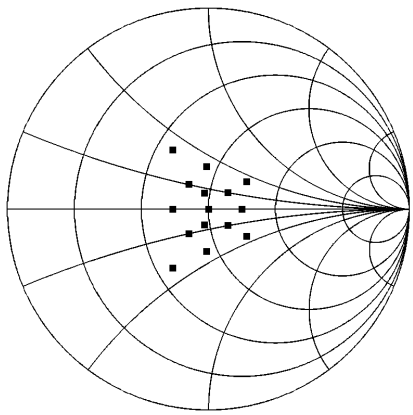

FIGURE 3.25: Smith chart plot of the fifteen impedances presented by the differential impedance tuner

The optimum source reflection coefficient of the receivers and of the differential LNA are expected to be found not far from $\Gamma = 0$ point. This explains why a constellation within the $|\Gamma| = 0.35$ circle is sufficient. There is no need of having impedances scattered all over the Smith chart.

For each of the 15 impedances synthesized by the differential tuner, the 4-port S-parameters of the latter are measured by using the 4-port Network Analyzer.

3.2.4.2 Noise parameters of receivers

Once the differential tuner has been measured for each impedance, the noise parameters of the receivers can be determined. As in section 2.2.3.2, the receivers consist of two low-noise preamplifiers from Kuhne electronic [33] connected to two R&S ZVA receivers. The input reflection coefficients S_{11}^{rec3} and S_{11}^{rec4} of the receivers are firstly measured by using the two other test-ports of the ZVA. Then, prior to the noise measurements, a power calibration is carried out in each receiver plane, as explained in section 2.2.3.2. For the noise characterization of the receivers, the differential tuner will be used as two separate single-ended tuners. The tuners are connected at the reference planes of the receivers as shown in Fig. (3.26). The

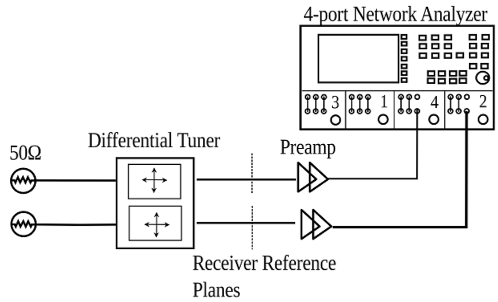

FIGURE 3.26: Setup for the noise parameters measurements of the receivers

input ports of the tuner are terminated with 50Ω matches and the noise powers at the output ports of the 'tuners+receivers' cascaded systems are measured. A photograph of the setup for output noise measurements of the cascaded systems is shown in Fig. (3.27).

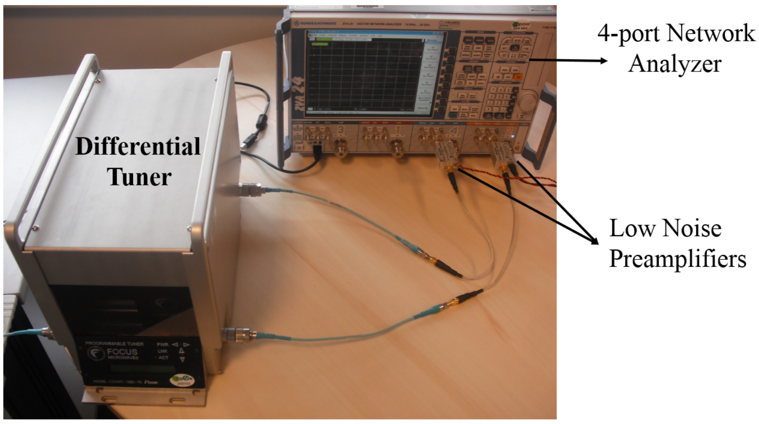

FIGURE 3.27: Photograph of the setup for noise parameters measurements of the receivers

The output noise powers are measured for each of the 15 impedances presented by the two single-ended tuners. The noise figures of the receivers are then determined from the output noise powers, the S-parameters of the tuners and the input reflection coefficients of the receivers as described in Appendix C. A least-square algorithm is finally applied on the overdetermined data for the extraction of the noise parameters of the receivers. This procedure is repeated for each of the frequency points. The measured noise parameters of both receivers are shown in Fig. (3.28). Minimum noise figures of 6 to 7 dB are obtained in the 2 to 3

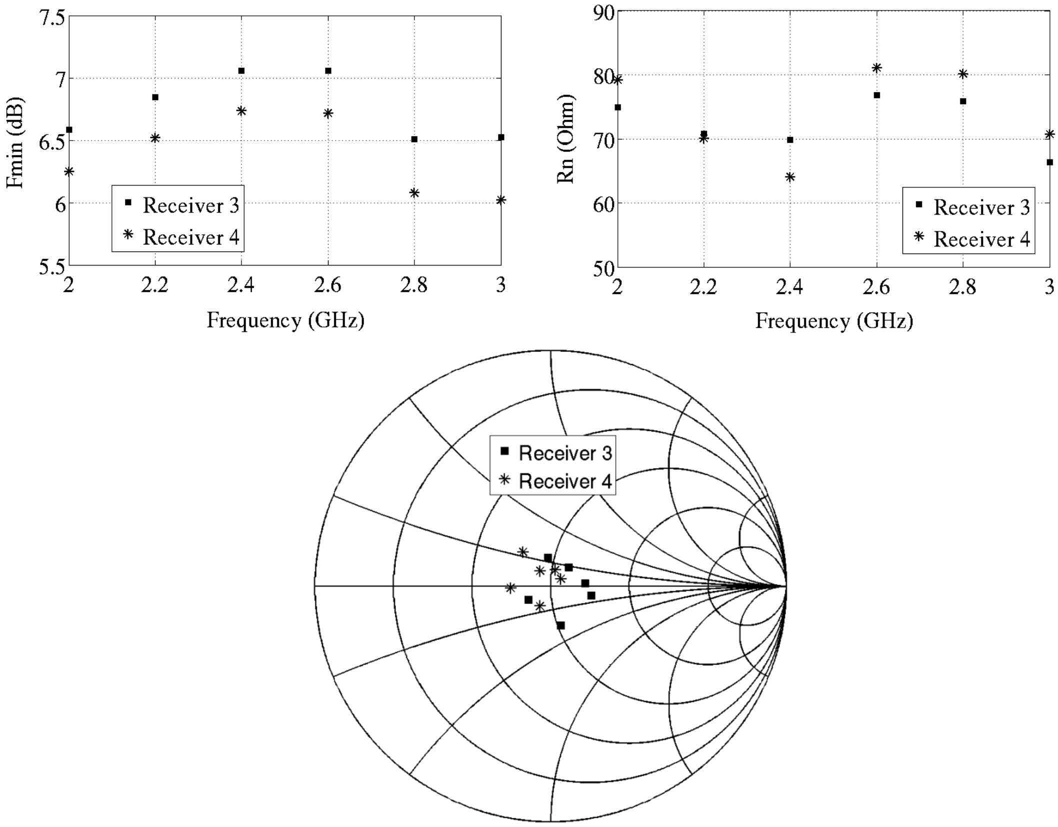

FIGURE 3.28: Single-ended noise parameters of the two receivers: minimum noise figures (left), equivalent noise resistances (right) and optimum source reflection coefficients (bottom)

GHz frequency range. The equivalent noise resistances vary from 65 to 80 Ω. And optimum source reflection coefficients are located within the $|\Gamma| = 0.18$ circle.

3.2.4.3 Noise parameters measurement of the dLNA

The next major part of the measurement procedure concerns the differential-source pull measurements on the dLNA. Firstly, the 4-port S-parameters of the 'dT+ dLNA' cascaded system are measured for each of the 15 impedances presented by the dT. The output reflection coefficients Γ_{out3} and Γ_{out4} of the cascaded system are thereby obtained. By using Γ_{out3}, Γ_{out4} and the receivers' noise parameters measured in the previous section, the noise figures F_{rec3} and F_{rec4} of the receivers are calculated for each impedance with (3.43).

The next step consists of measuring the noise powers N_{tot3} and N_{tot4} at the output ports of the whole 'dT+dLNA+receivers' system for each of the 15 impedances. A photograph of the measurement setup is shown in Fig. (3.29).

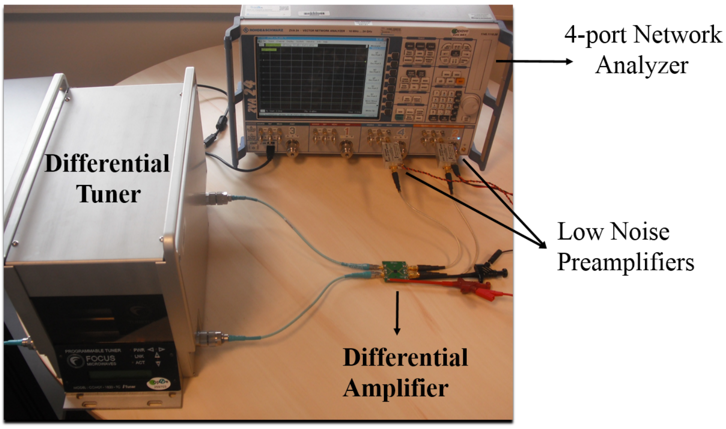

FIGURE 3.29: Photograph of the measurement setup for the noise powers N_{tot3} and N_{tot4} at the output ports of the whole 'dT+dLNA+receivers' system

The noise powers N_{out3} and N_{out4} at the output ports of the 'dT+dLNA' system are then extracted from N_{tot3} and N_{tot4} and from F_{rec3} and F_{rec4} by using (3.23). N_{out3} and N_{out4} are used together with the 4-port S-parameters to characterize the 'dT+dLNA' cascaded system. The correlation $\overline{b_{out3} \cdot b^*_{out4}}$ between the noise waves at the output ports of the system is calculated by using these measurement data and (3.25), (3.26) and (3.27).

The differential noise figure F^{diff}_{sys} is then calculated from the output noise powers, the correlation and the S-parameters of the 'dT+dLNA' system by solving (3.24).

The following step consists of calculating the noise figure F^{diff}_{dA} of the dLNA. It is extracted from F^{diff}_{sys} by using the available gain $G^{av^{diff}}_{tun}$ of the tuner and (3.29). The available gain is calculated previously using the differential S-parameters of the tuner.

The measurement procedure produces 15 differential noise figures corresponding to 15 differential source impedances. The procedure is repeated for each of the six frequency points.

The four differential noise parameters are finally evaluated by using a least-square fit on the overdetermined data as described in section 3.2.2.4. They are shown in Fig. (3.30).

The differential source-pull measurement procedure can be summarized as follows:

1. Calibration of the differential impedance tuner for each frequency
2. 4-port S-parameters measurements of the tuner for each desired impedance
3. 4-port S-parameters measurements of the 'dT+dA' cascaded system for each desired impedance
4. Measurements of input reflection coefficients of the two receivers
5. Noise power measurements at the output of the 'dT+receivers' cascaded system for each desired impedance
6. Noise power measurements at the output of the 'dT+dA+receivers' cascaded system for each desired impedance
7. Calculation of the noise parameters of the receivers
8. Calculation of the differential noise parameters of the differential amplifier

3.2.4.4 Evaluation of the measurement results

A minimum differential noise figure of 3 to 4 dB is obtained in the 2 to 3 GHz frequency range. The equivalent differential noise resistance varies from 25 to 40 Ω. The magnitude of the optimum differential source reflection coefficient is between 0.16 and 0.38. And its phase fluctuates between 140° and 160°.[3]

[3]The evaluation of the uncertainties of the measured noise parameters is left for future work due to lack of time.

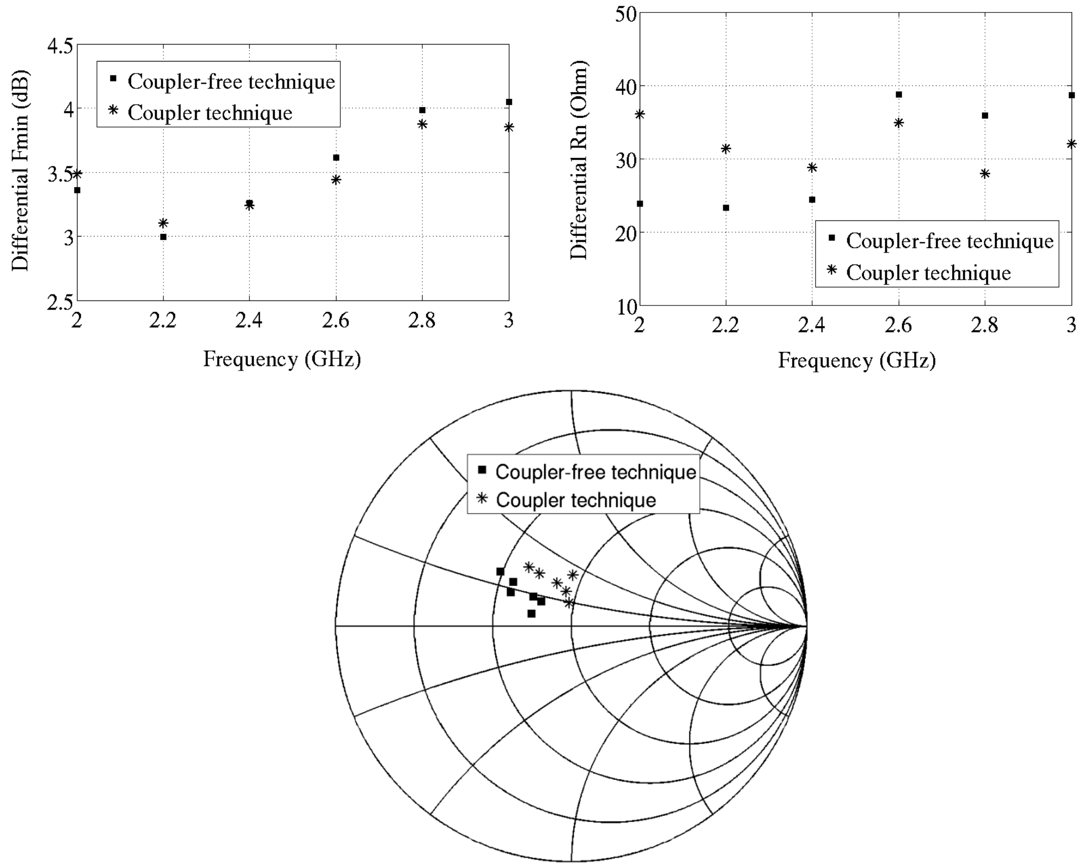

FIGURE 3.30: Differential noise parameters of the low noise amplifier measured with both the coupler-free technique and the coupler-technique: minimum differential noise figures (left), equivalent differential noise resistances (right) and optimum differential source reflection coefficients (bottom)

As the noise parameters measurements are very sensitive to experimental errors, the results have to be verified. Our verification method consists of comparing the noise parameters with those obtained with the conventional coupler-technique described in section 3.2.1.1. The noise parameters of the dLNA have therefore been measured from single-ended source-pull measurements by embedding the dLNA between two hybrid couplers. S-E source-pull measurements are performed by using one of the two S-E tuners of Focus Microwaves iDMT-1820 differential tuner. The same constellation of 15 impedances as in section 3.2.4.1 is used. The noise powers at the output port of the two-port cascaded system are measured by using one receiver of the R&S ZVA Network Analyzer. A photograph of the measurement setup is shown in Fig. (3.31). For each of the 15 source impedances, the noise figure of the dLNA is extracted from the measurements of the cascaded system and from the mixed-mode S-parameters of the hybrid couplers as explained

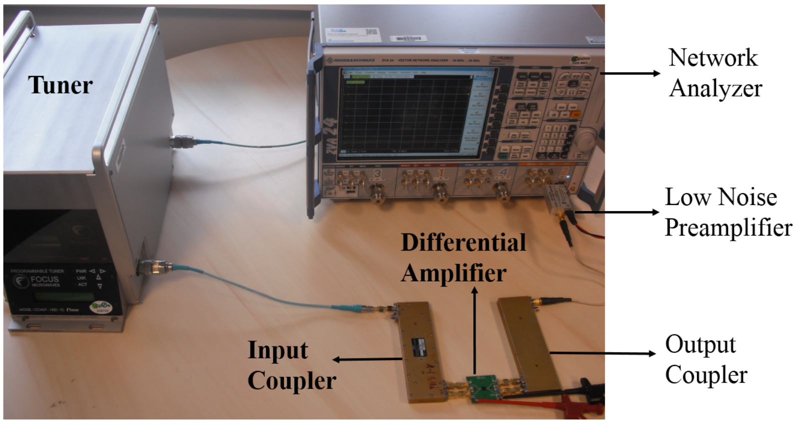

FIGURE 3.31: Photograph of the setup for differential noise parameters measurement by using the coupler technique

in section 3.2.1.1. The differential noise parameters are then determined from the 15 noise figures and from the source admittances by using Lane's procedure. The noise parameters obtained with this coupler technique in the 2 to 3 GHz bandwidth are also shown in Fig. (3.30).

A minimum differential noise figure of 3.1 to 3.9 dB is obtained in the 2 to 3 GHz frequency range. The differential equivalent noise resistance varies from 28 to 36 Ω. The magnitude of the optimum reflection coefficient is between 0.1 and 0.31. And the phase of Γ_{opt}^{diff} fluctuates between 90° and 125°.

The minimum noise figures obtained with the two techniques agree quite well, a maximum difference of 0.15 dB is observed. However, there are some discrepancies for R_n^{diff} and Γ_{opt}^{diff}. The maximum deviations reach around 12 Ω for the differential equivalent noise resistance, around 0.1 for the magnitude of Γ_{opt}^{diff} and around 60° for the phase of Γ_{opt}^{diff} .

These deviations are mainly due to the sensitivity of the noise parameters to measurement errors. Small errors or inaccuracies during the measurements have major influence on the relevance of the measured noise parameters [13], [38]. These errors and inaccuracies come firstly from the absolute noise power measurements of the 'dT+receivers', the 'dT+dA+receivers' and the 'tuner+couplers+dA+receivers' systems. The uncertainties in the noise power measurement are relatively important. Indeed, the power levels for noise measurements are very low and it is therefore challenging to measure them accurately. As explained in section 2.2.3.2, low noise receivers have been used for measuring such low levels of powers with an acceptable level of accuracy.

Errors and inaccuracies come also from the S-parameters measurements of the tuner, the amplifier, the couplers and the receivers. The uncertainties in the S-parameters measurements are relatively small compared to those in the noise power measurements. There are however some random errors that are caused by inaccuracies in the tuner repeatability. Repeatability designates how well the tuner' S-parameters repeat each time the tuner returns to a pre-determined position. In practice, the probes of the tuner do not return exactly to the same pre-determined position, which causes some measurement errors.

The results of Fig. (3.30) have shown that R_n^{diff} and Γ_{opt}^{diff} are more sensitive than F_{min}^{diff} to these measurement errors. A least square fit using a better choice of the impedance constellation could have improved the results. On one hand, choosing a few source impedance points close to Γ_{opt}^{diff} would improve the extraction of the latter. On the other hand, having a few distant points from Γ_{opt}^{diff} are more effective in determining R_n^{diff}.

The choice of the source impedances is pertinent when an approximate position of Γ_{opt}^{diff} is known. This position can be known by simulations. But when no schematic diagram is available for simulation as it was in our case, a two-step process [40] can be employed. The two-step process consists of using firstly a basic, reduced set of source impedances in order to determine the approximate location of Γ_{opt}^{diff}. And secondly, this information is used to choose additional source impedances localized in the Γ_{opt}^{diff} area to better determine the noise parameters.

Last but not least, the accuracy can be improved by the use of a weighting factor in the error criterion for the least square fit procedure. A weighting factor is used in the error criterion if certain measured differential noise figures are known to be less reliable than the average [13]. Methods exist for choosing the weighting factor [37] and have proved to increase the accuracy of the noise parameters extraction.

There are therefore some improvements to be made in our procedure for the measurement of the differential noise parameters. These improvements concern not only the accuracy problems but also time-consumption issues. Indeed, the technique takes quite a lot of time as it is based on single-frequency measurements. The development of a multi-frequency approach is left for future work.

3.2.5 Conclusion

An advanced measurement technique has been developed for the noise parameters measurement of differential amplifiers. It serves as a proof of concept, demonstrating that differential noise parameters can be measured from differential source-pull measurements without requiring any coupler. The calculations required for developing this new approach have been clearly explained in section 3.2.2. These calculations have been verified and validated by ADS simulations of a differential amplifier in section 3.2.3. The technique has then been tested in real measurement conditions where the noise parameters of a differential low noise amplifier are determined from source-pull measurements using a differential impedance tuner.

This is, to the best of our knowledge, the first coupler-free technique developed for measuring the noise parameters of differential amplifiers. The method has the advantage of not requiring isolators or couplers that would limit the bandwidth of measurements or complicate the noise figure de-embedding procedure. Moreover, it does not need any calibrated noise source that might bring some mismatch errors when the noise source is turned on and off. And finally, our approach can serve as a groundwork for the development of an automated differential noise parameter measurement system using a differential tuner and a 4-port Network Analyzer.

General Conclusion

The wide proliferation of differential circuits creates a need for the development of functional techniques for the proper noise characterization of these circuits. The goal of this work was to propose novel techniques for the noise figure measurement of differential circuits. It has been demonstrated in Chapter 1 that the noise figure of four-port circuits depends on the correlation of the noise waves at the two output ports of these circuits. The issue about noise measurements of differential circuits is that no commercially-available equipment is capable so far in measuring directly the correlation of output noises. The challenge of this work was therefore to develop measurement techniques for the measurement of this correlation.

In Chapter 2, an original technique for measuring the correlation of output noise waves has been proposed. It makes use of a 180° hybrid coupler connected to the differential DUT to be measured. The correlation is a complex term with a real and an imaginary part. These two unknown elements can be determined using two equations. These equations are determined by using two configurations of connection between the differential DUT and the coupler. The correlation is extracted by taking into account the amplitude and phase imbalances of the coupler. This approach has been employed for the development of a rigorous and general technique for the noise figure measurement of all sorts of differential amplifiers. The technique was validated by simulations and by measurements of RF amplifiers.

This coupler technique has however some drawbacks. Couplers have limited bandwidth and require a quite complex and long de-embedding procedure. This motivated us to build a novel technique that does not need any coupler. A coupler-free technique was developed in Chapter 3 for the determination of the correlation. A study of the classical architecture of a differential amplifier has been performed. It allowed us to define an expression of the correlation in terms of input-referred noise powers and of the 4-port S-parameters of the dA. This approach was used to build a fast and functional technique for the noise figure measurement of a differential low noise amplifier. The advantage of this new technique is that all measurements are easily performed on a 4-port network analyzer without the need for couplers that require complicated de-embedding procedures.

This coupler-free approach was extended in the second part of Chapter 3 to the measurement of the noise parameters of differential amplifiers. These noise parameters are important figures of merit as they allow the determination of the differential noise figure for arbitrary impedances presented to the dA. The noise parameters of a dA have been determined from differential source-pull measurements using a differential impedance tuner. The whole procedure for extracting the differential noise parameters has been successfully verified in simulations. The procedure was developed in real measurement conditions where the noise parameters of a differential low noise amplifier were measured. The measurement results were satisfying but could not be completely validated. This is due to the fact that noise parameters measurements are very sensitive to measurement errors and uncertainties.

This is, to the best of our knowledge, the first coupler-free technique developed for measuring the noise parameters of differential amplifiers. The differential noise parameters measurement technique still needs to be improved. Future work shall deal with improvements in accuracy and time-consumption issues.

The advanced techniques presented in this work can be considered as important proofs of concept. There is however still some work to be done for implementing them in equipment such as network analyzers. In particular, the coupler-free techniques give good results for differential amplifiers with classical one-stage architecture. Investigations need still to be carried out to verify that the methods work properly for differential amplifiers with complex multi-stage architectures.

List of Publications

Journal

Y. Andee, J. Prouvée, F. Graux and F. Danneville, "Determination of noise figure of differential circuits using correlation of output noise waves," in *Electronic Letters*, vol. 50, no. 9, pp. 665-667, Apr. 2014.

International Conferences

Y. Andee, J. Prouvée, F. Graux and F. Danneville, "A fast and functional technique for the noise figure measurement of differential amplifiers," in *Conference on Ph.D. Research in Microelectronics and Electronics (PRIME)*, 2014.

Y. Andee, A. Siligaris, F. Graux and F. Danneville, "On-wafer differential noise figure measurement without couplers on a vector network analyzer," in *Microwave Measurement Conference (ARFTG)*, Dec 2014.

Y. Andee, C. Arnaud, F. Graux and F. Danneville, "De-embedding differential noise figure using the correlation of output noise waves," in *Microwave Measurement Conference (ARFTG)*, May 2015.

Y. Andee, C. Arnaud, P. Seurre and F. Danneville, "A coupler-free differential noise figure measurement technique without noise source on a two-port network analyzer," in *IEEE Radio and Antenna Days of the Indian Ocean (RADIO)*, Sep 2015.

National Conference

Y. Andee, J. Prouvée, F. Graux and F. Danneville, "Technique de mesure du facteur de bruit différentiel avec un analyseur de réseau 4-ports," in *Journées Nationales du Réseau Doctoral en Micro-nanoélectronique (JNRDM)*, 2014.

Appendix A

Basic definitions for the calculation of the 2-port noise figure

This appendix deals with some important concepts that are necessary to understand the calculation of the noise figure.

In 1.3, the noise figure of a single-ended circuit is defined as the degradation of the available signal-to-noise ratio, evaluated for an available input noise power N_1^{av} of $kT_0\Delta f$ [8]:

$$F = \frac{P_1^{av}/N_1^{av}}{P_2^{av}/N_2^{av}} = \frac{N_2^{av}}{G^{av}N_1^{av}} = \frac{N_2^{av}}{G^{av}kT_0\Delta f} \tag{A.1}$$

where P_i^{av} is the available signal power at port i, N_i^{av} is the available noise power at port i and G^{av} is the available gain of the 2-port circuit.

In the following paragraphs, the terms of equation (A.1) are briefly defined.

The available gain is defined as the ratio of the available signal power at the output $P_{out}^{av}$to the available signal power from the source P_1^{av}, where P_1^{av} is given by:

$$P_1^{av} = \frac{|\hat{a}_1|^2}{1 - |\Gamma_1|^2} \tag{A.2}$$

where $\hat{a}_1$ is the generator wave [1] from the source and Γ_1 is its reflection coefficient.

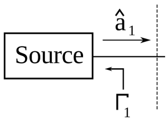

Figure A.1: One port formalism

The available signal power at the output P_{out}^{av} is given by:

$$P_{out}^{av} = \frac{|\hat{b}_2|^2}{1 - |\Gamma_{out}|^2} \tag{A.3}$$

where Γ_{out} is the reflection coefficient at the output port of the circuit. It is defined in terms of the scattering parameters and of the reflection coefficient of the source:

$$\Gamma_{out} = S_{22} + \frac{S_{21}S_{12}\Gamma_1}{1 - S_{11}\Gamma_1} \tag{A.4}$$

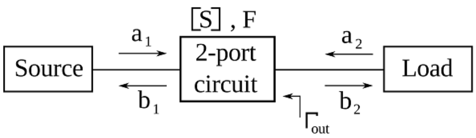

Figure A.2: Two port formalism

And $\hat{b}_2$ is the generator wave at the output port of the circuit. It is given by:

$$\hat{b}_2 = b_2 - a_2\Gamma_{out}$$
$$\hat{b}_2 = \frac{S_{21}\hat{a}_1}{1 - S_{11}\Gamma_1} \tag{A.5}$$

The expresssion of P_{out}^{av} is calculated from (A.3) and (A.5):

$$P_{out}^{av} = \frac{|S_{21}|^2|\hat{a}_1|^2}{|1 - S_{11}\Gamma_1|^2(1 - |\Gamma_{out}|^2)} \tag{A.6}$$

The available gain is therefore obtained from (A.2) and (A.6).

$$G^{av} = \frac{|S_{21}|^2(1 - |\Gamma_1|^2)}{|1 - S_{11}\Gamma_1|^2(1 - |\Gamma_{out}|^2)} \tag{A.7}$$

[1] A generator wave is the wave that would be delivered to a noiseless and reflectionless termination

In practice, a measured power is in fact a power delivered to a load/receiver. However, the determination of the noise figure requires the measurement of available powers. It is therefore interesting to have an expression of available power in terms of delivered power P_{del}. This is done by deriving an expression of P_{del}.

$$P_{del} = |b_2|^2 - |a_2|^2 \tag{A.8}$$

And as $a_2 = \Gamma_2 b_2$,

$$P_{del} = |b_2|^2(1 - |\Gamma_2|^2) = \frac{|S_{21}|^2|\hat{a}_1|^2(1 - |\Gamma_2|^2)}{|1 - S_{11}\Gamma_1|^2|1 - \Gamma_2\Gamma_{out}|^2} \tag{A.9}$$

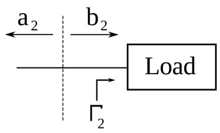

FIGURE A.3: One port load formalism

Using (A.3) and (A.9),the relation between available power and delivered power is given by:

$$\frac{P_{del}}{P_{out}^{av}} = \frac{(1 - |\Gamma_{out}|^2)(1 - |\Gamma_2|^2)}{|1 - \Gamma_2\Gamma_{out}|^2} \tag{A.10}$$

These power concepts allow us to build an expression of the noise figure in terms of parameters that can be measured using conventional equipment.

$$F = \frac{N_2^{av}}{G^{av}N_1^{av}} = \frac{|1 - \Gamma_2\Gamma_{out}|^2}{(1 - |\Gamma_{out}|^2)(1 - |\Gamma_2|^2)} \frac{N_{del}}{G^{av}kT_0\Delta f} \tag{A.11}$$

It is interesting to note that for the particular case of reflectionless terminations (source and load), the noise figure simplifies to:

$$F = \frac{N_{del}}{|S_{21}|^2 kT_0\Delta f} \tag{A.12}$$

Appendix B

Calculations using the complex representation

As explained in Chapter 1, noise waves are time-varying complex random variables. And for any noise wave, we can define a complex amplitude which determines both amplitude and phase. This appendix deals with the mathematical operations on complex numbers that have been used in this work.

Let X and Y be complex amplitudes, denoted by $X = a + jb$ and $Y = c + jd$.

$$\Re e(X) = \Re e(X^*) \quad \text{and} \quad \Im m(Y) = -\Im m(Y^*) \tag{B.1}$$

where X^* and Y^* are the conjugates of X and Y respectively.

The basic operations for the multiplication of complex values are given below:

$$XY = (a + jb)(c + jd) = (ac - bd) + j(ad + bc) \tag{B.2}$$

From (B.2),

$$\Re e(XY) = \Re e(X)\Re e(Y) - \Im m(X)\Im m(Y) \tag{B.3}$$

$$\Im m(XY) = \Re e(X)\Im m(Y) + \Im m(X)\Re e(Y) \tag{B.4}$$

And,

$$(X \cdot Y)^* = Y^* \cdot X^* \tag{B.5}$$

The equations of 2.2.1 are calculated using these basic operations:

According to (B.4),

$$2\Re e\left(S^c_{31} \cdot S^{c*}_{32}\,\overline{b_3 \cdot b_4^*}\right) = 2\Re e(S^c_{31} \cdot S^{c*}_{32})\Re e(\overline{b_3 \cdot b_4^*}) - 2\Im m(S^c_{31} \cdot S^{c*}_{32})\Im m(\overline{b_3 \cdot b_4^*}) \tag{B.6}$$

And,

$$2\Re e\left(S^c_{32} \cdot S^{c*}_{31}\,\overline{b_3 \cdot b_4^*}\right) = 2\Re e(S^c_{32} \cdot S^{c*}_{31})\Re e(\overline{b_3 \cdot b_4^*}) - 2\Im m(S^c_{32} \cdot S^{c*}_{31})\Im m(\overline{b_3 \cdot b_4^*}) \tag{B.7}$$

As $S^c_{32} \cdot S^{c*}_{31} = (S^c_{31} \cdot S^{c*}_{32})^*$,

$$\begin{aligned} \Re e(S^c_{32} \cdot S^{c*}_{31}) &= \Re e(S^c_{31} \cdot S^{c*}_{32}) \\ \Im m(S^c_{32} \cdot S^{c*}_{31}) &= -\Im m(S^c_{31} \cdot S^{c*}_{32}) \end{aligned} \tag{B.8}$$

Therefore, (B.7) becomes:

$$2\Re e\left(S^c_{32} \cdot S^{c*}_{31}\,\overline{b_3 \cdot b_4^*}\right) = 2\Re e(S^c_{31} \cdot S^{c*}_{32})\Re e(\overline{b_3 \cdot b_4^*}) + 2\Im m(S^c_{31} \cdot S^{c*}_{32})\Im m(\overline{b_3 \cdot b_4^*}) \tag{B.9}$$

Appendix C

Noise parameters of receivers

This section deals with the noise parameters measurement of the 2 receivers required for the differential source-pull measurements. The block diagram of the setup for the receivers's noise parameters measurement is shown in Fig. (C.1). The two independent receivers are denoted by rec3 and rec4. The differential tuner has two independent paths denoted by tun1 and tun2. As the receivers are

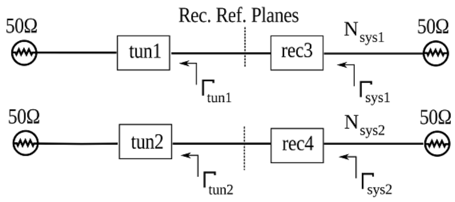

FIGURE C.1: Block diagram of the setup for the noise characterization of the receivers

independent, the calculations are done separately for each of them. Lets consider firstly rec3. The 2-port noise figure F_{sys1} of the 'tun1+rec3' cascaded system is given by Friis equation:

$$F_{sys1} = F_{tun1} + \frac{F_{rec3} - 1}{G^{av}_{tun1}} \tag{C.1}$$

As the tuner is a passive component, its noise figure F_{tun1} is related to its available gain G^{av}_{tun1} as $F_{tun1} = 1/G^{av}_{tun1}$. So, the noise figure of rec3 is given by:

$$F_{rec3} = F_{sys1} G^{av}_{tun1} \tag{C.2}$$

F_{sys1} is calculated from the available noise power N^{av}_{sys1} at the output of the cascaded system as:

$$F_{sys1} = \frac{N^{av}_{sys1}}{G^{av}_{sys1} k T_0 \Delta f} \tag{C.3}$$

The available gain of the cascasced system G^{av}_{sys1} is expressed in terms of the available gains of tun1 and rec3 as:

$$G^{av}_{sys1} = G^{av}_{tun1} G^{av}_{rec3} \tag{C.4}$$

The noise figure of rec3 is determined from (C.2),(C.3) and (C.4):

$$F_{rec3} = \frac{N^{av}_{sys1}}{G^{av}_{rec3} k T_0 \Delta f} \tag{C.5}$$

N^{av}_{sys1} can be calculated from the output noise power N_{sys1} delivered to a 50Ω load as:

$$N^{av}_{sys1} = \frac{N_{sys1}}{1 - |\Gamma_{sys1}|^2} \tag{C.6}$$

where Γ_{sys1} is the reflection coefficient seen at the output of the cascaded system.

And the available gain of the receiver is calculated as:

$$G^{av}_{rec3} = \frac{|S^{rec3}_{21}|^2 (1 - |\Gamma_{tun1}|^2)}{|1 - S^{rec3}_{11} \Gamma_{tun1}|^2 (1 - |\Gamma_{sys1}|^2)} \tag{C.7}$$

where Γ_{tun1} is the reflection coefficient presented by the tuner to the receiver. The forward gain of the receiver is set to unity ($|S^{rec3}_{21}|^2 = 1$) as a receiver power calibration is performed prior to the noise power measurements.

The final expression of F_{rec3} is otbained from (C.5) and (C.7):

$$F_{rec3} = \frac{N_{sys1} |1 - S^{rec3}_{11} \Gamma_{tun1}|^2}{(1 - |\Gamma_{tun1}|^2) k T_0 \Delta f} \tag{C.8}$$

For each tuner position, F_{rec3} is calculated from the noise power measured at the output of the cascaded system, from the input reflection coefficient of the rec3 and from the output reflection coefficient of the tuner.

Similar calculations are done for the determination of the noise figure of receiver 4:

$$F_{rec4} = \frac{N_{sys2}|1 - S_{11}^{rec4}\Gamma_{tun2}|^2}{(1 - |\Gamma_{tun2}|^2)kT_0\Delta f} \tag{C.9}$$

The two-port noise parameters of rec3 are then determined from F_{rec3} and Γ_{tun1} using Lane's procedure with the least-squares method. Likewise, the noise parameters of rec4 are then determined from F_{rec4} and Γ_{tun2}.

Bibliography

[1] A. Van der Ziel, *Noise in Solid State Devices and Circuits.* John Wiley & Sons, 1986.

[2] J. Johnson, "Thermal agitation of electricity in conductors," *Nature*, vol. 119, pp. 50–51, Jan 1927.

[3] H. Nyquist, "Thermal agitation of electric charge in conductors," *Physical Review Letters*, vol. 32, pp. 110–113, Jul 1928.

[4] M. Schottky, *On spontaneous current fluctuations in different electrical conductors (in German).* Annals of Physics, 1918, vol. 362, no. 23, pp. 541–567.

[5] A. Van der Ziel, *Noise.* Prentice-Hall, 1954.

[6] S. Kogan, *Electronic Noise and Fluctuations in Solids.* Cambridge University Press, 2008.

[7] H. Friis, "Noise figures of radio receivers," *Proceedings of the IRE*, vol. 32, no. 7, pp. 419–422, July 1944.

[8] "Ire standards on electron tubes: Definitions of terms, 1957," *Proceedings of the IRE*, vol. 45, no. 7, pp. 983–1010, July 1957.

[9] R. Haitz, "Noise of a self-sustaining avalanche discharge in silicon: Low-frequency noise studies," *Journal of Applied Physics*, vol. 38, no. 7, pp. 2935–2946, Jan 1967.

[10] *Noise figure measurements*, Application Note, Anritsu, 2012.

[11] *Noise figure measurement without a noise source on a Vector Network Analyzer*, Application note, Rohde&Schwarz, 2010.

[12] "Ire standards on methods of measuring noise in linear twoports, 1959," *Proceedings of the IRE*, vol. 48, no. 1, pp. 60–68, Jan 1960.

[13] R. Lane, "The determination of device noise parameters," *Proceedings of the IEEE*, vol. 57, no. 8, pp. 1461–1462, Aug 1969.

[14] S. Wedge and D. Rutledge, "Wave techniques for noise modeling and measurement," *Microwave Theory and Techniques, IEEE Transactions on*, vol. 40, no. 11, pp. 2004–2012, Nov 1992.

[15] N. Kanaglekar, R. McIntosh, and W. Bryant, "Wave Analysis of Noise in Interconnected Multiport Networks," *IEEE Transactions on Microwave Theory and Techniques*, vol. 35, no. 2, pp. 112–116, Feb. 1987.

[16] J. Penfield, P., "Wave representation of amplifier noise," *Circuit Theory, IRE Transactions on*, vol. 9, no. 1, pp. 84–86, Mar 1962.

[17] H. Bosma, "On the theory of linear noisy systems," Ph.D. dissertation, Dept. Elect. Eng., Eindhoven Univ. Technology, Eindhoven, The Netherlands, 1967.

[18] H. Haus and R. Adler, "Optimum noise performance of linear amplifiers," *Proceedings of the IRE*, vol. 46, no. 8, pp. 1517–1533, Aug 1958.

[19] R. Hecken, "Analysis of linear noisy two-ports using scattering waves," *Microwave Theory and Techniques, IEEE Transactions on*, vol. 29, no. 10, pp. 997–1004, Oct 1981.

[20] *Three and four port S-parameter measurements*, Application Note, Anritsu, 2002.

[21] D. E. Bockelman and W. R. Eisenstadt, "Combined Differential and Common-Mode Scattering Parameters: Theory and Simulation," *IEEE Transactions on Microwave Theory and Techniques*, vol. 43, no. 7, pp. 1530–1539, Jul. 1995.

[22] J. Lintignat, S. Darfeuille, Z. Sassi, B. Barelaud, L. Billonnet, and B. Jarry, "Original approach for extracting the exact noise factor of differential microwave circuits using mixed-mode and noise-wave formalisms," in *36th Eur. Microw. Conf.*, Sept 2006.

[23] Y. Andee, J. Prouvee, F. Graux, and F. Danneville, "Determination of noise figure of differential circuits using correlation of output noise waves," *Electronics Letters*, vol. 50, no. 9, pp. 665–667, April 2014.

[24] A. Abidi and J. Leete, "De-embedding the noise figure of differential amplifiers," *IEEE Journal of Solid-State Circuits*, vol. 34, no. 6, pp. 882–885, Jun. 1999.

[25] O. G. Perez, V. Gonzalez-Posadas, L. E. Garcia-Munoz, and D. Segovia-Vargas, "Noise-Figure Measurement of Differential Amplifiers Using Nonideal Baluns," *IEEE Transactions on Microwave Theory and Techniques*, vol. 59, no. 6, pp. 1658–1664, Jun. 2011.

[26] L. F. Tiemeijer, R. M. T. Pijper, and E. van der Heijden, "Complete on-wafer noise-figure characterization of 60-ghz differential amplifiers," *IEEE Transactions on Microwave Theory and Techniques*, vol. 58, no. 6, pp. 1599–1608, Jun. 2010.

[27] J. Dunsmore and S. Wood, "Vector corrected noise figure and noise parameter measurements of differential amplifiers," in *Eur. Microw. Conf.*, Sept 2009, pp. 707–710.

[28] Y. Andee, C. Arnaud, F. Graux, and F. Danneville, "De-embedding differential noise figure using the correlation of output noise waves," in *ARFTG Microwave Measurement Conference (ARFTG), 2015 85th*, May 2015, pp. 1–4.

[29] *Noise Figure Measurement Accuracy: The Y-Factor Method*, Application Note 57-2, Agilent Technologies, 2004.

[30] *R&S ZVA Vector Network Analyzer Specifications*, Datasheet, Rohde&Schwarz, 2012.

[31] *R&S ZV-Z5x Calibration Unit Specifications*, Datasheet, Rohde&Schwarz, 2014.

[32] *Accuracy of Noise Figure Measurement Systems*, Hewlett Packard, 1988.

[33] *KU LNA BB 0180 A-SMA Specifications*, Datasheet, Kuhne electronic, 2012.

[34] Y. Andee, A. Siligaris, F. Graux, and F. Danneville, "On-wafer differential noise figure measurement without couplers on a vector network analyzer," in *ARFTG Microwave Measurement Conference (ARFTG), 2014 84th*, Dec 2014, pp. 1–4.

[35] O. Perez, D. Segovia-Vargas, L. Garcia-Munoz, J. Jimenez-Martin, and V. Gonzalez-Posadas, "Broadband differential low-noise amplifier for active differential arrays," *Microwave Theory and Techniques, IEEE Transactions on*, vol. 59, no. 1, pp. 108–115, Jan 2011.

[36] H. Fukui, "The noise performance of microwave transistors," *Electron Devices, IEEE Transactions on*, vol. ED-13, no. 3, pp. 329–341, March 1966.

[37] L. Escotte, R. Plana, and J. Graffeuil, "Evaluation of noise parameter extraction methods," *Microwave Theory and Techniques, IEEE Transactions on*, vol. 41, no. 3, pp. 382–387, Mar 1993.

[38] A. Davidson, B. Leake, and E. Strid, "Accuracy improvements in microwave noise parameter measurements," *Microwave Theory and Techniques, IEEE Transactions on*, vol. 37, no. 12, pp. 1973–1978, Dec 1989.

[39] C. Giuseppe and M. Sannino, "Computer-aided determination of microwave two-port noise parameters," *Microwave Theory and Techniques, IEEE Transactions on*, vol. 26, no. 9, pp. 639–642, Sep 1978.

[40] S. Van den Bosch and L. Martens, "Improved impedance-pattern generation for automatic noise-parameter determination," *Microwave Theory and Techniques, IEEE Transactions on*, vol. 46, no. 11, pp. 1673–1678, Nov 1998.